Calibration of the muon barrel chambers for the EMMA experiment

Master's thesis, June 16, 2017

Author:

Jukka Sorjonen

Supervisors:

Timo Enqvist (University of Oulu), Pasi Kuusniemi (University of Oulu), Kai Loo

UNIVERSITY OF JYVÄSKYLÄ
DEPARTMENT OF PHYSICS

Abstract

Sorjonen, Jukka
Calibration of the muon barrel chambers for the EMMA experiment
Master's thesis
Department of Physics, University of Jyväskylä, 2017, 107 pages.

The topic of this thesis was position calibration of muon barrel chambers used in the EMMA experiment. A detector ergo plank consist of seven chambers, and there were six uncalibrated detectors. The planks were set in a calibration stack, where there were four reference planks and six uncalibrated planks. Every chamber was divided into channels, and for every chamber, there was a specific position in the chamber. The position for each channel was ascertained by using manually calibrated reference planks and atmospheric muons. The calibration table was created for every chamber to obtain corresponding position for every channel in the chamber. The data collection was being done for approximately a month.

There were 42 chambers in total to be calibrated, and it was possible to be created the calibration tables for 31 of them. The failed calibration originated from low statistic, probably due to broken chambers. There were some troublesome planks in the calibration stack, which have been through several calibrations.

The experimental uncertainty was approximated by residual histograms. The residual histograms were done for reference planks, and for uncalibrated planks. When comparing the peak width and mean of these histograms, an information about the quality of the calibration was obtained.

Keywords: cosmic rays, drift chambers, calibration

Tiivistelmä

Sorjonen, Jukka
EMMA-kokeen ajautumiskammioiden kalibraatio
Pro gradu-tutkielma
Fysiikan laitos, Jyväskylän yliopisto, 2017, 107 pages.

Tutkimuksessa paikkakalibroitiin EMMA-kokeessa käytettäviä ajautumiskammioita. Yksi ilmaisin eli plankki koostui seitsemästä kammiosta, ja kalibroitavia ilmaisimia oli yhteensä kuusi. Plankit oli sijoitettu telineeseen, jossa oli neljä referenssiplankkia ja kuusi kalibroimatonta plankkia. Jokainen kammio oli jaettu kanaviin, ja jokaista kanavaa vastasi tietty paikka kammiossa. Kanavaa vastaava paikka pystyttiin selvittämään hyödyntäen manuaalisesti kalibroituja referenssiplankkeja sekä ilmakehän myoneja. Kalibraatiotaulukko luotiin jokaiselle kammiolle siten, että siitä saatiin tiettyä kanavaa vastaava paikka. Dataa kerättiin noin kuukausi.

Kammioita oli yhteensä 42 ja niistä onnistuttiin tekemään kalibraatiotaulukko 31:lle. Epäonnistuneet kalibraatiot johtuivat heikosta statistiikasta, joka johtui toimimattomista kammioista. Kyseisessä kalibraatioasetelmassa oli joitakin ongelmallisia plankkeja, jotka olivat jo käyneet monia kalibraatioita läpi.

Epätarkkuutta arvioitiin residuaali-histogrammilla. Residuaali-histogrammi tehtiin sekä referenssiplankeille että kalibroitaville plankeille. Vertaamalla näiden residuaalihistogrammin piikin leveyttä sekä keskikohdan paikkaa, saatiin tieto kalibraation onnistumisesta.

Avainsanat: kosmiset säteet, ajautumiskammio, kalibraatio

"Hey, hey, hey. A life. A life, Jimmy, you know what that is? It's the shit that happens while you're waiting for moments that never come."

Det. Lester Freamon, HBO: The wire, season 3, episode 9.

Contents

1 Cosmic radiation

In this chapter, concepts of cosmic ray (CR) radiation will be discussed. The first subsection covers briefly about the history of discovering CRs and some notable discoveries. The main bulk of the chapter then describes the core elements of CR radiation: Crs, acceleration mechanism of Crs, extensive air showers, and hadronic cascade in extensive air shower. Studying extensive air showers and respectively their muon component is the key objective of the EMMA experiment [1].

1.1 A brief history of cosmic rays

During the years of 1911-1912 an Austrian physicist Victor Hess did a series of balloon flights to several altitudes to measure the ionizing radiation, or rather "durchdringenden strahlung" (penetration radiation), of the atmosphere with Wulf's devices. He discovered that there was a component in the ionizing radiation that was coming outside of the earth, and it increased as a function of the height [2]. Before the flights of Hess, the general view among scientists was that cosmic radiation was a bare product of the earth's natural radioactivity [3]. Hess received a Nobel prize "*for his discovery of cosmic radiation*" in 1936 [4].

There were many pioneers before Hess, whose passion for physics paved the way for Hess and his discovery. The first one to be named is Charles Augustin de Coulomb who discovered that electroscope loses its electricity spontaneously over time [5]. William Crookes builds Crookes' tube (discharge tube with partial vacuum) in 1879 [6]. It was used by Wilhelm Röntgen for his experiments for discovery of ionization radiation for the first time in 1895 [7]. Henri Becquerel discovered spontaneous radioactivity by an experiment where he concluded that "...phosporescent substance in question emits radiation..." in 1896 [8]. Slightly later, Thomson discovered electron, or measured mass-to-charge-ratio of electrons to be exact, with an upgraded Crookes' tube in 1897 [9].

The first scientist who discovered that "penetrating radiation" was not purely of terrestrial origin was Theodor Wulf by measuring ionizing radiation on the top of Eiffel's tower using the Wulf electrometer in 1909. Wulf's idea was to prove his theory that penetration radiation was caused by radioactive sources in the upper-levels of the soil. [10] However, there was still radiation on the top of Eiffel tower which made his theory inadequate. Albert Gocke did also a balloon flight to measure the ion density of air, and came to the same conclusions as Wolf that radiation varies as a distance of the ground and source of the radiation was not (only) coming from the earth in 1909-1910 [11] [12].

The "penetration radiation" was named as 'cosmic rays' by an American scientist Robert Millikan in 1926. However, Millikan falsely thought that CRs were mainly γ-rays. [13] This was disproved by Bennett et al. afterwards [14]. It was found out in 1934, Crs are not only γ-rays, but mostly charged particles [15]. In 1937, CR-produced extensive air shower was detected for the first time by Auger [16]. Enrico Fermi published models of acceleration mechanisms of cosmic rays in 1949 [17]. The knee in CR energy spectrum was discovered in 1956 [18]. First experimental evidences of the source of cosmic rays to be supernova remnants was founded in 2002. [19] [20] [21]

Nowadays, it is known that CR's energy spectrum consist of a wide range of energies and they are entering Earth's atmosphere from multiple sources. The annual exposure of cosmic radiation is approximately 0.33 mSv in Finland [22]. Outside of Earth's atmosphere, as well as at high altitudes, CRs may cause hazards to microelectronic circuits. Thus proper shielding of electronics must be taken into account.

1.2 Cosmic rays

1.2.1 Classification of cosmic rays

CRs can be divided into three subcategories on the basis of three different aspects. First, on a most general level, CRs can be divided into primary and secondary CRs. Primary CRs are those particles that are accelerated at astrophysical sources (e.g. supernova remnants) and secondary CRs are particles that are produced in the interaction of the primary CRs with interstellar gas [23]. Second, on the basis of their origin, a separation can be made between solar, galactic and extragalactic cosmic rays [24]. For example, CRs exceeding 10^{17} eV, in energy at least part of them, are considered as extragalactic origin [25] [26] [27]. Third, and the most elementary level, CRs can be divided by particle type into nuclei, hadrons, electrons, gammas and neutrinos [28]. The nuclei can be further classified into subgroups, presented in Table 1.

Table 1: Classification of primary nuclei [29]

Particle, element	Group	Atomic charge	Element
Protons	-	1	H
Helium nuclei	-	2	He
Light nuclei	L	$3 \leq Z \leq 5$	Li, Be, B
Medium nuclei	M	$6 \leq Z \leq 9$	C, N, O, F
Heavy nuclei	H	$10 \leq Z \leq 19$	Ne - K
Very heavy nuclei	VH	$20 \leq Z$ 30	Ga - Zn
Ultra-heavy nuclei	VHH	$Z > 30$	Ga - U
Super-heavy nuclei	SH	$Z > 92$	-
Other occasional used sub groups			
Light group	L	$1 \leq Z \leq 5$	H - B
Light heavy (Silicone) group	LH	$10 \leq Z \leq 14$	Ne - Si
Iron group	-	$15 \leq Z \leq 26$	P - Fe

1.2.2 Energy spectrum of cosmic rays

CR energy spectrum consists of a wide range of energies from 10^{10} eV up to 10^{20} eV. Experimental energy spectrum of CR is shown in Figure 1. The spectrum can be expressed using a simple power law $\propto \mathrm{E}^{-\gamma}$, where γ is the spectral index. A change of the spectral index around 3 PeV is called the *knee* in CR spectrum. In the knee region, the spectral index increases from $\gamma \approx 2{,}7$ to $\gamma \approx 3{,}1$. *The second knee* is located approximately at 400 PeV, where the spectral index steepens to $\gamma \approx 3.3$. Another change of spectral index takes place around EeV (10^{18} eV), and it is called *ankle*. Knowledge of the origin of cosmic rays can be obtained by studying the features (the *knee*, the *2nd knee* and the *ankle*) in the cosmic ray energy spectrum. [30] The highest energy CR, also known as *Oh-My-God-Particle*, was measured in Utah on 15th of October in 1991, by University of Utah's Fly's Eye Cosmic Ray detector with an energy of approximately 3.2×10^{20} eV. [31] [32]

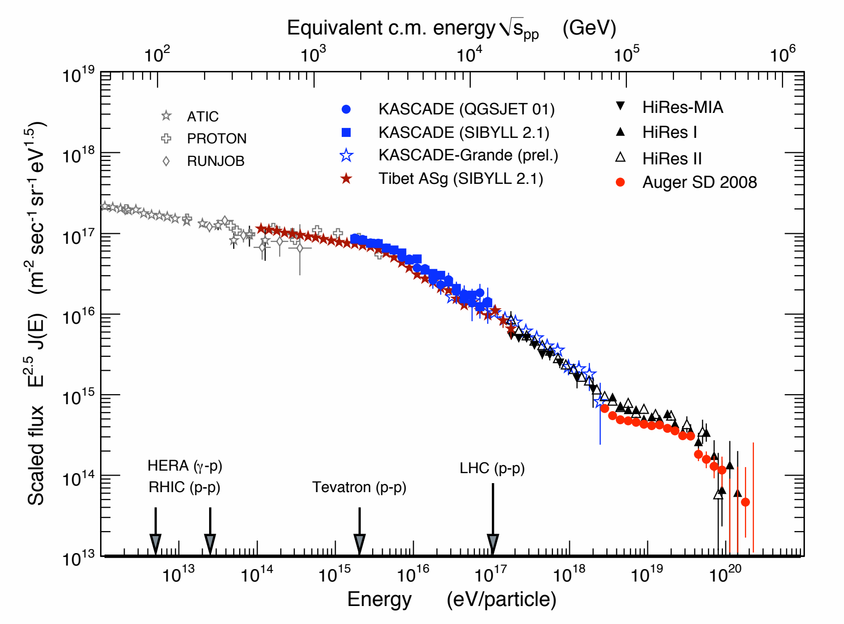

Figure 1: **The cosmic ray all particle flux, multiplied by a factor of $E^{2.5}$, constructed from measured data. The arrows in the bottom indicate the energies used in accelerator experiments.** [33]

Still, a half-century later the origin of the knee is shrouded in secrecy. One of the reasons for this is the turbulent magnetic field in our Galaxy (Milky Way), which makes the observed flux identical in all directions on Earth, and hence any specific point source cannot be observed. The knee feature of CR spectrum was the first time deduced by Kulikov et al. from a shower size spectrum in 1956 [18]. According to S.Thoudam et al. [34], the measured cosmic ray energy spectrum and its composition is best explained in the light of current knowledge by a contribution of Wolf-Rayet supernovae. This of course does not explain fully the shape of the knee, because supernova does not produce all CRs. KASKADE-Grande experiment measured a knee-like break for heavier components at $8{\times}10^{16}$ eV in energy spectrum in 2011 [35]. This suggests that the knee-like behaviour in the cosmic ray energy spectrum would be a superposition of heavy/light CRs. A transition between galactic to extra-galactic CR can explain the shape of the 2nd knee and the ankle in the CR energy spectrum. [36] There are many models for explaining the knee-like behaviour as can be seen in Table 2.

There is a theoretical upper limit (for protons) for the CR energy to be observed at the Earth called Greisen-Zatsepin-Kuzmin-limit (GZK-limit). This limit is $\sim 10^{19}$ eV. GZK-limit is due to the slow-interaction of protons with the photon gas during a long period of time (proton age $\geq 10^8$ y). Interaction of protons with the cosmic background radiation (CMB) resulting Δ-resonance and its subsequent decay can be written as

$$\gamma_{\mathtt{CMB}} + \mathbf{p} \rightarrow \Delta^{+} \rightarrow \mathbf{p} + \pi^{0},$$

Table 2: Models of explaining the knee in the CR energy spectrum. The table modified from [39].

Model	Author(s)
Source Acceleration	
Acceleration in SNR	Berezhko and Ksenofontov
Acceleration in SNR + radio galaxies	Stanev et al.
Acceleration by oblique shocks	Kobayakawa et al.
Acceleration in variety of SNR	Sveshnikova
Single source model	Erlukin and Wolfendale
Reacceleration in the galactic wind	Völk and Zirakashvili
Cannonball model	Plaga
Propagation/Leakage from Galaxy	
Minimum pathlength model	Swordy
Anomalous diffusion model	Lagutin et al.
Hall diffusion model	Ptuskin et al., Kalmykov and Pavlov
Diffusion in turbulent magnetic fields	Ogio and Kakimoto
Diffusion and drift	Roulet et al.
Interactions with background particles	
Diffusion model + photo-disintegration	Tkaczyk
Interaction with neutrinos in galactic halo	Dova et al.
Photo-disintegration (optical and UV photons)n	Candia et al.
New interactions in the atmosphere	
Gravitons, SUSY, technicolor	Kazanas and Niclolaidis

or

$$\gamma_{\texttt{CMB}} + \mathbf{p} \rightarrow \Delta^{+} \rightarrow \mathbf{n} + \pi^{+},$$

where $\gamma_{\texttt{CMB}}$ is cosmic background radiation gamma na $\mathbf{p}$, $\mathbf{n}$, $\Delta^{+/0}$, and $\pi^{0/+}$ is proton, neutron, Δ-resonance, and π-meson, respectively. The reactions reduce the energy of proton and result in cut-off energy around 10^{19} eV. Nonetheless, the experimental data do not agree with the limit, as the highest measured CR energy is $\sim 3.2\times 10^{20}$ eV. The reason of this discrepancy might be that the measured high-energy event was due to interaction of heavier nucleus than proton. [37] [38]

1.2.3 Acceleration mechanisms of cosmic rays

There are many ways for acceleration of CRs. As CRs are mostly charged particles. Consequently, what is needed for accelerating them is an electric field, and for creating an electric field a magnetic field is required. In general form, the relativistic equation of motion for a charged particle is

$$\mathbf{F} = \frac{\mathrm{d}}{\mathrm{dt}}(\gamma \mathrm{m}\mathbf{p}) = \mathrm{q}(\mathbf{E} + \frac{\mathbf{v} \times \mathbf{B}}{\mathrm{c}}), \tag{1}$$

where $\gamma \equiv (1 - v^2/c^2)^{-1/2}$ is the Lorentz factor and m,q and $\mathbf{v}$ are the mass, charge, and velocity of the particle, respectively. Two most general acceleration mechanism, introduced by Enrico Fermi, models are diffusive shock wave acceleration (1st order Fermi acceleration) and turbulent acceleration (2nd order Fermi acceleration). Some other acceleration sources are e.g. spinning magnetized neutron stars (pulsars) and a pulsar or neutron star and a normal star system (binaries). [17] [40]

Diffusive shock wave acceleration

In diffusive shock way acceleration, CR is propagating through a shock wave, generated e.g. by supernova remnants. The shock wave is divided into two parts: upstream and downstream. Upstream is the area before the shock front, and downstream after the shock front, where interstellar gas is streaming away from the shock front. If CR encounters a magnetic field after the shock wave, it can be reflected back (from downstream to upstream) through the shock wave with increased velocity. Consequently, particle can encounter multiple reflections and reach very high gain in kinetic energy. This is called *First order Fermi acceleration.* [41]

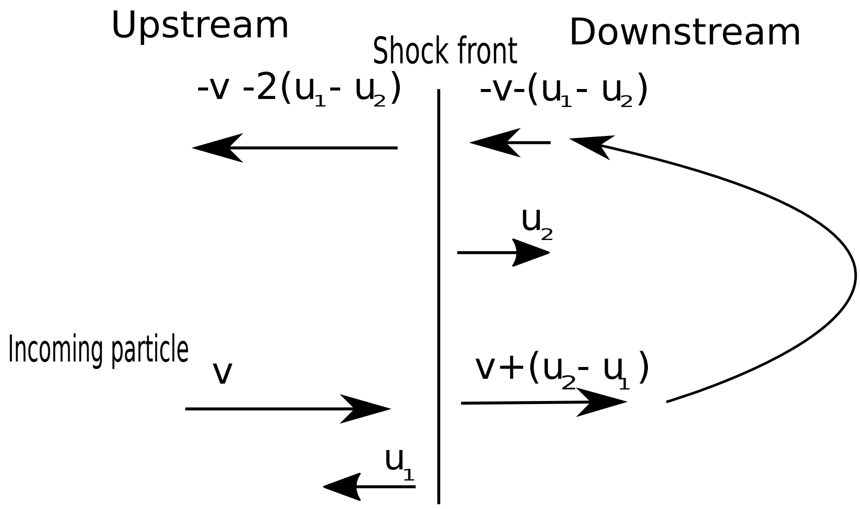

Figure 2: **Shock wave acceleration where incident particle velocity is v, shock front velocity is $\mathbf{u_1}$ and interstellar gas streaming away from the shock with velocity $\mathbf{u_2}$. $\mathbf{u_1}$ - $\mathbf{u_2}$ =Δu is velocity of the gas in the upstream frame of reference(laboratory frame of reference). A particle with initial velocity v enters the shock front (u_1) from upstream to downstream. The particle then gains kinetic energy v + ($\mathbf{u_1}$ - $\mathbf{u_2}$) and is then reflected back into its arrival direction with velocity -v - 2($\mathbf{u_1}$ - $\mathbf{u_2}$)**

Energy gain in shock fronts can be demonstrated with simplistic calculations. A particle with velocity **v** collides elastically with a shock front with velocity of $\mathbf{u_1}$ and is being reflected back. $\mathbf{u_2}$ is velocity of the interstellar gas streaming away from the shock front, and $\mathbf{u_1}$ is antiparallel with $\mathbf{u_2}$ as illustrated in Figure 2. Kinetic energy of a reflected particle is

$$\mathbf{E}_2 = \frac{1}{2}\mathrm{m}(-2\Delta\mathbf{u} - \mathbf{v})^2,$$

where $\Delta\mathbf{u} = \mathbf{u_1}$-$\mathbf{u_2}$ with $\mathbf{u_1}>\mathbf{u_2}$ is the gas front velocity in the laboratory frame. Now the energy difference of the CR particle is

$$\Delta\mathrm{E} = \mathbf{E}_2 - \mathbf{E}_1 = \frac{1}{2}\mathrm{m}(-2\Delta\mathbf{u} - \mathbf{v})^2 - \frac{1}{2}\mathrm{m}\mathbf{v}^2 = \mathrm{m}(2\Delta\mathbf{u}\mathbf{v} + \Delta\mathbf{u}^2).$$

Since $\mathbf{v} \gg \Delta\mathbf{u}$, the linear term dominates ($\frac{\Delta\mathbf{u}^2}{\mathbf{v}^2} \to 0$). The energy gain related to the incoming particle's kinetic energy is

$$\frac{\Delta\mathbf{E}}{\mathbf{E}_1} = \frac{\mathrm{m}(2\Delta\mathbf{uv} + \Delta\mathbf{u}^2)}{\frac{1}{2}\mathrm{m}\mathbf{v}^2} \approx \frac{4\Delta\mathbf{u}}{\mathbf{v}}$$

[40] The result is of the 1st order, hence the name *1st order Fermi acceleration.* More detailed calculations can be found in Bell's paper [42], where it is shown that for differential energy spectrum, following formula can be obtained

$$\mathbf{N(E)dE} = \frac{\mu - 1}{\mathbf{E}_0}(\frac{\mathbf{E}}{\mathbf{E}_0})^{-\mu}\mathbf{dE},$$

where μ is a constant, $\mathbf{N(E)}$ is energy density and $\mathbf{E}_1$ is the system energy where particle is injected. [41]

Turbulent acceleration

In the second model, CRs gain kinetic energy in collisions with moving magnetized interstellar clouds due to magnetic mirror effects. [17] This can be demonstrated with simplistic calculations. Let $\mathbf{v}$ be the velocity of the particle and $\mathbf{u_1}$ to be velocity of a magnetized interstellar cloud. Let us assume that the particle is deflected 90° and the collision is elastic. Then we can have two cases: first where the cloud's velocity is parallel with particle velocity, and secondly, where they are anti-parallel. These two cases are illustrated in Figure 3. [41]

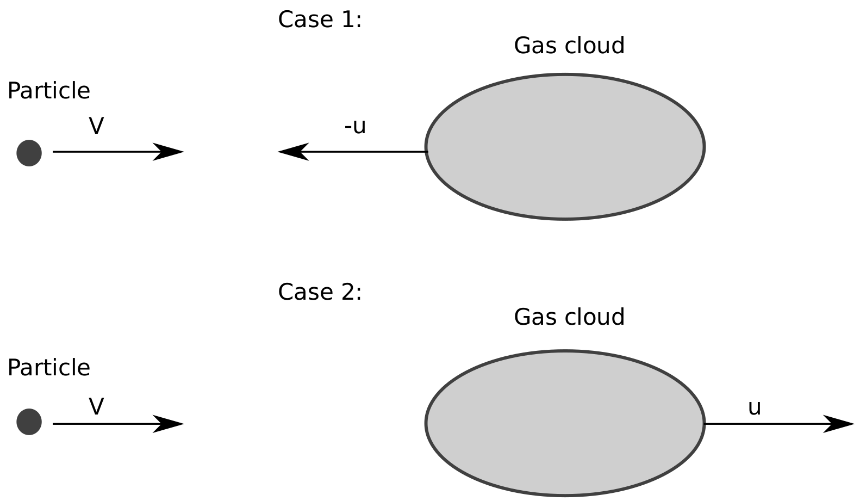

Figure 3: **Turbulent acceleration. A particle with velocity v collides with a magnetized cloud head-on (case 1) and tail-on (case 2), the velocity of the cloud being -u and u respectively, and the particle is reflected back in both cases**

Let us first assume that the velocity of the cloud is parallel to the particle's velocity (head-on-collision). In this case, the kinetic energy difference of incoming and outgoing particle is

$$\Delta\mathbf{E}_{\mathrm{head}} = \mathbf{E}_2 - \mathbf{E}_1 = \frac{1}{2}\mathrm{m}(-\mathbf{v} - 2\mathbf{u})^2 - \frac{1}{2}\mathrm{m}\mathbf{v} = \frac{1}{2}m(4\mathbf{uv} + 4\mathbf{u^2}).$$

When velocities are anti-parallel (tail-on-collision), the kinetic energy difference can be written as

$$\Delta\mathbf{E}_{\mathrm{tail}} = \mathbf{E}_3 - \mathbf{E}_1 = \frac{1}{2}m(-\mathbf{v}+2\mathbf{u})^2 - \frac{1}{2}m\mathbf{v^2} = \frac{1}{2}m(-4\mathbf{uv}+4\mathbf{u^2}).$$

By using average kinetic energy gain, a relative net gain can be written as

$$\frac{\Delta\mathbf{E}_{\mathrm{tail}} + \Delta\mathbf{E}_{\mathrm{head}}}{\Delta\mathbf{E_1}} = \frac{\frac{1}{2}\mathrm{m}(-4\mathbf{uv}+4\mathbf{u^2}) + \frac{1}{2}\mathrm{m}(4\mathbf{uv}+4\mathbf{u^2})}{\frac{1}{2}\mathrm{m}\mathbf{v^2}} = 8\frac{\mathbf{u^2}}{\mathbf{v^2}}.$$

This is called *Second order Fermi acceleration* because of the quadric result. The probability for a particle to collide with head-on is higher than with tail-on, and thus particle accelerates. [17] [40] [41]

1.3 Extensive air showers

An air shower is cascade of ionized particles and electromagnetic radiation produced by CR. It is called extensive air shower (EAS) if it is many kilometres wide. EASs originate from extremely energetic primary CRs (E $> 10^{13}$ eV) entering the atmosphere isotropically from outer space. The EASs can be divided into different categories on the basis of the initiator of the EAS. These categories are: nucleus, hadron, gamma ray, electron and neutrino initiated EAS. A particle that produces an EAS in the atmosphere is called parent particle or primary particle. Particles produced in the interaction of a parent particle with the molecules of the atmosphere are referred to as secondary particles. [28]

In the interstellar medium, CR has a fewer chances to collide with medium's particles. However, when CR enters Earth's atmosphere it's greater chance to collide with particles in the atmosphere. A cosmic ray interacts mainly with O_2, N_2 and Ar. The interaction produces an immense amount of secondary particles which keep interacting with molecules in the atmosphere producing more and more secondary particles as they propagate deeper in the atmosphere. The first interaction of the primary with the molecules of atmosphere depends on the mass of the primary particle. The more massive (e.g. proton vs. Fe-nucleus) is the primary, the more rapidly it interacts with the atmosphere, because it has larger inelastic cross-section. This is illustrated by using the **CORSIKA**-simulation program with a proton and an iron-nucleus in Figure 4. Simulations were done by using the **CORSIKA**-program with 5 000 events and primary's energy of 10^{15} - 10^{16} eV for both proton and iron. [43]

As a primary particle interacts with the atmosphere's molecules, it generates a hadron cascade. As the hadron cascade propagates in the atmosphere, it generates, as a side product, an electronic cascade, as well as muons and pions. These all together form an extensive air shower. When CRs in the atmosphere are discussed, a parameter called *atmospheric depth* (X) is used. The *atmospheric depth* is measured in g/cm^2, and it is integral in altitude of the atmospheric density observation level h, i.e.

$$\mathbf{X} \equiv \int_h^\infty \rho(\tilde{h})d\tilde{h}.$$

The extensive air shower expands until it reaches its maximum size at X_{max}. After the maximum, it begins to diminish. Extensive air showers of the most energetic primaries

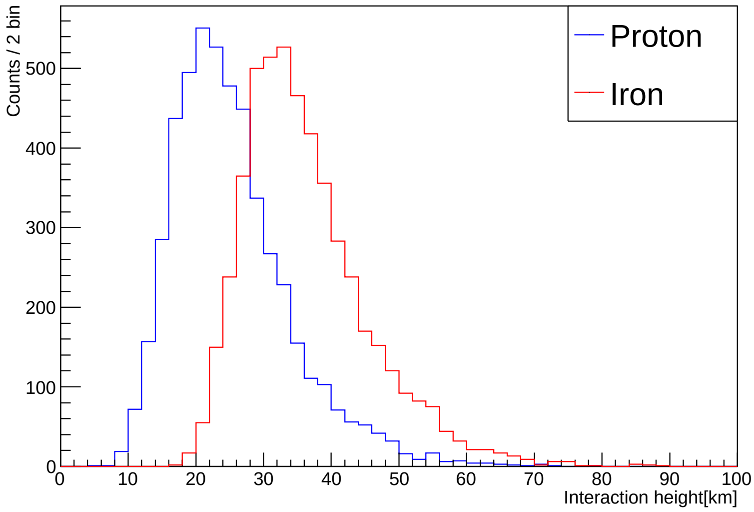

Figure 4: **Simulated first interaction height of CR particles in atmosphere. Blue line shows the result for proton and red line for iron, respectively. The energy of the primary CR particle were 10^{15}-10^{16} eV (knee-region).**

reach their maximum size at the sea level. However, there are fluctuations in the shower size with the same primary energy because of the density of air is quite thin at higher altitudes. If considering a size spectra of muons (N_μ), following estimation for relation for primary's energy E_0 to muon shower size is [44]

$$E_0(\mathrm{eV}) = 1.7 \times 10^{17}[\frac{N_\mu}{10^6}]^{1.21}$$

for $10^{14.5}$ eV $< E_0 < 10^{18}$ eV at 920 - 1020$\frac{\mathrm{cm}}{\mathrm{g}^2}$. [45]

1.4 Hadronic cascade

Hadron initiated EAS can be divided into three parts: hadron core and electromagnetic and muon sub-cascades, illustrated in Figure 5. Hadron cascade undergoes numerous inelastic collision of the molecules in the atmosphere, and in every successful collision an energy dependent number of new particles is generated, until the energy of the particles falls below the one-pion threshold. Usually, the first decay products are pions ($\pi^0, \pi^\pm$) and kaons ($\kappa^\pm$). Neutral pions have a short life time ($\tau_0 = 8.52 \times 10^{-17}$ s) and decay quickly into two gammas ($\pi^0 \rightarrow 2\gamma$ with a branching ratio of 98%) which triggers electromagnetic sub-cascade. Charged pions have a longer lifetime ($\tau_0 = 2.6 \times 10^{-8}$ s), thus they propagate further away from the shower axis and initiate a muon sub-cascade via decay channels ($\pi^\pm \rightarrow \mu^\pm + \nu_\mu(\overline{\nu}_\mu)$) with the branching ratio of 99.9877 %). Consequently, electromagnetic cascade is closer to the hadron core of air shower than muon sub-cascade. Hadronic core is thus responsible for energy transfer within an air shower. The decay of kaons also contributes to the sub-casacdes in the air shower by decaying mainly into muons ($\kappa^\pm \rightarrow \mu^\pm + \nu_\mu(\overline{\nu}_\mu)$) with the branching ratio of 63.56 %, into charged pions ($\kappa^\pm \rightarrow \pi^\pm + \pi^0$) with branching ratio of 20.67 % or into neutral pions ($\kappa^\pm \rightarrow \pi^0 + \mu^\pm + \nu_\mu(\overline{\nu}_\mu)$ with the branching ratio of 5.07 %. [46] [47]

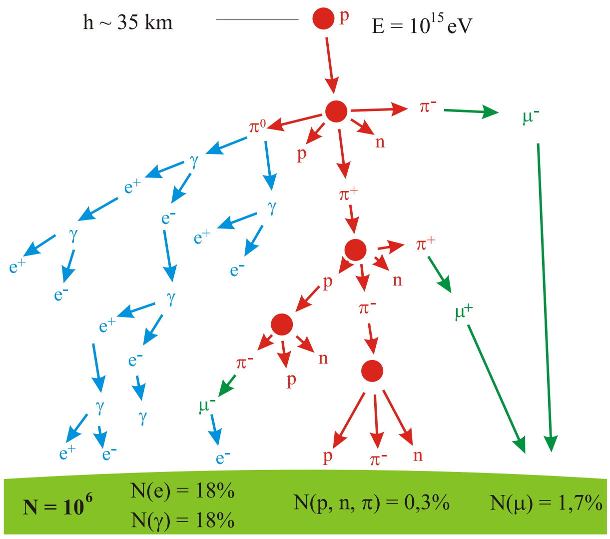

Figure 5: **An illustration of the development of a proton initiated air shower in the atmosphere. The hadronic core of the air shower is shown in red, electromagnetic (EM) sub-cascade in blue, and muonic sub-cascade in green, respectively. Here a proton as the primary particle initiates an air shower. The percentages shows the approximate portion of electrons, gammas, muons and other particles at the sea level.[GNU FDL]**

1.4.1 Electromagnetic part of EAS

Electromagnetic sub-cascade, as well as muons, are daughter products of a hadronic cascade. As mentioned above, neutral pions decay into gammas. Each gamma produces its own photo-electric cascade through pair production ($\gamma \rightarrow e^+ + e^-$), which is strengthened by Bremsstrahlung of hadron cascade. Pair production continues until it is below its threshold energy (1.02 MeV). Thereafter, photoelectric effect and Compton scattering makes a low energy contribution to the shower. Moreover, the decay of muons ($\mu^\pm \rightarrow e^\pm + \overline{\nu}_e(\nu_e) + \nu_\mu(\overline{\nu}_\mu)$ with the branching ratio of $\approx 100\%$) contributes to EM-cascade. Ultimately, the EM-cascade magnitude depends on the energy of initial pions and thus the energy of the primary CR particle. [46] [47]

1.4.2 Muons of EAS

Muon sub-cascade of the EAS are initiated mainly by charged pions and kaons, but also charmed particles, such as $D^\pm$, D^0, J/ψ and others. In Table 3 the main production channels for muons are listed. Muons have a relatively long life time ($\tau_0 = 2.2\ \mu$s at rest) and small energy loss, when propagating in medium. Consequently, the muon decay rate is low. Thus, a large fraction of muons, generated in the air shower, reach the sea level and even propagate some distance in the ground, depending on the energy of the primary. This is capitalized in underground cosmic ray experiments, such as the EMMA experiment [1], where the rock overburden works as a filter for low energy muons and only high energy muons are able to penetrate the rock and reach the experiment. [1] [46] [47]

Table 3: Summary of the major muon production channels in the EAS. [48]

Particle symbol	Particle decay modes	Branching fraction [%]	Mean life [s]
$\pi^{\pm}$	$\mu^{\pm} + \nu_{\mu}(\overline{\nu}_{\mu})$	99.99	$2.6 \cdot 10^{-8}$
$K^{\pm}$	$\mu^{\pm} + \nu_{\mu}(\overline{\nu}_{\mu})$	63.43	$1.2 \cdot 10^{-8}$
	$\pi^{0}\mu^{\pm} + \nu_{\mu}(\overline{\nu}_{\mu})$	3.27	
$D^{\pm}$	$K^{0}(\overline{K^{0}}) + \mu^{\pm} + \nu_{\mu}(\overline{\nu}_{\mu})$	7.0	$1.0 \cdot 10^{-12}$
D^{0}	$\mu^{\pm}$ + Hadrons	6.5	$4.1 \cdot 10^{-13}$
	$K^{-} + \mu^{+} + \nu_{\mu}$	3.19	
$\tau^{\pm}$	$\mu^{\pm} + \nu_{\mu}(\overline{\nu}_{\mu}) + \nu_{\tau}(\overline{\nu}_{\tau})$	17.36	$2.9 \cdot 10^{-13}$
J/ψ	$\mu^{+}\mu^{-}$	5.88	$\sim 10^{-20}$

1.4.3 Propagation of muons throughout medium

Generally, muons lose their energy by ionization, bremsstrahlung, direct electron pair production or photonuclear interactions. Muon can lose energy also due to direct muon pair production, but the mechanism occurs rarely. Ergo, the energy loss for muon in medium can be formulated as

$$-\frac{\mathrm{dE}}{\mathrm{dx}} = \mathtt{a_{ion}}(\mathtt{E}) + [\mathtt{b_{br}}(\mathtt{E}) + \mathtt{b_{pp}}(\mathtt{E}) + \mathtt{b_{ni}}(\mathtt{E})]\mathtt{E}, \tag{2}$$

where the terms $\mathtt{a_{ion}}$, $\mathtt{b_{br}}$, $\mathtt{b_{pp}}$ and $\mathtt{b_{ni}}$ represent energy losses due to ionization, bremsstrahlung, pair production and photonuclear interactions, respectively. The probability of different mechanisms of muon energy losses in standard rock is demonstrated in Figure 6. Values for the coefficients ($\mathtt{a_{ion}}$, $\mathtt{b_{br}}$, $\mathtt{b_{pp}}$ and $\mathtt{b_{ni}}$) for muon's energy loss in iron are listed in Table 4. [49]

Table 4: Muon's energy loss ($-\frac{\mathrm{dE}}{\mathrm{dx}}$) in iron (GeV g^{-1} cm^{2}). [50]

Muon energy [GeV]	$\mathtt{a_{ion}}$	$\mathtt{b_{br}}$	$\mathtt{b_{pp}}$	$\mathtt{b_{ni}}$	Total
1	$1.56 \cdot 10^{-3}$	$5.837 \cdot 10^{-7}$	$5.837 \cdot 10^{-7}$	$4.4145 \cdot 10^{-7}$	$1.561 \cdot 10^{-3}$
10	$1.925 \cdot 10^{-5}$	$1.397 \cdot 10^{-5}$	$1.492 \cdot 10^{-5}$	$4.229 \cdot 10^{-6}$	$1.958 \cdot 10^{-3}$
100	$2.162 \cdot 10^{-3}$	$2.236 \cdot 10^{-4}$	$3.174 \cdot 10^{-4}$	$3.851 \cdot 10^{-5}$	$2.7 \cdot 10^{-3}$
1000	$2.336 \cdot 10^{-3}$	$2.866 \cdot 10^{-3}$	$4.192 \cdot 10^{-3}$	$3.878 \cdot 10^{-4}$	$9.782 \cdot 10^{-3}$
10000	$2.502 \cdot 10^{-3}$	$3.172 \cdot 10^{-2}$	$4.523 \cdot 10^{-2}$	$4.326 \cdot 10^{-3}$	$8.377 \cdot 10^{-2}$

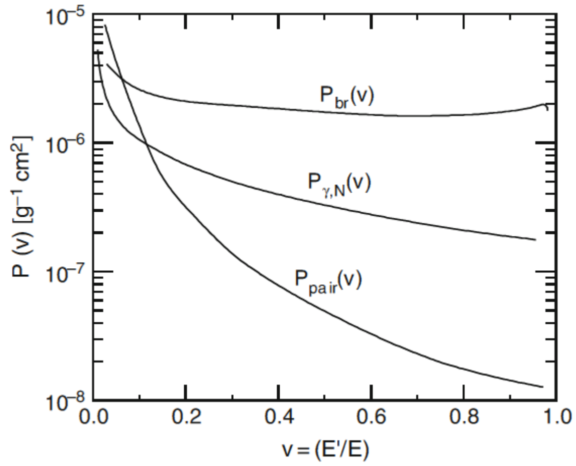

Figure 6: **The probability of a 2 TeV to lose a fraction (v = E'_μ/E_μ) per gram of its energy via bremstrahlung (br), photonuclear reaction (γ,N), and pair production (pair) in standard rock.** [51]

2 Cosmic ray experiments

The variation of CR experiments is large because the CR energy spectrum is wide. CRs can be detected either directly or indirectly - determined by energy of the CR. Direct measurement means detecting primary CR using a satellite or an air balloon. Indirect measurement means measuring extensive air showers produced by primary CR.

Low energy CRs, energy being below the knee, are detected by direct measurements as shown in Figure 7. This is mainly because of the rapid decrease in the flux of cosmic ray radiation as a function of energy, and also the limitations of size, weight and power of on-board equipment. For example, detecting ultra-high energy regime CRs directly by using satellite or air balloons is not sensible, because of extremely low rates. Energies exceeding the knee are measured indirectly as shown in Figure 7. Indirect measurements mean measuring the air shower produced in the interaction of the CR with earth's atmosphere.

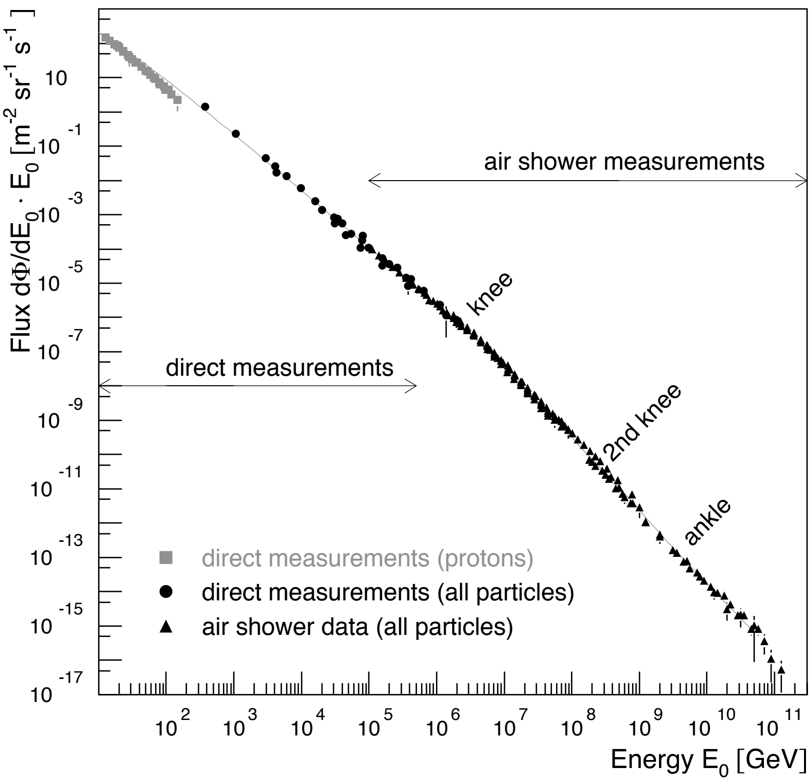

Figure 7: **The spectrum of CR flux. The arrows indicate the energy gaps where air shower measurements or direct measurements are valid. Regions where cosmic ray flux changes are also marked (the knee, the 2nd knee and the ankle).**[33]

2.1 Detection of cosmic rays

CRs are mainly charged particles and they can be detected by using normal particle detectors. Detection method is selected on the basis what is wanted to be measured and what information is needed to extract. Typical particle detectors are: magnetic spectrometers, calorimeters, Cherenkov detectors, scintillators, and gas filled detectors.

The basic principle of a magnetic spectrometer is based on Lorentzian force. When a charged particle enters constant magnetic field its path curves due to Lorentzian force. Magnetic spectrometer is used to measure energy spectrum of particles, and to identify particles. For example, the alpha magnetic spectrometer which is located in the international space station purpose is understanding of dark matter, anti-matter, the origin of CR and the exploration of new physics phenomena. It measures Crs in the energy range from 0.5 to ∼2000 GeV. [54]

Calorimeter was originally created for the study CRs. It is a block of instrumented material and when a charged particle enters calorimeter, it loses its energy via interactions with medium by electromagnetic or strong interactions. The entering particle creates a particle shower in the calorimeter, and a fraction of deposited energy of the incoming particle can transform into a signal which can be detected. The signal depends on the instrumented material and it can be scintillation light, Cherenkov ligh, or ionization charge. [55]

Calorimeters can roughly divided into two categories: electromagnetic and hadronic calorimeters. Calorimeter is sensitive for all types of particles - charged and neutral, unlike magnetic spectrometer. It is used for particle energy measurement, to determine the shower position and direction, to identify different particles, and to measure the arrival time of the particle. Depending on the instrumented material, calorimeter allows accept high event rate, and thus it is commonly used for trigger purpose. [55]

Detectors, which use Cherenkov technique, are based on Cherenkov radiation. It is electromagnetic radiation and it is emitted by a charged particle when it passes medium with a greater speed than phase velocity of light in that medium. It was discovered experimentally for the first time by the Union of Socialist Republics physicist Pavel Cherenkov in 1934 [56]. The primary particle interacts with Earth's atmosphere and produces secondary particles with velocity around speed of light, thus they emit Cherenkov light which can be detected by telescopes. This is illustrated in Figure 8. In Pierre Auger experiment, water Cherenkov detectors are used to measure CRs with energy beyond 10^{18} eV. [57] [58] Scintillators and gas filled detectors are main detectors of the EMMA experiment [1], and they will be discussed in more detail in section 3.

2.2 Direct experiments

Direct CR experiments measure primary CRs. They are usually at high altitude in the atmosphere or in space. An example of experiment the in atmosphere is BESS-polar experiment which is a balloon borne experiment for studying low-energy antiprotons and searching for antinucle in the galactic CRs at altitude of 37 km. It was launched in 2004. The detector consists of spectrometer and scintillation systems.[53]

An example of CR experiment in space is PAMELA experiment which is a satellite borne experiment designed to study CRs of galactic, solar, and trapped nature in a wide energy range (protons 80 MeV-700 GeV, electrons 50 MeV- 400 GeV). Main aim is to study antimatter component of CRs. The experiment, housed on board the Russion Resurs-DK1 satellite and it was launched in June 15th 2006 in a 350×600 km orbit wit an inclination

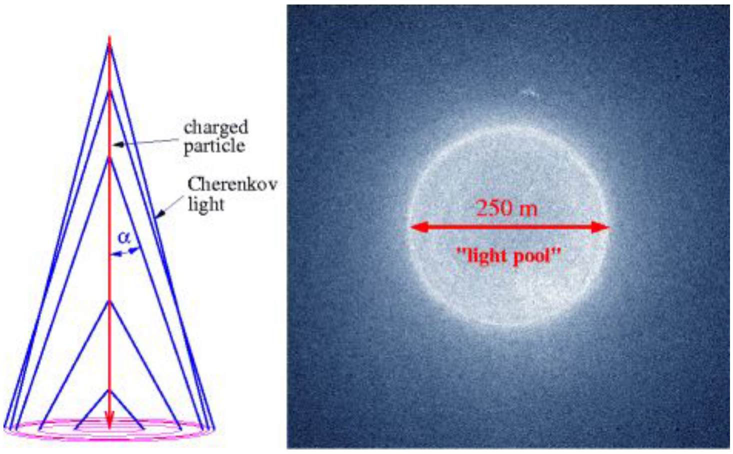

Figure 8: **Left: a single charged particle (red line) moving downward and emitting Cherenkov light (blue lines). Right: A Cherenkov "light pool" which is observed at 1800 m above sea level. It is produced by a γ-ray shower with a primary energy of 1 TeV.**[59]

of 70 degrees. The detector consist of magnetic spectrometer, scintillator system, silicon tungsten calorimeter, shower tail scintillator, neutron detector and anticoincidence system. [52] As a result of PAMELA experiment, it provided more insight to explaining trends in CR positron fractions [60].

2.3 Indirect experiments

In indirect CR experiments, CRs are studied by the air shower which they produce when entering Earth's atmosphere. Indirect CR experiments are located typically on the Earth's surface or underground, and they are used for studying high energy CRs. An example of high energy CR experiment is KASKADE-Grande (KArlsruhe Shower Core and Array DEtector-Grande) which is a cosmic ray experiment located in Forschungszentrum Karlsruhe, Germany, corresponding to an average atmospheric depth of 1022 cm/g^2. The experiment site consists of an area of 370 m^2 of plastic scintillators (Grande array), 80 m^2 of plastic scintillators (Piccolo array), 490 m^2 liquid scintillators (KASCADE array), 622 m^2 of shielded pl. scintillators (KASCADE array), 4 $\times$ 128 m^2 streamer tubes (Muon tracking detector), 2$\times$129 m^2 multi wire proportional chambers at CD (central detector), 250 m^2 limited streamer tubes at CD, and 9 $\times$ 304 calorimeter at CD. KASKADE-Grande studies cosmic rays with an energy range of 10^{14} - 10^{18} eV. [61]

An example of ultra-high-energy CR experiment is Pierre Auger observation which is located in the Province of Mendoza, Argentina, and it is designed to study cosmic rays at highest energy (energies beyond 10^{18} eV). The construction of the experiment started in 2004, and it was fully complete in 2008. It has been collecting data since 2004. The observatory consists of two parts: a large surface detector, and fluorescence detector. The surface detector consists of 1660 water Cherenkov detectors of overall covering area of 3000 km^2. The detectors are located in mean altitude of $\sim$1400 km, corresponding to an atmospheric overburden of $\sim$ 875 g cm^{-2}. As a result of the experiment, there was found no point sources for EeV neutrons [62] or photons [63]. [58]

3 The EMMA experiment

EMMA (Experiment with MultiMuon Array)[1] is located at the depth of 75 m, corresponding 240 m.w.e in the Pyhäsalmi mine, Finland. The purpose of the EMMA experiment is to study the composition of cosmic rays in the knee region (10^{15} - 10^{16} eV). The rock overburden filters out all particles with energy less than the threshold energy, except the high-energy muons and neutrinos. The rock overburden is visible in Figure 9, where the measured muon flux at different in the different depths in the Pyhäsalmi mine is shown. As mentioned in section 1.3, high-energy muons are usually produced in the proximity of the high-energy primary at high altitudes. Therefore, they provide good information of the properties of the primary particle.

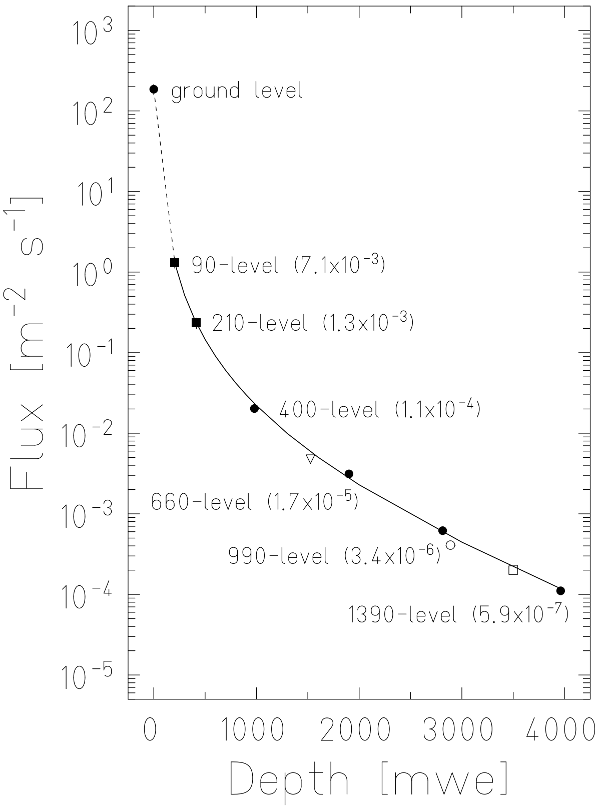

Figure 9: **Measured muon flux in the Pyhäsalmi mine as a function of depth in m.w.e.** [64]

The EMMA experiment consist of 84 Muon Barrel Chambers (MUBs) from LEP-DELPHI experiment at CERN [65], 72 SC16 scintillators and 60 Limited streamer tubes (LSTs) from KASCADE experiment [61]. Detectors are placed in the detector stations as in two- or three-layers. Stations in two different areas - level 85 and level 45, at different depths 75 m and 45 m from the surface. Detectors are placed inside the cottages to protect them against hazardous environment in the cavern. As the efficiency of MUBs depend on the temperature, the detector stations have insulation and heating, to guarantee their optimal performance.

There are nine detector stations in 75m-area and three in 45m-area as shown in Figure 10. The areas are connected with a drill hole which is needed for cabling. The 75m-area is also connected to the surface via a drill hole. The drill hole provides the gas, electricity for the detectors, and optical fibre for monitoring.

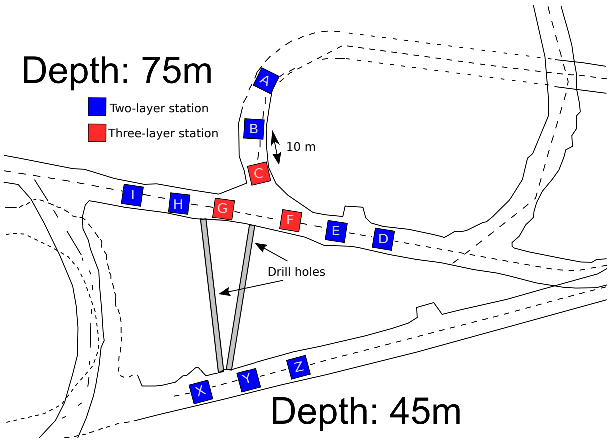

Figure 10: **A schematic picture of the area of the EMMA experiment in the Pyhäsalmi mine. Stations labelled from A to I are on the level 85 and squares X,Y and Z on the level 45. Red colour indicates three-layer and blue two-layer stations. In addition, drill holes between the levels are indicated**

3.1 Detectors of the EMMA experiment

3.1.1 SC16 scintillators

The SC16 scintillators (SC16s) were manufactured specifically for the EMMA experiment by the Institute for Nuclear Research of the Russian Academy of sciences. Each of SC16 consists of 16 pixels called SC1 scintillator (SC1), which are arranged into 4 × 4 matrix. There are 72 SC16s used in the EMMA experiment covering the area of 18 m^2. The SC1s/SC16s technical information are following:

- The dimensions of one SC1 pixel: 122 × 122 × 30 mm^3.
- The material used in SC1: polystyrene coated with reflector.
- The weight of SC16: 20 kg.
- The dimensions of SC16: 50 × 50 × 25 cm^3

There is a light collecting (Y11 Kurayra wave length shifting) fibre embedded into a SC1 pixel. The fibre collects light produced in the SC1 pixel, and the light is guided to avalanche photo diode (APD). The detection efficiency of SC16 is 98 ± 1%, and the time resolution is approximately 1.7 ns. [1] [66] [67]

The SC16s array set-up serves three purposes: muon number estimation, measurement of an initial guess of air showers arrival angle, and start time generation for drift chambers. The angular accuracy of SC16s is poor, approximately 10-15 degrees, but if the MUBs are saturated, they can be used to measure the arrival angle. The SC1 and SC16 are illustrated in Figure 11. [1] [66] [67]

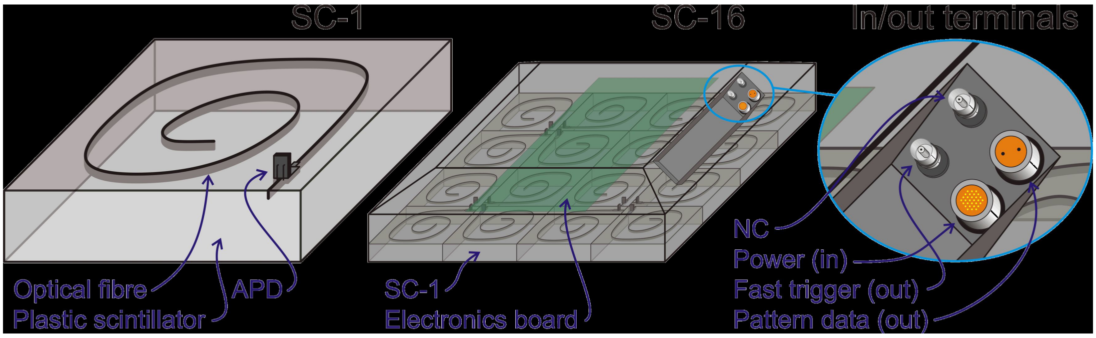

Figure 11: **An illustration of SC1 and SC16 scintillator. [67]**

3.1.2 Limited streamer tubes

The limited streamer tubes (LSTs) were obtained from the KASCADE experiment on the spring of 2012. In total of 66, the LSTs will be placed outer stations as well as an additional detector array layers in the central stations. The dimensions of the LST unit are 100 $\times$ 290 cm^2 and it consists of six LST chambers. Each chamber has dimensions of 16.7 $\times$ 280 $\times$ 1.34 cm^3 and consists of 16 tubes with dimensions of 9 $\times$ 9 mm^2 and filled with CO_2 gas. The weight of one LST is $\approx$20 kg. An anode wire runs through the central axis of the tube, and it is connected to ground. -4.8 kV high voltage is applied to the cathode profile. Dimensions of LST are illustrated in Figure 12. [68] [69]

3.1.3 Muon barrel chambers

The main detectors used in the EMMA experiment are drift chambers (muon barrel chambers, MUB) from former LEP-DELPHI experiment at CERN [65]. A MUB is divided into seven chambers: three on top and four below. The upper one are named Y1, Y2 and Y3, where Y2 is the middle chamber. The lower ones are named similarly: X1, X2, X3 and X4. This is illustrated in Figure 13a. All the chambers have been shielded by a layer of aluminium. The dimensions of a MUB are the following:

- Gas volume per drift chamber: 365 cm (length) $\times$ 20 cm (width) $\times$ 1.5 cm (height) cm^3.
- The thickness of aluminium shielding: 2 mm.
- Weight of a MUB: $\approx$ 130 kg.
- The gas mixture: 92% Ar and 8% CO_2. The gas is delivered from the ground level gas station via 100 meter long gas pipe to EMMA-level.

There is a tungsten anode wire ($\oslash$47 μm) located in the middle of each chamber. The wire is supported by three plastic holders placed 1.2 metres apart to keep the wire on the chamber's center axis. The anode wire is connected to 6 kV high voltage.[1] [66] [71]

On the bottom of each chamber, a delay line is located as illustrated in Figure 13b. The delay line consists of winded copper strips which are connected to 4 kV high voltage (grading voltage). There are also 26 grading copper strips glued on the wall of a chamber. These strips are evenly distributed on the chamber walls and connected to grading voltage. Each of these strips have a specified voltage, which is decreasing almost

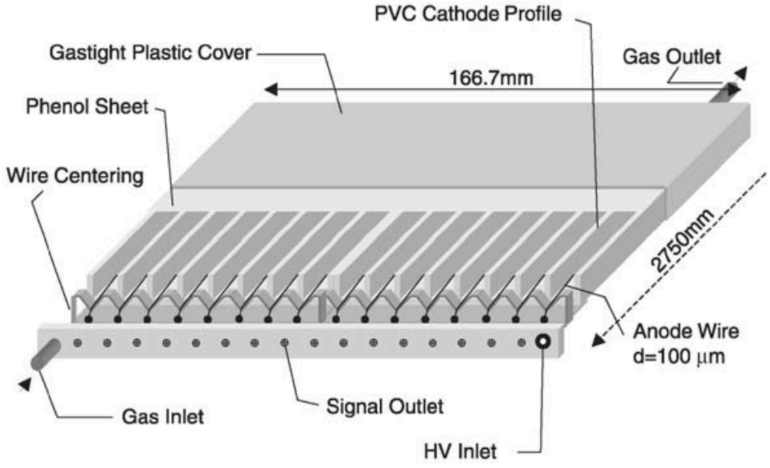

(a)

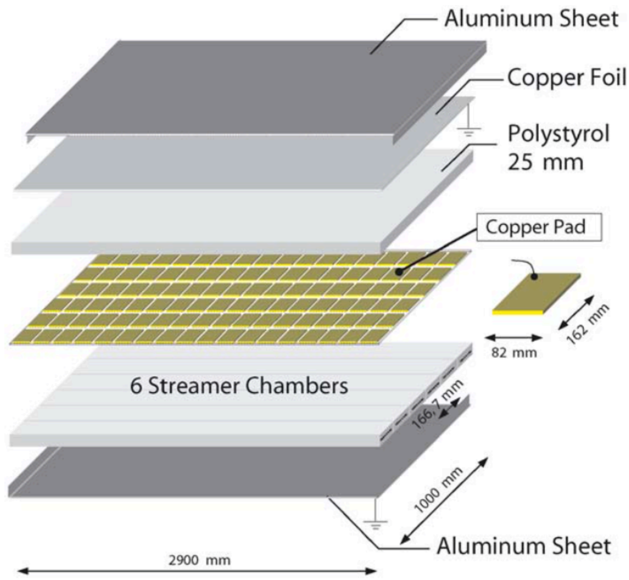

(b)

Figure 12: **A schematic view of LST and its dimensions. [70]**

to ground at the end of the chamber, producing a uniform electric field with a strength of 400 V/cm. Consequently, it provides constant drift velocity of approximately 4 cm/μs (=v_{drift}) towards the anode wire. The efficiency of drift chambers is typically better than 90 % and have a position resolution approximately < 1 cm^2. [1] [66] [71]

When a high energy particle hits the MUB, it collides with the gas molecules in the MUB and produces electrons. Thereafter, electrons drift towards the anode line, because of the electric field inside a chamber, and they will produce an anode signal.Each chamber produces three signals: one from anode the wire (A) and two from the delay line - near (N) and far (F). Near and far-signals are collected at the opposite end of the chamber, and the near signal is collected at the same end where the anode-signal is received." *The signals* *are fed into Front Electronics Boxes (FEBs), which host amplificator and discriminator cards providing an ECL-level output to CAEN V767B TDC (time-to-digital-converter) via twisted pair cable. V767B has 128 channels, a least significant bit resolution of 0.8 ns and a double hit resolution of 10 ns in single channel* [71]." MUBs are used to obtain information of the shower arrival direction by reconstructing the track of the high energy particle. [1] [66]

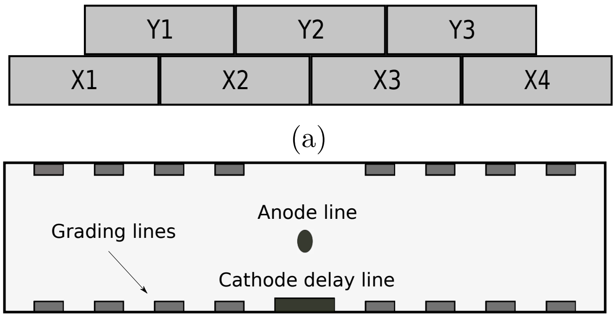

(b)

Figure 13: **An illustration of MUB's chambers' names (a) and the inside of a chamber (b).**

However, some energetic UV-photons may be generated in the drift process, and they will be emitted at random directions. UV-photons may produce more electrons when they hit on a cathode surface e.g cathode delay line. Such electrons will also drift towards the anode line and trigger a "fake" anode signal. This kind of event is called an afterpulse or a false hit, and the signal produced by a high energy particle (e.g. muon) is called a real hit. Afterpulses come always after the real hit, so they can be sorted out from the data fairly easily. [72]

As mentioned in the section above, the chambers' gas mixture is Ar:CO_2 (92:8% respectively), where CO_2 serves as a quenching gas. At CERN in the operation of the drift chambers, also CH_4 (methane) was used as a quenching gas. However, CH_4 was not suitable for mine environment due to safety measures. Thus, a new ratio for Ar:CO_2 of 92:8 was looked for. CO_2 has two-rotational and four-vibrational degrees of freedom, it can absorb different photon wavelengths effectively. Therefore, CO_2 role is to absorb UV-photons to reduce afterpulses in the chamber. In addition, electronics produces afterpulses. Such afterpulses are generated near the end of the chamber. These afterpulses can be identified by their extremely short time value. As UV-photon-generated afterpulses, also electronics-generated afterpulses come always after the real signal, so filtering the data can be done easily. [72]

4 Calibration of MUBs

MUBs are used for the tracking high energy muons going through the tracking stations of the EMMA experiment. To reliable obtain information where the particle crosses the detector, the position calibration have to be conduct. The calibration of MUBs is introduced in this section. In section 4.1 the calibration set-up and calibration of the reference MUBs is described. In section 4.2 format, problems, and analysing of data files are discussed. In section 4.3 the fit in the delay direction, and in section 4.4 the construction of delay positions, and creating calibration tables are discussed. Ultimately, fit in the anode direction is discussed in section 4.5. From here on, a word "plank" is used when referring to MUB.

4.1 Calibration set-up and the calibration of reference MUBs

Four of the MUBs were position-calibrated manually by ^{22}Na source. These four MUBs were called reference planks. The calibration stack, in Figure 14, consisted of ten MUBs at maximum, of which four of the MUBs were reference MUBs and the rest were calibrated by using CR muons. The height of the calibration stack was (1681$\pm$1) mm. The uncertainty comes from the usage of the measurement tape. [66]

4.2 Reading of *.emma-files

Data are stored in *.emma-files in a binary format, which has byte order in little endian. There were $\sim$ 1000 hours of recorded data for each stack. For example, stack 15 had 164 Gb of data. From now on, I will refer to raw data as binary data, which is written into *.emma-files by the electronics of the calibration stack. The format of binary files can be found in Appendix A. A program called *Binaryreader*(BR) was created to read *.emma-files and slightly sort out raw data. Basically, its main job is to sort out afterpulses, to link TDC's channels to right signals and save data into *.root-files. BR was created by using c++-programming language and data analysis framework **ROOT** [73].

4.2.1 Structure of *.emma-files

The binary structure of *.emma-files is the following: First comes Header (0x00-0x2f) and TDC-configuration (0x30-0x3f). The Header and the TDC-configure will come only once per file. Every file has its own id-number, and the number of TDC-units. These can be found in the Header. TDC's GEO address, which is unique for each TDC-unit, can be found in the TDC-configuration.

Data are distributed in events. Each event consists of a single Event header (32 bits) and data words (32 bits each). This is illustrated in Figure 15. If event is null, then there will be only an Event header. There is no limit for data words, thus there can be random amount of data words in each event. In the end of each raw data file, there is a file tailer which has the end signal in the "Start of tailer" in the position 0x00-0x03. The end signal is 0x00600000. When BR detects the end signal, it ends the data processing and proceeds to map data to right TDC channels, sorting data, and saving data into *.root-files.

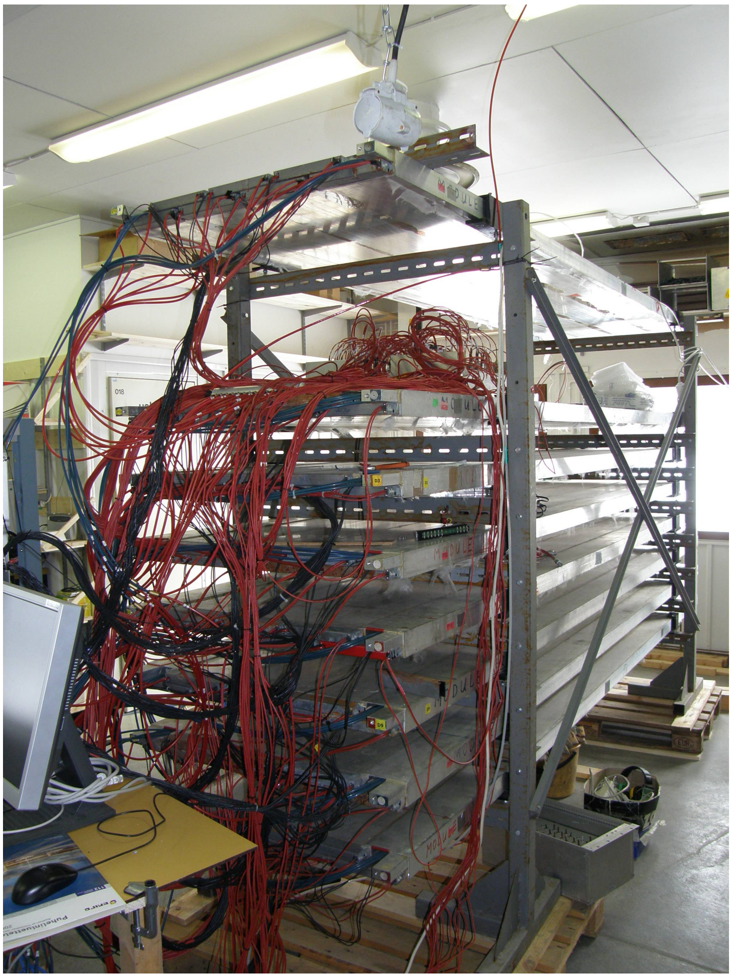

Figure 14: **The calibration stack in the surface laboratory "Leipomo". Photo by Tomi Räihä.**

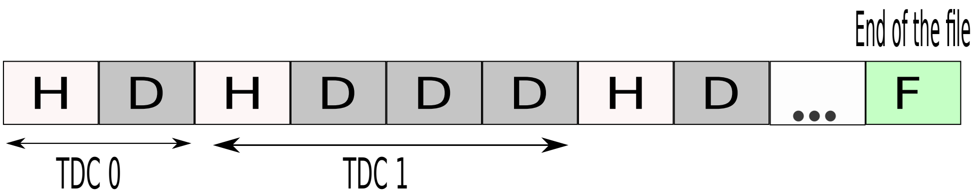

Figure 15: **Structure of raw data in *emma-files. There comes always first TDC 0's data header and random amount of data words and then TDC 1's header and data words. The event ends when the file tailer with an ending signal comes. The symbol "H" means event header, "D" data word, and "F" file tailer.**

4.2.2 Linking raw data signals to TDCs' channels

To be able to link raw data signal to the right MUB's chamber, a map called "plankmap" is needed. It provides information of the TDC's channel to which particular chamber's signal it is connected. A plankmap is valid only for a specific time period, and the reason why there are several plankmaps is due to for example in electronics, replacing a broken TDC's channel and so on. In the logbook (fig. 16, Appendix B), one can always see which plankmap is valid for specific *.emma-files. For example, the first plankmap is valid for the first 241 data files. Likewise, poor chamber efficiencies or broken chamber can be read from the logbook and taken into account in data processing. The plankmaps can be found in Appendix C. Primarily, the logbook is used for checking whether there are no data in a chamber, is the reason in the code done by the author or whether that chamber is missing. The logbook for stack 15 in its entirety can be found in Appendix B.

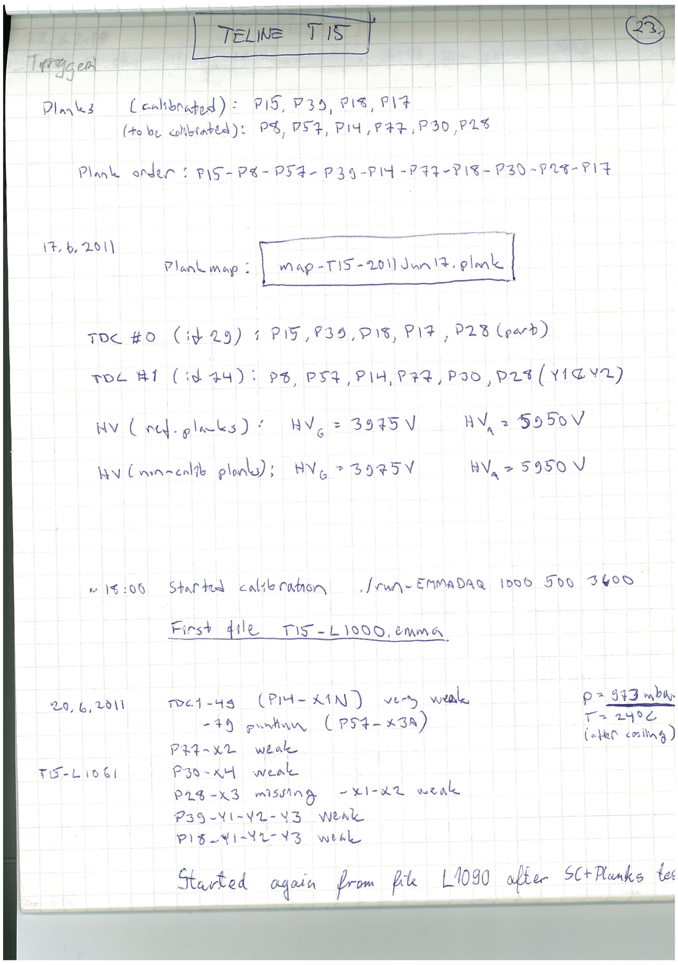
TELINE T15

23

Trigger

Planks (calibrated): P15, P39, P18, P17

(to be calibrated): P8, P57, P14, P77, P30, P28

Plank order: P15 - P8 - P57 - P39 - P14 - P77 - P18 - P30 - P28 - P17

17.6.2011

Plankmap: map-T15-2011Jun17.plmk

TDC #0 (id 29): P15, P39, P18, P17, P28 (part)

TDC #1 (id 74): P8, P57, P14, P77, P30, P28 (Y1 & Y2)

HV (ref. planks): HV_G = 3975 V HV_A = 5950 V

HV (non-calib planks): HV_G = 3975 V HV_A = 5950 V

~18:00 Started calibration ./run-EMMADAQ 1000 500 3600

First file T15-L1000.emma

20.6.2011 TDC1-49 (P14-X1N) very weak

-79 puuttuu (P57-X3A)

P77-X2 weak

T15-L1061 P30-X4 weak

P28-X3 missing -X1-X2 weak

P39-Y1-Y2-Y3 weak

P18-Y1-Y2-Y3 weak

p = 973 mbar

T = 24°C

(after cooling)

Started again from file L1090 after SC+Planks tes

Figure 16: **The first page of logbook of the calibration of MUBs of stack 15.**

4.2.3 Event jumps and false hits in data

As mentioned above, one event consists of one event file header and arbitrary amount of datawords for each TDC. However, a problem of an unknown origin arose - an event jump. It is a mismatch of events in data from two or more TDCs. This is illustrated in Figure 17. An initial thought was to disregard the raw data-files that contained event jumps. Unfortunately it was later found out that this would mean to disregard half of the *.emma-files.

Event jumps are detected by a function called "eventchecker()". It calculates differences between subsequent events. There is no event jump if

$$\mathbf{x_i} - \mathbf{x_{i-1}} = 1,$$

and there is an event jump if

$$\mathbf{x_i} - \mathbf{x_{i-1}} \geq 2,$$

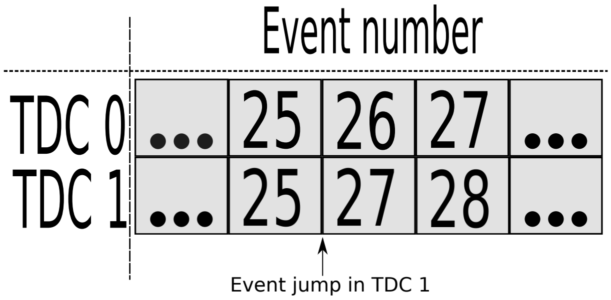

Figure 17: **An illustration of an event jump happening in TDC 1 in raw data. Event number 26 has been skipped in TDC1.**

where $\mathbf{x_i}$ is the event number $\mathbf{i}$, where $\mathbf{i} \in \mathbb{N}$ and $\mathbf{i} \in [\mathbf{1}, \mathbf{N}]$ and $\mathbf{N}$ is the last event of the file. All the event jumps are save into a std::vector, and every time there is an event jump in the data processing, the event in which an event jump has happened is rejected from the analysis in both TDCs.

As mentioned in section 3.1.3, there can be numerous false hits in raw data. False hits are sorted out by function called sorter(). It uses a basic algorithm to inspect that there is only one of each signal (NEAR, FAR and ANODE) from each chamber, and these signals are the first ones to arrive to the TDC. All other signals are disregarded. There are usually multiple false hits in every chamber for every signal type.

The biggest problem of the calibration process was the chambers themselves, and the way they were working. The air temperature and pressure have an effect on the rate of afterpulses and trigger rates of the chamber. The stack 15 set-up was done in summer, during June 17 - August 1. The high temperature, over 27 degrees, and high air pressure increased afterpulse rate. Temperature reached its highest value around 29,8 degrees during the calibration run. Also, many of the low triggering rates in the chambers are speculated to be due to high pressure. Afterpulses do not produce much harm for calibration, due to the sorting process done by the BR, but low trigger rate affects statistics of chamber, and hence makes the calibration results worse. More details of the temperature, air pressure, and trigger rates can be found in the logbook in Appendix B.

4.3 Fit in delay-direction

The delay-direction is longitudinal direction of the MUBs as illustrated in Figure 21a. Because there are four reference MUBs in the stack, the exact hit position is known in these MUBs. Therefore a position in the delay direction can be constructed. A program called "Sorter" is responsible of creating a delay fit (as well as creating anode fit).

4.3.1 Requirements for delay fit

Sorter demands a single muon track. This means that there is only one track per each event and the track must consist of 8 hits in each reference MUBs' chambers. Multiple tracks are disregarded. Thus the delay fit, which is a 1st order polynomial fit, can be constructed by using hit positions in reference MUBs. An event is considered to be of good quality when it fulfils the following requirements:

- There must be two hits (one hit in both the X- and Y-chamber) in each reference MUBs. Eight hits in total.
- Hits must be located in proximate chambers. For example, if there is a hit in Y2-chamber, then there must be a hit in X2- or X3-chamber. This is illustrated in Figure 18. The central chambers (Y2,X2,X3) benefit from this requirement the most and have more data than external chambers. However, this would be the case anyway because of the geometry of the stack and the requirement of 8 hits.

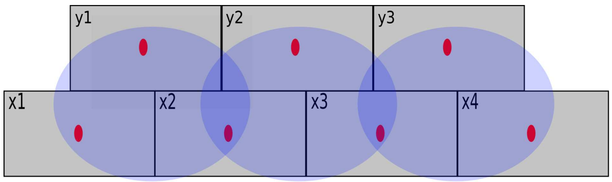

Figure 18: **An illustration of the trinity-demand. Sorter demands that there is a hit in the Y-chamber and the proximate X-chambers. This is illustrated by blue ellipses. The red dots represent anode lines.**

- The position between the hits in the Y-chamber and the X-chamber must be 60 mm or less [74]. The distance of 60 mm comes from the geometry of the stack, and the value in question is the maximum value which a high energy particle can propagate to trigger all MUBs in the stack.

4.3.2 Construction of delay hit positions

The delay hit position in the reference MUBs was constructed from NEAR-, ANODE- and FAR-signal of each chamber by using equations

$$
\begin{aligned}
\mathtt{X}_{\mathtt{NA}} &= \mathtt{X}_{\mathtt{N}} - \mathtt{X}_{\mathtt{A}}, \\
\mathtt{X}_{\mathtt{FA}} &= \mathtt{X}_{\mathtt{F}} - \mathtt{X}_{\mathtt{A}}, \\
\mathtt{X}_{\mathtt{NAFA}} &= \frac{\mathtt{X}_{\mathtt{NA}} + \mathtt{X}_{\mathtt{FA}}}{2},
\end{aligned}
\tag{3}
$$

where $\mathtt{x}_{\mathrm{N}}$ is a NEAR-signal in mm, $\mathtt{x}_{\mathrm{A}}$ is an ANODE-signal in mm and $\mathtt{x}_{\mathrm{F}}$ is a FAR-signal in mm. The hit position in a MUB's chamber is $\mathtt{x}_{\mathrm{NA}}$ and $\mathtt{x}_{\mathrm{FA}}$. $\mathtt{x}_{\mathrm{NAFA}}$ is the average of the two hit positions in the plank's chamber and it is constructed by using three independent parameters called triplet. The signals are first in channels, but they are transformed into mm using calibration tables of the reference MUBs. Basically this is done by a function named *Calparameters::inputdata()*. It takes as input:

- N,F and F-signals in channels,
- chamber id,
- plank id, and

- a vector, which contains a calibration table for current plank.

Then it reads calibration tables and matches the correct channel to the corresponding hit position and gives as output a data structure where all hits in reference MUBs are saved in mm.

The plastic holders inside the chamber can be located in the raw data as showed in Figure 19. In those locations, there are less statistic than usually. Another location for poor statistic is in the ends of each chambers, approximately 20 cm from each chamber end. Channel-hit position can be constructed by extrapolating good data into poor data.

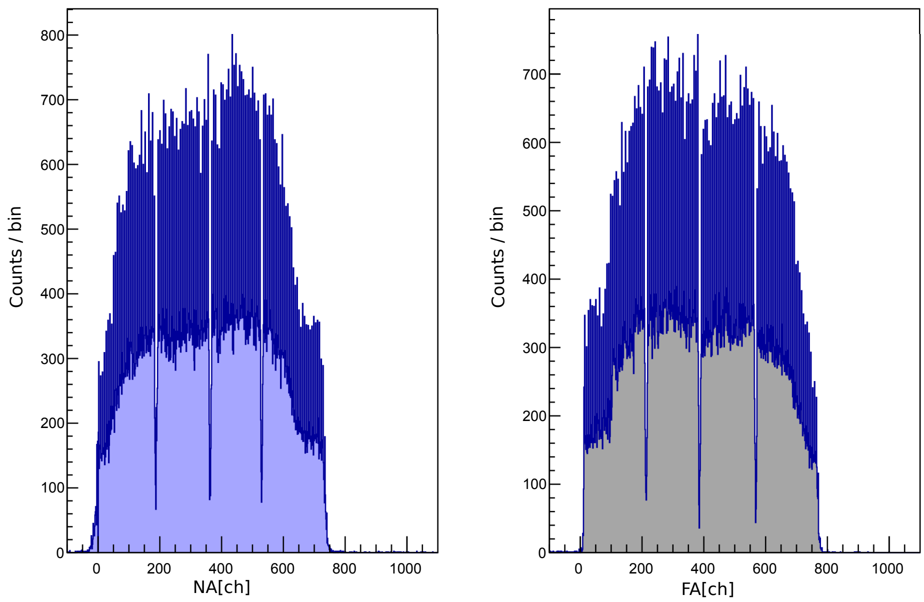

Figure 19: **Chamber X1 of P15 NA- and FA-signal are illustrated in this histogram. Sharp decreases in counts are due to plastic holders inside the chamber.**

4.3.3 Construction of delay fit

The track of a high energy particle is illustrated in Figures 21a and 21b. When an event is considered to be of a good quality, a linear fit is done to hit-positions of the reference planks. The linear fit is done by using **ROOT**'s ROOT::Fit-class and fitting a 1st order polynomial to the data points. The slope and the constant can be retrieved from the fit parameters. Now the hit track can be recreated and the hit position in the un-calibrated planks can be constructed. Here we approximate that a high energy particle goes along a straight track when propagating through the calibration stack.

The positions of reference planks have been measured and can be found in Table 5. The exact position of the anode line in X- and Y-chambers is calculated by

$$\mathtt{Y_{P15}} = 16.5\ \mathtt{mm\ and}$$

$$\mathtt{X_{P15}} = 16.5 + 27\ \mathtt{mm},$$

where 16.5 mm is the distance between the Y-chamber ceiling and the anode line, and the 27 mm is the distance between the Y-chamber anode line and the X-chamber anode line. P15 is the utmost reference plank and it is considered as origin as its Y-chamber ceiling is reference point for other planks' positions in the stack. Of course, to get the other reference planks' corresponding values, one have to add the distance from table 5. Ultimately, the position of a reference plank in the delay direction is then constructed for the Y-chamber

$$\mathtt{POS_Y} = (\mathtt{Y_{P15}}, \mathtt{X_{NAFA}})$$

and for the X-chamber

$$\mathtt{POS_X} = (\mathtt{X_{P15}}, \mathtt{X_{NAFA}}).$$

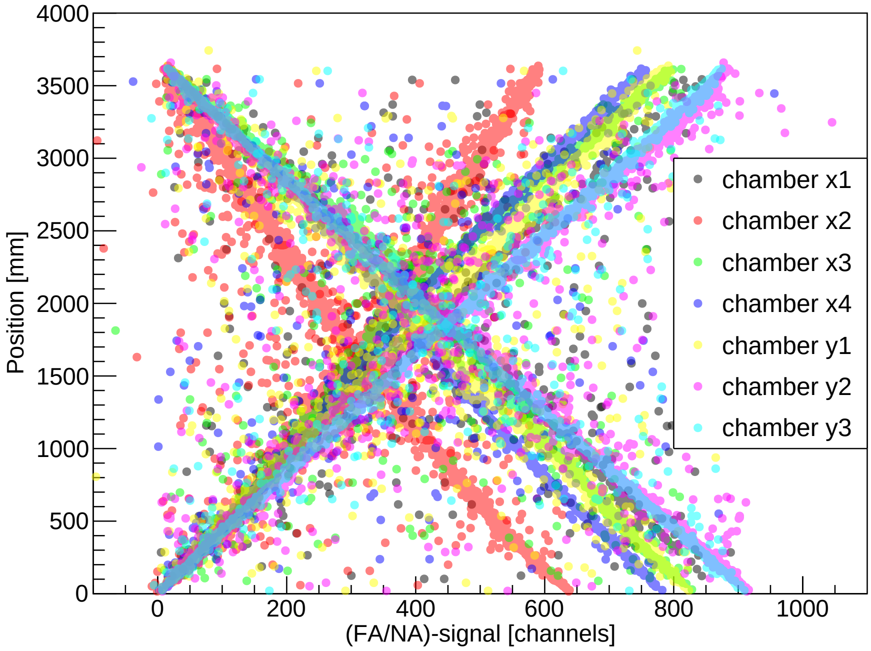

Figure 20: **Position is plotted as a function of NA- or FA-signal using Equation** (3) **for each chamber in plank P8 as 2D-histogram. It can be seen here that the anode line is not linear and it is slightly different in each chambers. This is due to the fact that MUBs are man-made. Also, the difference between NA- and FA-signals can be seen in the figure. NA is monotonically increasing whereas FA is monotonically decreasing as a function of hit-position. It is also noteworthy that the anode lines (NA/FA) are similar in each chamber, but they are reversed.**

Table 5: Reference planks ID and their position in the calibration stack.

Reference plank ID	Distance from P15 Y-chamber's ceiling (mean value)
P15	0 ± 1 mm
P39	539 ± 1 mm
P18	1082 ± 1 mm
P17	1602 ± 1 mm

As shown in Figure 20, MUBs are not perfect, and the position in the delay direction cannot thought as a linear line, or the different chambers seen as alike. This had to be taken account in the measurement of the height of the calibration stack. The MUB vertical position in the stack was measured in three location: 100 mm from the end of the plank, at 1750 mm middle point and 100 mm from the other end, with errors of 1 mm. Therefore a mean of these values were calculated and used when doing the fit of the track.

4.3.4 Uncertainty of the height of the stack

The uncertainties of the height of the MUB, and the position in delay and anode direction in the reference MUBs have been approximated to be ±1 mm, and have been taken account in the fitting process. The uncertainty for the height of the stack comes from using a measurement tape. Each plank has three measurement points, and the height fluctuates ± 1 mm. Thus, propagating of uncertainty can be calculated

$$\sigma_{\mathtt{err}} = \sqrt{\sum_{i=1}^{3} (\frac{\partial \overline{\mathrm{x}}}{\partial \mathbf{x_i}} \Delta \mathbf{x_i})^2},$$

where $\overline{\mathrm{x}}$ is the mean of the MUB's positions

$$\overline{\mathrm{x}} = \frac{1}{3} \sum_{i=1}^{3} \mathbf{x_i}, \text{ and}$$

$\Delta \mathbf{x_i}$ is the uncertainty of each position. Therefore, $\sigma_{\mathtt{err}}$ is

$$\sigma_{\mathtt{err}} = \sqrt{(\frac{1}{3})^2 + (\frac{1}{3})^2 + (\frac{1}{3})^2} = \frac{1}{3} \text{ mm}.$$

However, the uncertainty has been overestimated to be 1 mm. This is the value used in as parameter range when using **ROOT**'s ROOT::FIT-class.

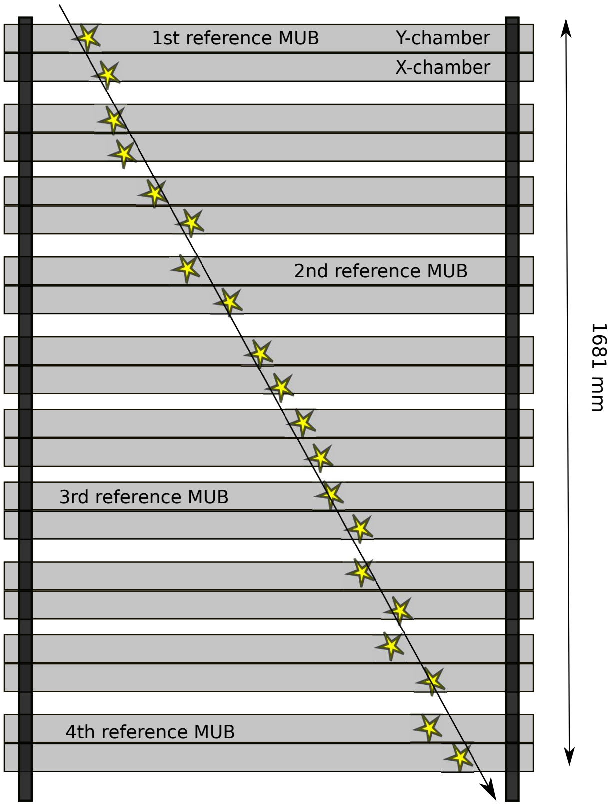

(a) **An illustration of a high energy particle track, the fit process for calibrating the uncalibrated MUBs and the location of reference MUBs in the calibration stack. The yellow stars are the hits in MUBs and the line through them represents a linear fit.**

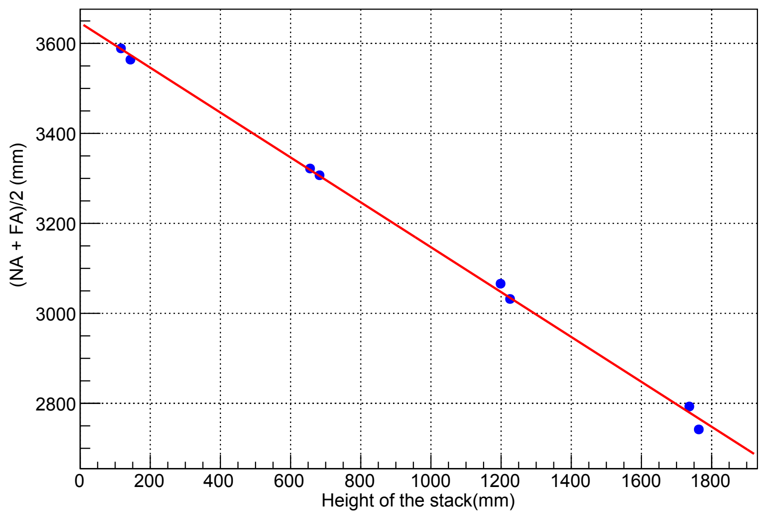

(b) **An example of a delay fit procedure. The horizontal axis shows the stack's height and on the vertical axis is the delay hit position in MUBs' chambers. Figure 21a rotated 90 degrees counter clockwise so the top reference MUB (P15) is the nearest of the origin. Blue dots represent the hits in the X- and the Y-chambers in the reference MUBs. The red line is the linear fit.**

Figure 21: **An illustration of a high energy particle's track in (a) and the delay fit process in (b).**

4.4 Construction of position in delay-direction from parameters of linear fit

Due to data acquisition electronics delay hit-positions are represented in channels in all uncalibrated planks, and for every channel there is a specific location in the chamber in delay-direction. This location can be reconstructed from the fit parameters of linear fit in reference planks. Thus a histogram was done for each channel for chamber of uncalibrated planks. This histogram is illustrated in Figure 22. The histogram is done for channel 258 for plank 8's chamber Y2 from FA-signal. Ultimately, there were altogether 2400 histograms per chamber, because there were 1200 channels per chamber, and the chamber position had to be done in FA- and NA-direction.

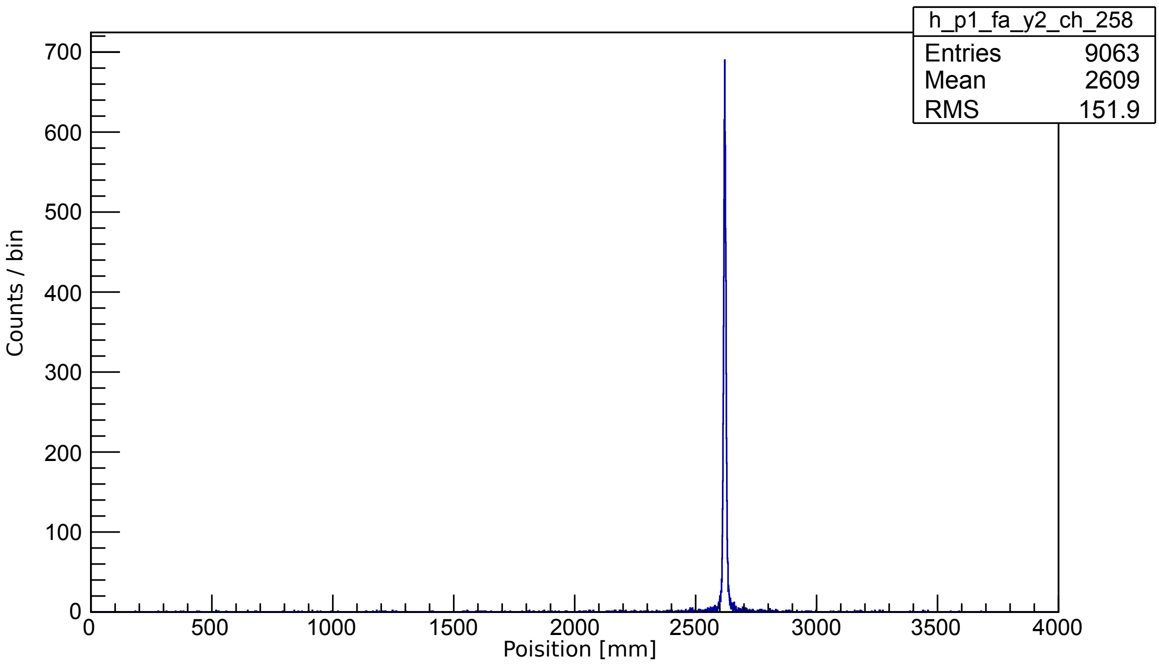

Figure 22: **Plank 8's chamber Y2 channel 258 corresponding position in mm. The position is reconstructed from the linear fit parameters of reference planks.**

After the reconstruction of the position, FA/NA-signal can be plotted as a position-channel histogram, which is illustrated in Figures 23a and 23b. It can be seen, the anode-line in chambers behaves differently, and thus each chamber has to analysed separately. Statistics of both ends of the chamber is usually poor. Therefore, small parts at the ends of chambers are disregarded. The poor statistics at the ends of chamber depends solely of chamber, and of how good statistic it has. Also, plastic holders of the anode wire can be located in the line, as there is no data in small interval in channels. For example, 1st plastic holder is located around 1000 mm in Figure 23a.

Positions are needed for channels from -100 to 1100. Therefore an extrapolation is needed. This is done by creating a linear fit for the known data points and by extrapolating the needed positions by using the fit function. The fit is done for data points and it, usually, must be done in five different locations: in the beginning, in the end and in location of every plastic holder. The reason for that is that for every chamber the position in delay-direction behaves differently and it is not usually linear.

The filling of low statistics locations and extrapolation is done semi-manually. The code, which handles the extrapolation and filling, takes several input parameters: the amount of data points in the channels from the fit is constructed, as well as the locations of the extrapolation, and low statistics locations. The fit is done using an interval of 200-300 data points from the x-axis, nearby of the preferred fit. An example of the fits are shown in Figure 24.

After the filling of data points of low statistics and extrapolation regions, the position of each channel was saved into a *.txt-file. This was done for every seven chambers of an uncalibrated plank and for both FA- and NA-signals. After that, all the same chambers of the plank FA- and NA-signal locations are combined so that there is only one text file. This is the calibration table of the plank. Because of the myriad amount of lines in calibration tables, they were not included in this thesis. However, the fits, out of which the calibration tables were composed, are included in the appendix D. Table 6 contains the summary of the successful and unsuccessful creation of calibration tables.

The unsuccessful calibrations were due to low statistics. The list of causes of low statistic in a chamber were: a missing signal, a broken chamber, and a weak signal. These where the most typical reasons for no data from a specific chamber, and this is documented in the logbook in Appendix B. However, no reason has been found why the chambers X1 of P8 and P57 are not working. P8 and P57 have gone three calibrations before stack 15, so there might have been something wrong with these planks. For all the other chambers, the reason for low statistics have been documented in the logbook.

Table 6: Summary of chambers for which it was possible to produce calibration tables. Red color indicates failed calibration. FA or NA in the table element indicates which direction has failed. Green color indicates successful calibration.

	Chamber Id						
Plank Id	X1	X2	X3	X4	Y1	Y2	Y3
P8	FA and NA						
P57	FA and NA						
P14	FA and NA				FA		
P77	FA and NA	FA and NA			FA		
P30				FA and NA	FA		
P28			FA and NA		FA		

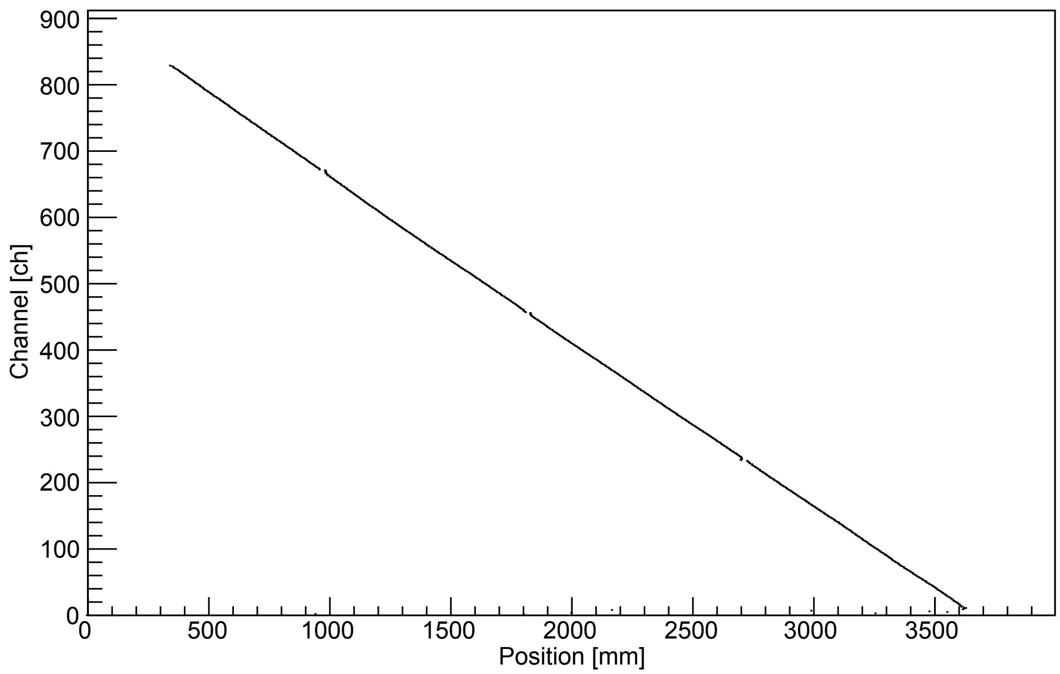

(a) **P8, Y3, FA-signal**

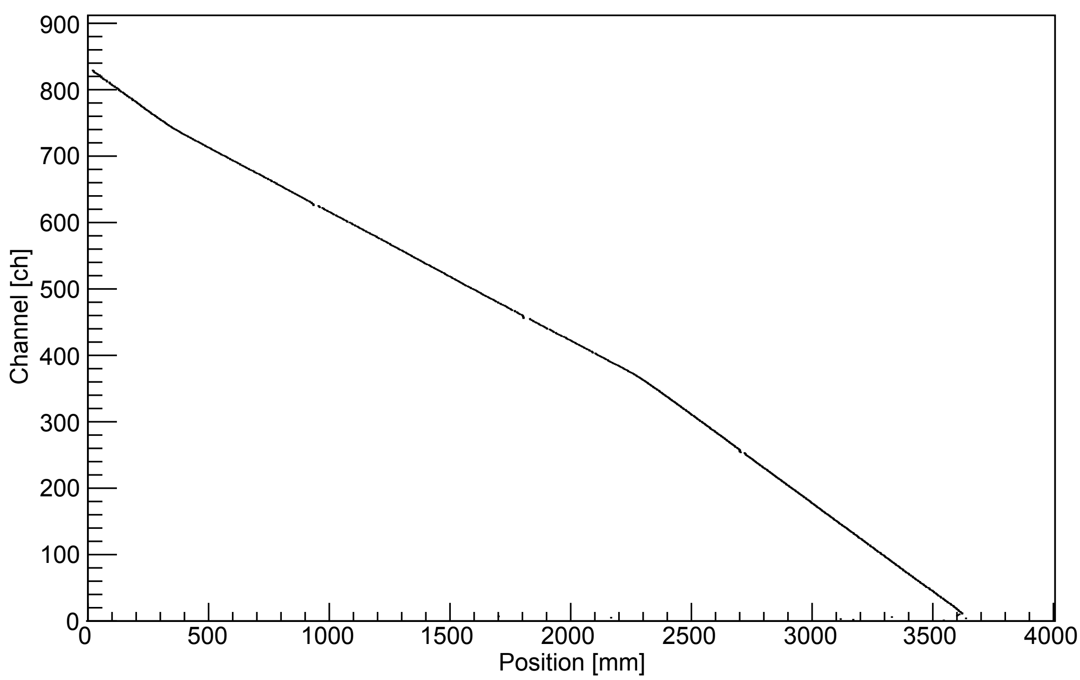

(b) **P8, X3, FA-signal**

Figure 23: **Plank P8's channels are plotted as a function of position in the delay direction. Y3 chamber is plotted in upper Figure (a) and X3 chamber is plotted in lower Figure (b). The variation of anode line position is visible. In the upper figure, the anode line is almost linear but in the lower figure, it is not linear.**

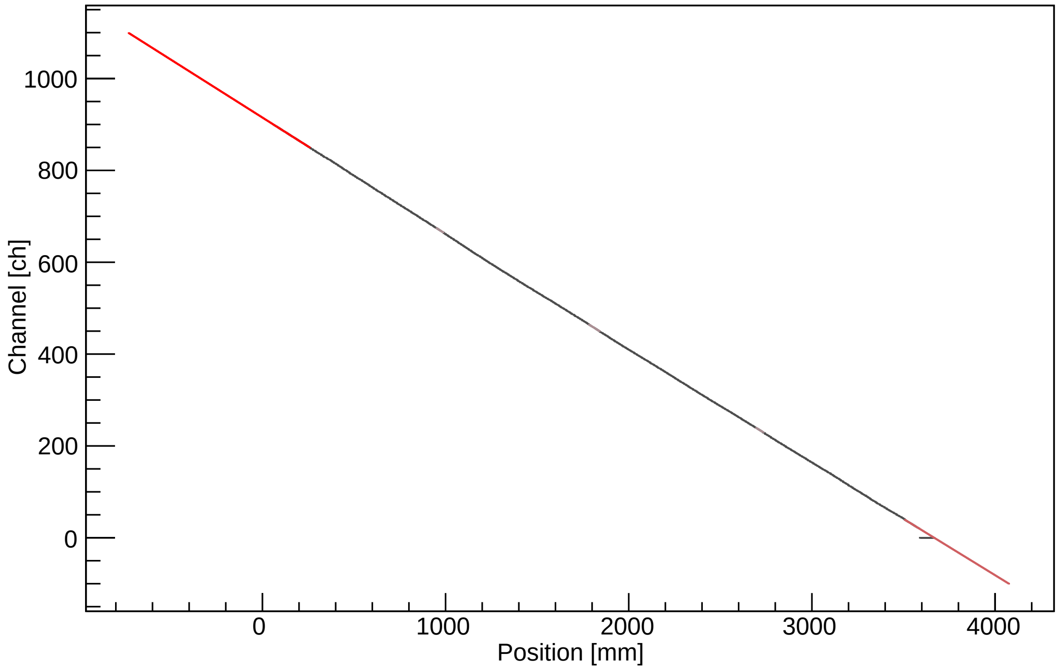

(a) **P8, Y3, FA-signal + fit**

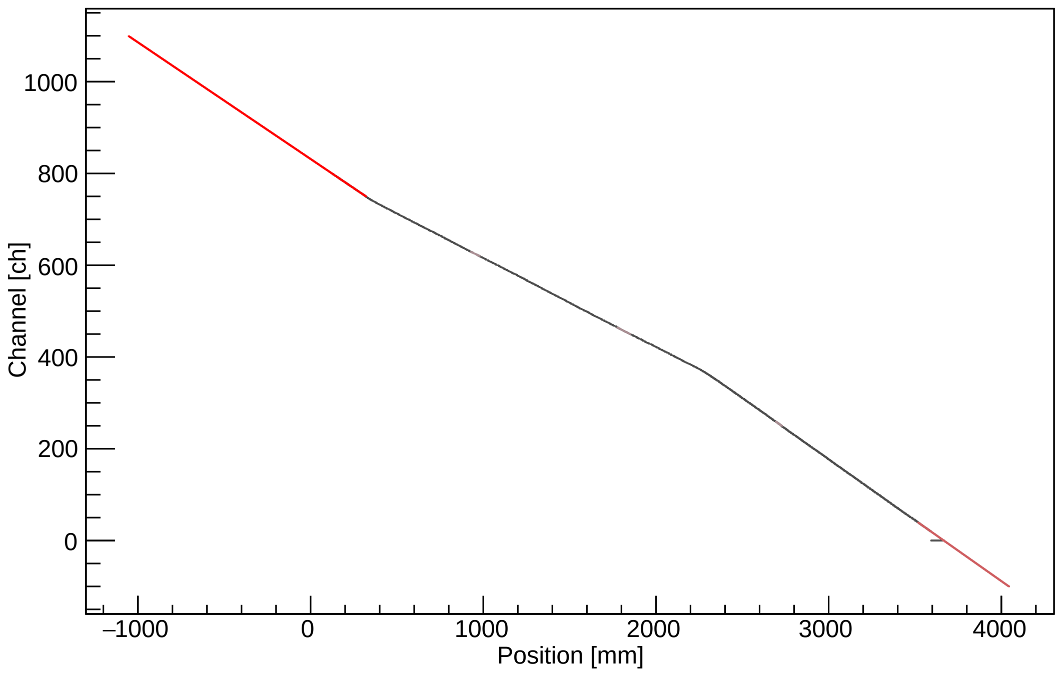

(b) **P8, X3, FA-signal + fit**

Figure 24: **An example of the extrapolation in the chambers. Red and amaranth exhibit extrapolations from the beginning and ending data points, constructed from linear fit function. Usually 200-300 data points were included in the fit-process from the end and the beginning. There are also three greyish fits in the histogram. These are the location of the plastic holders inside of the chambers. Black dots nearby amaranth extrapolation, are just a visual bug, and they take no part in the creation of calibration tables.**

4.5 Fit in anode direction

Like in the delay direction, the same kind of fitting procedure is used to make sure that the anode direction is also good. Anode direction means vertical direction in the stack while the delay direction is the horizontal direction. The anode direction is illustrated in Figure 25.

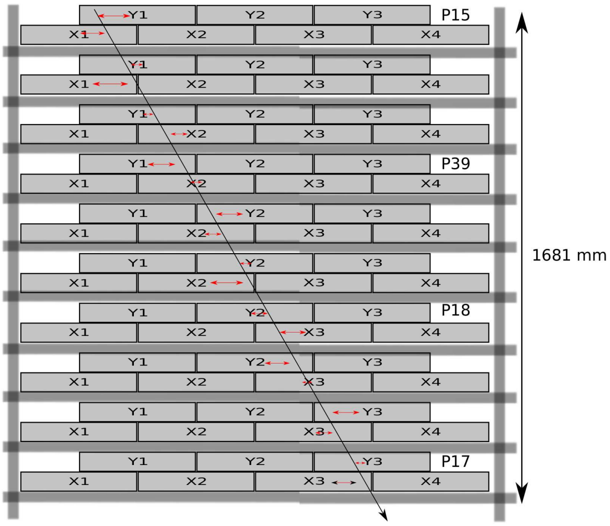

Figure 25: **An example of how the anode fit has been done. The black arrow indicates hit-track of a high energy particle in anode direction. Red arrows indicate the distance from the hit to the anode wire. The anode position is created using a hit in both chambers, Y and X of the plank.**

4.5.1 Construction of anode fit

The reconstruction of anode hit-position was much alike as the reconstruction of position in the delay direction. However, the difference was that the hit position in MUB was built by using a signal from both chambers - Y and X. Therefore, there were only four hit positions in the anode direction. This is shown in Figure 27. The anode hit position was created by using the following formula

$$\mathtt{x}_{\mathtt{a1a2}} = [3 + 52 \cdot (1 + \frac{\mathtt{x}_{\mathtt{A1}} - \mathtt{x}_{\mathtt{A2}}}{3250})] \ \mathtt{mm}, \tag{4}$$

where 3 mm is the thickness of MUB's case, 3250 is the estimated length of the chamber in lengthwise direction and `A1`/ `A2` (Y/X) - anode chamber signals in channels as in Figure 26a. Of course, the position must be shifted depending which anodes are used for the position calculating. The origin in the anode fit has been taken in the X1 anode. To make sure that the direction is kept on the right track, the position must be calculated a bit differently depending on where the hits have occurred. For chambers Y1-X1, Y2-X2 and Y3-X3, the deduction of anode signals is X-chamber hit minus Y-chamber hit , ergo position is calculated by A1 - A2, and for chambers Y1-X2, Y2-X3 and Y2-X4 vice versa. This is illustrated in Figure 26b.

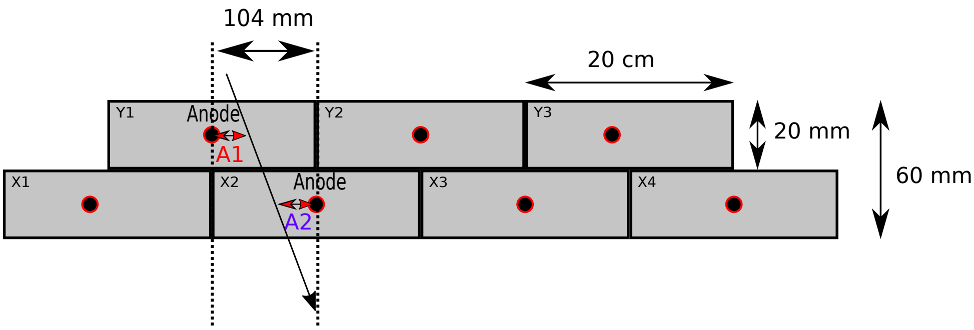

(a) **Here, an anode hit direction is illustrated. 104 mm is the distance between chamber X and Y anode lines. Also, chamber dimensions are shown and the height of a MUB in anode direction.**

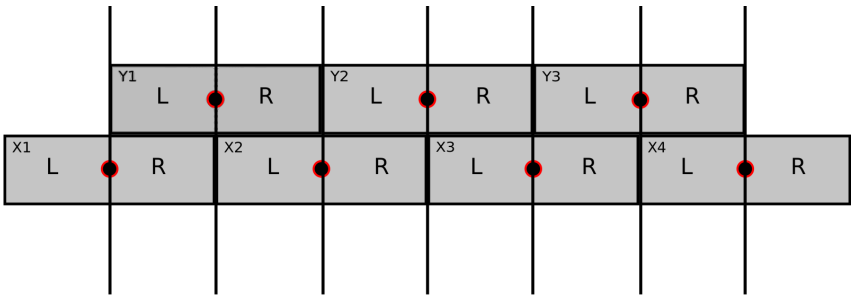

(b) **Chambers are divided into two parts in anode direction - left(L) and right(R). Calculation of the position for anode fit is done by using by L minus R. Basically this means Y-hit minus X-hit for chamber pairs Y1-X1, Y2-X2 and Y3-X3, and vice versa for chamber pairs X2-Y1, X3-Y2 and X4-Y3.**

Figure 26: **An illustration of the dimensions used in the anode fit (a) and the division of chambers into left and right-pairs (b).**

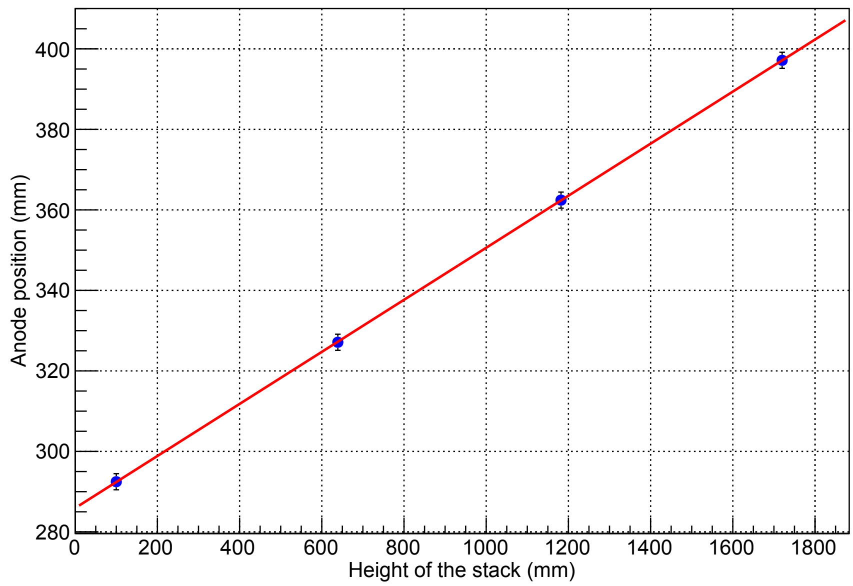

Figure 27: **A fit to anode hit positions. The height of the stack is on the horizontal axis, and the anode position in mm is on the vertical axis. The blue points are anode positions with errors and the red line is a 1st order polynomial fit.**

5 Analysis of the errors in the calibration process

Experimental, or as in this case, calibration uncertainty can be divided into two categories: random and experimental uncertainty. Random uncertainty can be treated statistically based on repeated measurements, whereas systematic cannot be handled in that way. Random uncertainty can be revealed by repeating the measurements, and it is called random error. Random errors are caused by unknown or unpredictable sources in calibration, for example, noise from electronics, air temperature, and pressure effects in chambers. Systematic uncertainty can not be treated by repeated measurement and it is called systematic error. Systematic errors are usually caused by the measuring instrument or the observer. For example, they may result from the process of measuring the height of the stack, measuring the distance of anodes, and from the code done by the author. However, a value for random and systematic errors can be received from the residual histogram. The peak width tells us the random error of the calibration, and the mean tells us the systematic error of the calibration. These errors can be combined as a quadric sum of errors. Taking the square root of the sum, we get the estimation for precision for the calibration, ergo

$$\delta\sigma_{\mathrm{precion.}} = \sqrt{(\delta\sigma_{\mathrm{rand.}})^2 + (\delta\sigma_{\mathrm{sys.}})^2}, \tag{5}$$

where $\delta\sigma_{\mathrm{rand.}}$ is the peak width in residual histogram, and $\delta\sigma_{\mathrm{rand.}}$ is data/fit mean in residual histogram. [75]

5.1 Residual of anode and delay fit in reference MUBs

Because of the unknown nature of the calibration, the only way to estimate errors of the created calibration tables was using a residual histogram. This was done in both anode and delay direction. Basically, the residual histogram was done by subtracting reconstructed position from the actual hit position, ergo

$$\Delta_{\mathrm{res}} = \mathrm{x}_{\mathrm{pos}} - \mathrm{x}_{\mathrm{fit}},$$

where Δ_{res} is the residual, $\mathrm{x}_{\mathrm{pos}}$ is the actual hit location from the calibration tables, and $\mathrm{x}_{\mathrm{fit}}$ is the position constructed from the linear fit parameters.

Residual histograms were done for reference planks and also for uncalibrated planks. The estimation of error was obtained from the reference residuals, and by comparing uncalibrated planks residuals with reference plank's residuals, errors of the calibration can be justified.

5.1.1 The fit functions in residual histograms

The fit for the delay residual histograms of uncalibrated MUBs were done by using two methods: the double Gaussian with linear background and an integral method. Double Gaussian fit with linear background did fit better than just one Gaussian, but the problem was it could not be used in the fit process for the reference planks' residual histogram. The integral method was better in the end, but the double Gaussian fit provided also more information for the error analysis. Lorentzian function was used for the fit in the anode direction for both reference and uncalibrated MUBs, and also for reference MUBs in the delay direction. This was done because Lorentzian function has a sharper peak than in Gaussian, and the peak in the anode direction was much more sharper than in the delay direction. The Lorentzian function did fit also in the reference planks residual histogram.

Gaussian distribution is defined in **ROOT** as

$$\mathrm{f(x)} = [0]\mathrm{exp}(-\frac{1}{2}(\frac{x-[1]}{[2]})^2),$$

where [0] is normalizing constant, [1] is mean (μ), and $[2]^2$ is variance (σ^2) of the Gaussian distribution. The double Gaussian fit with constant background takes seven parameters. Six comes from the two Gaussian functions and one from the constant function. These fits have to be done first, and then feed the parameters of these fits to the double Gaussian with background fit. Hence an estimation for mean and variance was needed.

The total sigma of the two Gaussian was calculated as

$$\sigma_{\text{total}} = \sqrt{(\sigma_1)^2 + (\sigma_2)^2},$$

and mean is calculated by

$$\mu_{\text{total}} = \mu_1 + \mu_2.$$

The lower indices indicate different Gaussian fit. Quadric sum of variance works only if the variables are independent, here they are not. However, this was done to overestimate the errors of variance and mean. The real error analysis was done with different method and the double Gaussian fit with constant background was done to provide extra insight for the error analysis.

The second method for the delay residual was to integrate the area of the peak, and from it to approximate the peak width and mean. In integral method, the area was integrated where 68.25 % (=σ) of data is located, and also for 80% of data. This was done first and foremost to get a more accurate estimation for the error, and to be able to compare more easily reference residual histogram with uncalibrated residual histograms. The problem arose as the shape of the peak of reference and uncalibrated residuals were a bit different, so it demanded the use of different fits. The integral method could be used for the reference and the uncalibrated residuals in the delay direction, thus it was more solid method. Some of the chambers seem to have good σ when the double Gaussian fit was used, but when the integral method was used, it turned out that data was not really normally distributed.

Lorentzian function was fitted for the residual histogram in the anode direction. This could be done for both reference and uncalibrated residuals. This was done also for the reference residuals in the delay direction. The Lorentzian function [76] is the singly peaked function given by

$$\mathcal{L}(x) = \frac{\mathrm{A}}{\pi}\frac{\frac{1}{2}\Gamma}{(x-x_0)^2 + (\frac{1}{2}\Gamma)^2}, \tag{6}$$

where x_0 is the center of the distribution, A is an offset-parameter, and Γ is a parameter specifying the width, or more likely full width at half maximum (FWHM). The build-in Lorentzian of **ROOT** needs an additional offset parameter to be applied in this case.

The general problem with residual fits was that the data do not fully obey normal distribution. That was the main reason why such the double Gaussian, integral, or

Lorentzian method was used in the fitting process. The reason why data did not obey normal distribution, was probably because of the anode wire and delay-line are not ideal. For example, the anode line is not a straight line as it is fixed in three points in the roof of the chamber.

5.2 Residuals of reference MUBs

Systematic and random error of the calibration can be approximated from the residual histogram. Systematic error can be found from the mean of data/fit, and this should be close to zero. The peak width gives random error in residual histograms.

The reference MUBs residuals give an indication of what the residual of the uncalibrated MUBs should look like. For the anode direction, as can be seen in Figure 28, the FWHM of the residual histogram is around 3.7 mm. However, one has to remember that the fit does not perfectly explain the data, so this is just a guideline. The center of the fit is at 0 as it should be. Ultimately, the anode residual distribution has a sharper peak than delay residual distribution. This is due to the fact that anode position is constructed using two chambers. Hence, it is a bit more accurate.

Two different kinds of fit methods were used for the delay direction - the Lorentzian function and the integral method. The Lorentzian function was used in Figure 29. FWHM is around 7.7 mm in the delay direction, and the center is -0.01 mm. The second method was used in Figure 30. It can be seen that σ, where at least 68.25% data are located, is around 10 mm and mean of distribution is zero. Ultimately, the integral method is better, because it was also used for residuals of uncalibrated planks.

The error for reference planks can be calculated by using Equation 5 for both the anode and the delay direction. The error in the delay direction is

$$\delta\sigma_{delay} = \sqrt{(\delta\sigma_{\text{rand.}})^2 + (\delta\sigma_{\text{sys.}})^2} = \sqrt{0^2 + 10^2}\ \text{mm} = \pm 10\ \text{mm}.$$

For the anode residual, systematic error is zero, so there are only random error in reference planks. In the anode direction one gets

$$\delta\sigma_{\text{anode}} = \sqrt{(\delta\sigma_{\text{rand.}})^2 + (\delta\sigma_{\text{sys.}})^2} = \sqrt{(0)^2 + (3,66)^2}\ \text{mm} = \pm 3.66\ \text{mm}.$$

Now an estimation for the precision of the calibration of uncalibrated chambers can be acquired, by the errors of the uncalibrated chamber and the errors of the calibrated ones.

5.3 Delay residuals of uncalibrated MUBs

The residuals for uncalibrated planks in the delay direction were done by two methods: Double Gaussian with background fit, and an integral method. Values from the integral method are used in error analysis to guarantee identical basis for the error analysis. These values are comparable with the reference delay residual, which is done by same method. Demonstrations of the use of both methods can be found in Figures 31a and 31b. Other chambers' figures are in Appendix E.The error value of the reference planks is calculated in section 5.2, and that is 10 mm. By comparing this value to uncalibrated chambers, one gets an estimate for precision of the calibration.

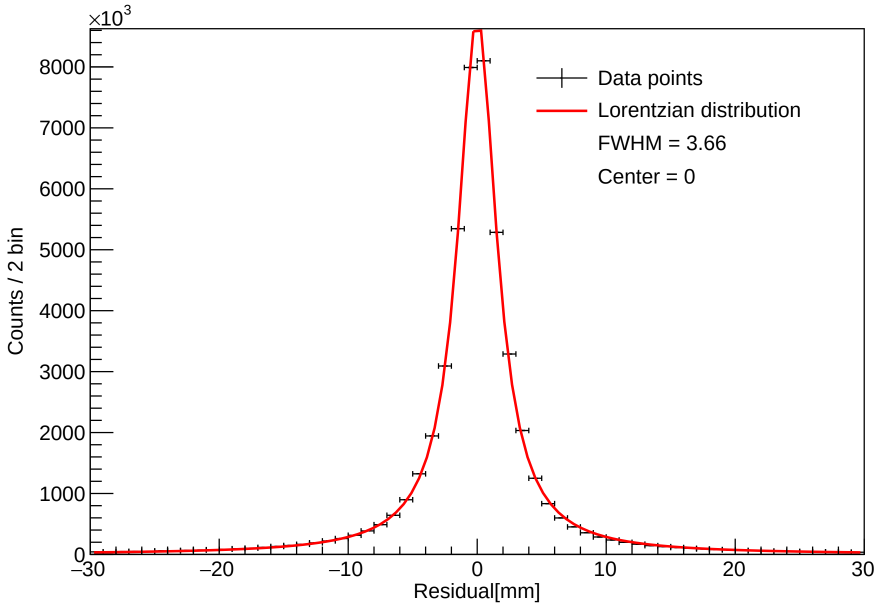

Figure 28: **Anode residual for the sum of reference MUBs in total 27 chambers. The black points are data, and the red line is the Lorentzian fit in Equation** (6)**.**

Errors of the uncalibrated chambers is shown Table 7 , and the difference between the reference planks and uncalibrated planks in Table 8. A couple of questionable chambers with large error differences have been found. For example, there is over 50 mm difference between P30's and P28's chamber X2. This is due to the fact that the peak of the distribution is not steep enough. However, if one compares the result of the other method, the double Gaussian with constant fit from Appendix E, one gets the peak width around 12 mm for both chambers. Hence, the difference would be around two millimetres. The probable reason is that the data are not well distributed result was in a large σ. If the residual histogram is good, both the integral method and the double Gaussian fit with linear background should give approximately the same results for mean of the peak and the peak width. Ultimately, P30's chamber X1 and P28's chamber X1 calibration did not succeeded. P77's chamber X4 shows an interesting behaviour. The histogram is not symmetric, but right-skewed. This explains why the fit mean is heavily on the right side. The cause for that might be a bug in code or the chamber having not worked correctly.

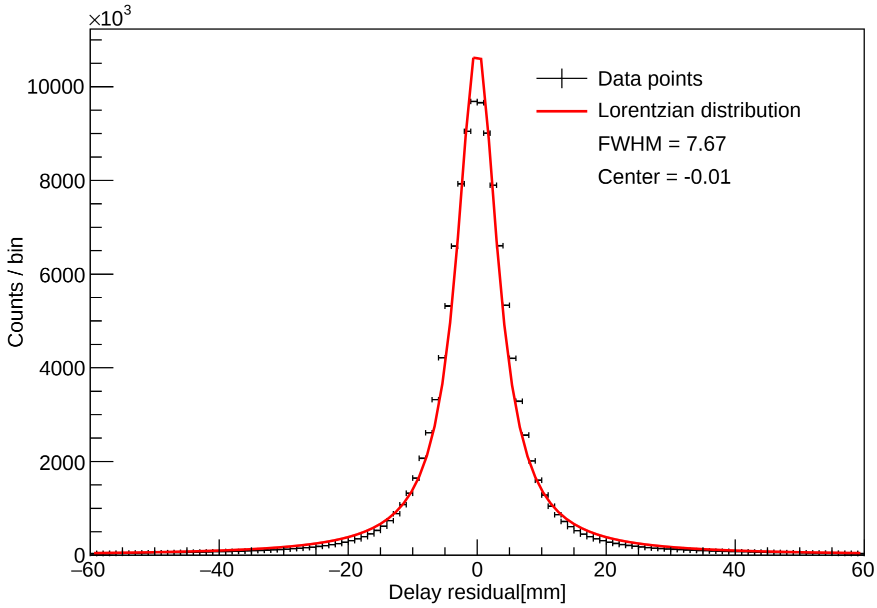

Figure 29: **Delay residual histogram for the sum of reference MUBs in total 27 chambers. The black points are the data, and the red line is the Lorentzian fit from Equation** (6)**.**

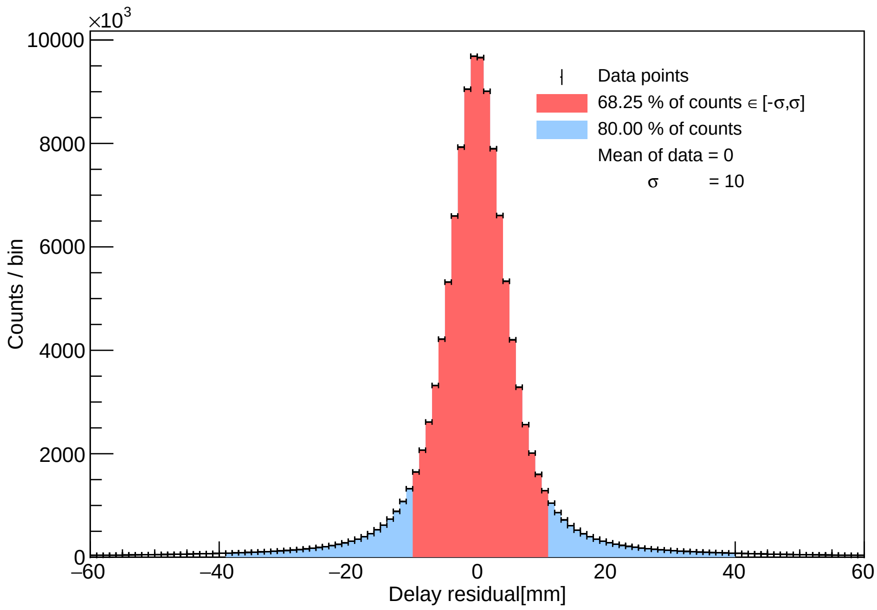

Figure 30: **Delay residual histogram for the sum of reference MUBs as in Figure 29. The peak width is approximated by the integral method. The red area is where at least 68.25** % **of data are located. The teal area is where at least 80**% **of the data are located. The mean of data has been taken straight from the data.**

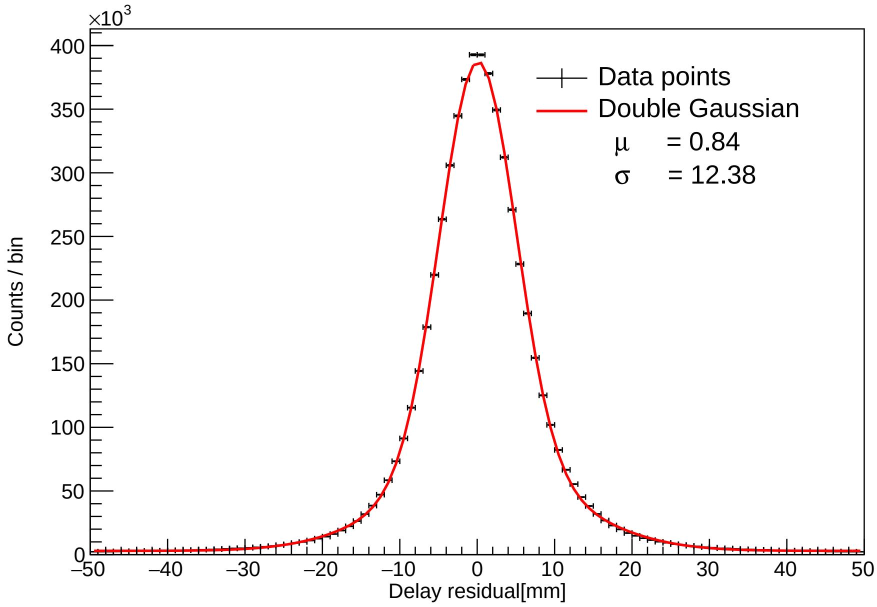

(a) **Delay residual histogram for P8's chamber X2. The red line is the double Gaussian fit with constant background. The mean is calculated by summing together the two means of the Gaussian fits, and σ is calculated by sum of squared of both sigma.**

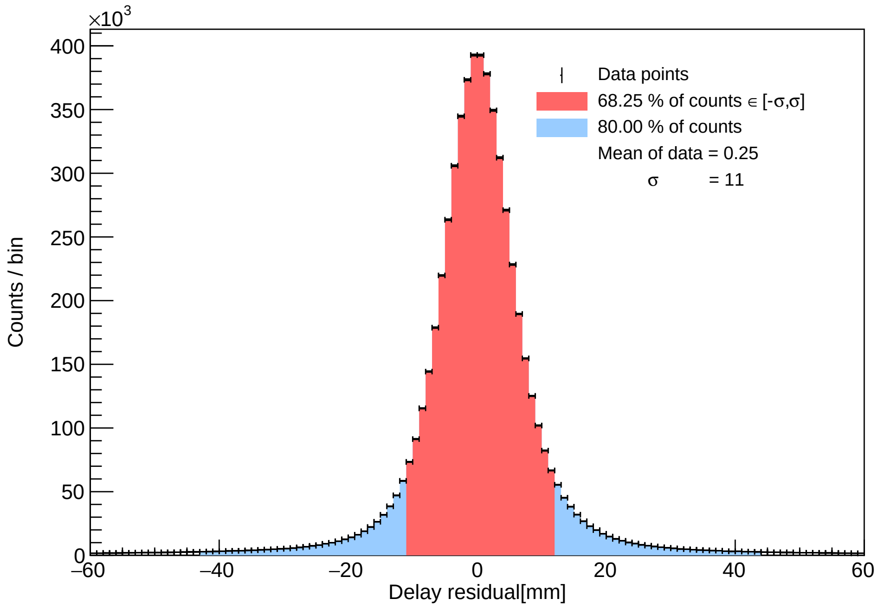

(b) **Delay residual histogram of P8's X2-chamber. The peak width is approximated by the integral method. The red area is where at least 68.25 % of the data are located. The teal area is where at least 80% of data are located. The mean of the data was taken straight from the data.**

Table 7: **Summary of errors of uncalibrated chambers in the delay direction in mm. The errors are calculated by using equation 5.**

	Chamber Id						
Plank Id	X1	X2	X3	X4	Y1	Y2	Y3
P8	No table	11	13.02	12.04	12	15	10.02
P14	No table	16.01	11	9	No table	11.01	14
P57	No table	9	13	10.14	20	14.01	8
P77	No table	No table	11	9	No table	14.01	8
P30	12	60	7.01	No table	No table	11.01	11.03
P28	8	61	No table	9.02	No table	9	9

Table 8: **Summary of the difference in errors of uncalibrated chambers and reference chambers in mm. The error values of uncalibrated chambers are from table 7, and the error of reference residual are from section 5.2. The negative value indicates that the uncalibrated chamber has had smaller error than the reference chambers.**

	Chamber Id						
Plank Id	X1	X2	X3	X4	Y1	Y2	Y3
P8	No table	1	3.02	2.04	2	5	0.02
P14	No table	6.01	1	-1	No table	1.01	4
P57	No table	-1	3	0.14	10	4.01	-2
P77	No table	No table	1	-1	No table	4.01	-2
P30	2	50	-2.99	No table	No table	1.01	1.03
P28	-2	51	No table	-0.98	No table	-1	-1

5.4 Anode residuals of uncalibrated MUBs

The Lorentzian fit was used to approximate the peak width and its location in the anode direction. This is demonstrated in Figure 32, where the fit has been done for P8. The precision of the anode direction is calculated by using Equation (5), where σ_{random} is FWHM and $\sigma_{\text{sys.}}$ is the mean of data from the Lorentzian fit. These values and the fit can be found in appendix F. Table 9 summarises the results. P8 seems to have better accuracy than the reference planks. P57, P77, P30 and P28 had less than 1.5 mm larger uncertainty than reference planks. The larger error of P14 is explained by the largest systematic error.

A couple of planks had questionable anode residuals. P28 and P30 both had double peaks in their residual histogram. The histograms can be found in appendix F. The peaks in P30 are quite close to zero and coalesced together, but in P28 peaks are more separated. This might originate from the structure of chambers, because the value used for the distance of two anodes is same for all chambers. Basically, there could be small offset in the distance of anodes for different planks, which might cause double peak in the anode direction. The anode direction is more accurate than the delay direction, because it has been constructed from two chambers. Therefore, even the smallest fluctuations in the value of the distance of anodes might have been affected to the result. The uncertainty in the stack height, which is one millimetre, might also be a reason. P28 and P30 are the lowest ones in the stack, so there might also be a cumulative error regarding the height of the stack. This error might be visible only in the anode direction, because the anode direction is more accurate. Ultimately, the reason might also be a bug in the code by the author.

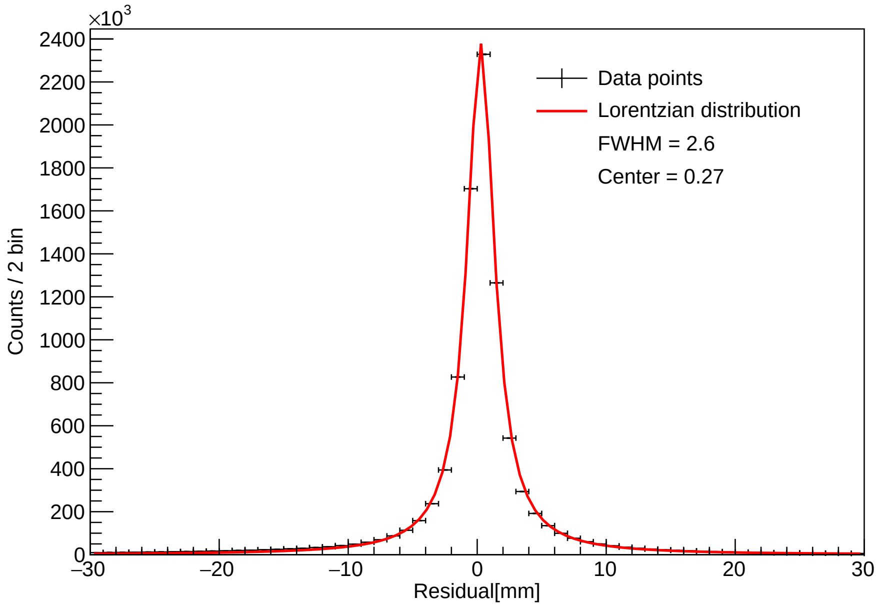

Figure 32: **Anode residual histogram of P8 with Lorentzian fit. FWHM and the center of the fit have been taken from the fit parameters.**

Table 9: **Summary of uncalibrated planks errors in residual fit in the anode direction. $\sigma_{\mathbf{precision}}$ is calculated by using Equation (5), where $\sigma_{\mathbf{rand.}}$ is used FWHM value and $\sigma_{\mathbf{sys.}}$ is used the center value. $\Delta\sigma$ is calculated by $\Delta\sigma = \sigma_{\mathbf{uncal.}} - \sigma_{\mathbf{ref.}}$, where $\sigma_{\mathbf{ref.}}$ is the error of reference planks. The negative value indicates that the uncalibrated chamber has had smaller error than the reference chambers.**

Plank Id	$\sigma_{\text{precision}}$ (mm)	$\Delta\sigma$ (mm)
P8	2.62	-1.05
P14	5.31	1.65
P57	4	0.29
P77	5.05	1.39
P30	5.07	1.35
P28	5	1.28

6 Conclusions

The goal of my thesis was to calibrate muon barrel chambers for the EMMA experiment. The muon barrel chambers that I was calibrating were from calibration stack 15. There were four reference MUBs (P15, P39, P18, P17), and six uncalibrated MUBs (P8, P57, P14, P77, P30, P28).

The first task was to be able to read raw data files, which were in binary format. I used C++ and **ROOT** to make a program called Binaryreader. It reads the data, excludes afterpulses from the raw data, takes into account event jumps, and finally saves sorted data into *.root-file.

As a next step I created another C++ and **ROOT**-based program called Sorter to do the actual position calibration. It reads the files produced by Binaryreader and makes anode- and delay-fit to the hit-positions in reference MUBs with a couple of restricting conditions. Then a position in uncalibrated MUBs was created by using the function of the reference fit. Sorter then creates 2D-histogram, position versus channel, for each channel for both NA- and FA-signal for every chamber of uncalibrated planks.

Finally, the third program, Extrapolation, fills the gaps caused by plastic holds in the 2D-histogram, and that calibration full length of the chamber i.e. channels range from -100 to 1100. This is to guarantee that all the hits have a hit-position. Errors of the positions are approximated by creating residual histograms, and a fit function is fitted to residual histogram to get variance or FWHM of the residual.

Calibration tables were successfully created for 31 chambers out of 42. For four of those 11 failed chambers, it was possible to do only delay position calibration (NA). Hence these chambers were only "half" calibrated. For the rest of the seven chambers, it was not possible to produce calibration tables at all. These 11 chambers had poor statistic, which were the reason why calibration was not successful. Poor statistics were due to weak or non-existing signal.

Residual histograms were done for both reference and uncalibrated planks, in both anode and delay direction. That was done in order to get information on how good the calibration has been. The following chambers had better precision in the delay direction than reference planks: P57's chambers' X2 and Y3, P77 chambers' X4 and Y3, P30's chamber X3, and P28's chambers' X1, Y2 and Y3. Over five millimetres difference was observed in P14's chamber X2, P30's chamber X2, and P28's chamber X2. In the anode direction, only P8 had better precision than the reference planks. P57, P77, P30, and P28 had less than 1.5 mm difference, and P14 had over 1.5 mm difference compared to the reference planks' precision.

References

[1] T. Enqvist et al. A new underground cosmic-ray experiment. *J.Phys.Conf.Ser.39:478*, arXiv:astro-ph/0512398, dec 2006.

[2] V. Hess. Über beobachtungen der durchdringenden strahlung bei sieben freiballonfahrten. *Physikalische Zeitschrift*, 13:1084--1091, nov 1912.

[3] M. Bertolotti. Celestial messengers: cosmic rays : the story of a scientific adventure (1st ed.). *New York, NY: Springer*, page 2, 2013.

[4] Nobel Media AB. "Victor F. Hess - Facts." Nobelprize.org. http://www.nobelprize.org/nobel_prizes/physics/laureates/1936/hess-facts.html, 1936. [Online; accessed 3-July-2016].

[5] C. Coulomb. Troisième mémoire sur l'electricité et le magnétisme. *Histoire de l'Académie Royale des Sciences*, pages 612--638, 1785.

[6] W. Crookes. On the illumination of lines of molecular pressure, and the trajectory of molecules. *Phi. Trans. R. Soc. Lond.*, pages 135--164, jan 1879.

[7] M. Röntgen. Über eine neue art von strahlen. *Der Physikalisch-medizinishen gesellschaft zu wurzburg*, 1895.

[8] H. Becquerel. Sur les radiations émises par phosphorescence. *Comptes rendus hebdomadaires des séances de l'Acadèmie des sciences*, 122:420--421, 1896.

[9] J. Thomson. Cathode rays. *Phi. Mag.*, 44:293, 1897.

[10] J. Hörandel. Early cosmic-ray work published in german. *arXiv:1212.0706v1*, 2012.

[11] A. Gockel. Über die in der atmosphäre vorhandene durchdringende strahlung. *Phys. Zeit*, page 845, 1909.

[12] A. Gockel. Luftelektrische beobachtungen bei ener ballonfahrt. *Phys. Zeit*, page 280, 1910.

[13] R. Millikan. High frequency rays of cosmic origin. *Proceedings of the National Academy of Sciences of the United States of America*, 12:48--55, 1926.

[14] R. Bennett et al. Diurnal variation of cosmic rays. *Phys. Rev.*, 41:119.

[15] B. Rossi. Directional measurements on the cosmic rays near the geomagnetic equator. *Phys. Rev.*, 45:212--214, feb 1934.

[16] P. Auger et al. Extensive cosmic-ray showers. *Reviews of modern physics*, 11, jul-aug 1939.

[17] E. Fermi. On the origin of the cosmic radiation. *Phys. Lett.*, 75(8), apr 1949.

[18] G. Kulikov et al. On the size spectrum of extensive air showers. *Zh. Eksp. Teor. Fiz.*, 35:635--640, sep 1958.

[19] R. Enomoto et al. The acceleration of cosmic-ray protons in the supernova remnant rx j1713.7-3946. *Nature*, 416:823--826, apr 2002.

[20] M. Bertolotti. Celestial messengers: cosmic rays : the story of a scientific adventure (1st ed.). *New York, NY: Springer*, page 33, 2013.

[21] L. Dorman. Cosmic ray history. *Hauppauge, New York : Nova Science Publishers*, pages 1--2, 2014.

[22] STUK. "Luonnon taustasäteily. (in Finnish). `http://www.stuk.fi/aiheet/sateily-ymparistossa/luonnon-taustasateily`. [Online; accessed 2-August-2016].

[23] J. Beringer et al. Cosmic rays. *PR D86, 010001*, `http://pdg.lbl.gov/2013/reviews/rpp2013-rev-cosmic-rays.pdf` 2013.

[24] T. Gaisser. Origin of cosmic ray radiation. *AIP Conf.Proc.558:27-42,2001*, `arXiv:astro-ph/0011524`, nov 2000.

[25] J. Hörandel. Cosmic-ray composition and its relation to shock acceleration by supernova remnants. *Adv.SpaceRes.41:442-463,2008*, `arXiv:astro-ph/0702370`, jun 2007.

[26] P. Grieder. Extensive air showers, high energy phenomena and astrophysical aspects, a tutorial, reference manual and data book (2nd ed.). *Springer Heidelberg Dordrecht London New York*, page 480, 2010.

[27] J. Abraham et al. Correlation of the highest-energy cosmic rays with nearby extragalactic objects. *SCIENCE9*, 318, nov 2007.

[28] P. Grieder. Extensive air showers, high energy phenomena and astrophysical aspects, a tutorial, reference manual and data book (2nd ed.). *Springer Heidelberg Dordrecht London New York*, pages 3--27, 2010.

[29] P. Grieder. Extensive air showers, high energy phenomena and astrophysical aspects, a tutorial, reference manual and data book (2nd ed.). *Springer Heidelberg Dordrecht London New York*, page 482, 2010.

[30] A. Haungs. Cosmic rays from the knee to the ankle. *Physics Procedia 61 (2015) 425*, `arXiv:1504.01859` ,apr 2015.

[31] The Fly's Eye (1981-1993). . `http://www.cosmic-ray.org/reading/flyseye.html#SEC10`, 1991. [Online; accessed 2-August-2016].

[32] J. Matthews et al. First results from the high resolution fly's eye experiment. *Nuc. Phys. B*, 87:411--413, 2000.

[33] J. Blümer et al. Prog. Part. Nucl. Phys. 63 (2009) 293-338. `arXiv:0904.0725`, 2009. [Online; accessed 26-February-2016].

[34] S. Thoudam et al. Cosmic-ray energy spectrum and composition up to the ankle - the case for a second galactic component. *arXiv:1605.03111*, may 2016.

[35] W. Apel et al. Kneelike structure in the spectrum of the heavy component of cosmic rays observed with kascade-grande. *Phys. Rev. Lett., arXiv:1107.5885*, 107, 2011.

[36] P. Grieder. Extensive air showers, high energy phenomena and astrophysical aspects, a tutorial, reference manual and data book (2nd ed.). *Springer Heidelberg Dordrecht London New York*, pages 11--12, 2010.

[37] K. Greisen. End to the comic-ray spectrum? *Phys. Rev. Lett.*, 16:748--750, apr 1966.

[38] G. Zatsepin et al. Upper limit of the spectrum of cosmic rays. *JETP LETT.*, 4:78--80, may 1966.

[39] J. Hörandel. Models of the knee in the energy spectrum of cosmic rays. *Astro. phys.*, 21:241--265, jan 2004.

[40] C. Grupen. Astroparticle physics (2nd ed.). *Springer Berlin Heidelberg New York*, ISBN-10 3-540-25312-2:66--69, 2005.

[41] D. Fokkeman. The hisparc experiment data accuisition and reconstruction of shower direction. *National Institute for Subatomic Physics*, pages 11--15, 2012.

[42] A. Bell. The acceleration of cosmic rays in shock fronts. *Mon. Not. R. astr. Soc.*, 182:147--156, jun 1977.

[43] P. Grieder. Extensive air showers, high energy phenomena and astrophysical aspects, a tutorial, reference manual and data book (2nd ed.). *Springer Heidelberg Dordrecht London New York, Second edition*, pages 3--4, 2010.

[44] M. Nagano et al. Energy spectrum of primary cosmic rays between $10^{14.5}$ and 10^{18} ev. *J. Phys. G10, 1295*, jan 1984.

[45] T. Stanev. High energy cosmic rays (2nd ed.). *New York, NY: Springer*, page 122, 2010.

[46] P. Grieder. Extensive air showers, high energy phenomena and astrophysical aspects, a tutorial, reference manual and data book (2nd ed.). *Springer Heidelberg Dordrecht London New York*, pages 77--79, 2010.

[47] K. Olive et al. Particle data group. *Chin. Phys.C, 38*, 2015.

[48] P. Grieder. Extensive air showers, high energy phenomena and astrophysical aspects, a tutorial, reference manual and data book (2nd ed.). *Springer Heidelberg Dordrecht London New York*, page 207, 2010.

[49] P. Grieder. Extensive air showers, high energy phenomena and astrophysical aspects, a tutorial, reference manual and data book (2nd ed.). *Springer Heidelberg Dordrecht London New York*, pages 208--225, 2010.

[50] W. Lohmann. Energy loss of muons in the energy range 1-10000 gev. *Cern Yellow Reports*, 1985.

[51] P. Grieder. Extensive air showers, high energy phenomena and astrophysical aspects, a tutorial, reference manual and data book (2nd ed.). *Springer Heidelberg Dordrecht London New York*, page 222, 2010.

[52] A. Morselli et al. The pamela space experiment. -, `arXiv:0905.2551` ,may 2009.

[53] T. Yoshida et al. Bess-polar experiment. *Advances in Space Research*, 33(10):1755--1762, 2004.

[54] A. Kounine. The alpha magnetic spectrometer on the international space station. *Lab. for Nuc. Scien.*, 21(08), 2012.

[55] C. Fabjan et al. Calorimetry for particle physics. *Rev. Mod. Phys.*, 75(1243), 2003.

[56] P. Cerenkov. Visible radiation produced by electrons moving in a medium with velocities exceeding that of light. *Phys. Rev. Lett.*, 52(378), 1937.

[57] H. Völk et al. Imaging very high energy gamma-ray telescopes. *Exp Astron*, 25:173--191, 2009.

[58] The Pierre Auger Collobration. The pierre auger cosmic ray observatory. *Nucl.Instr. and Meth. A, 798, arXiv:1502.01323*, 2015.

[59] T. Bernhörn et al. Simulations of imaging atmospheric cherenkov telescopes with corsika. *Astropart. Phys.*, 30(149), 2008.

[60] I. Cholis et al. Constraining the origin of the cosmic ray positron fraction with the boron-to-carbon ratio. *Phys. Rev. D*, 89, 2014.

[61] W.D Apel. The kascade-grande experiment. *Nucl.Instr. and Meth. A 620*, pages 202--216, 2010.

[62] A. Aab et al. A targeted search for point sources of eev neutrons. *Astrophy. Journ. Lett.*, 789(2), 2014.

[63] A. Aab et al. A search for point sources of eev photons. *Astrophy. Journ. Lett.*, 789(2), 2014.

[64] T. Enqvist et al. Measurements of muon flux in the Pyhäsalmi underground laboratory. `arXiv:hep-ex/0506032`, 2005. [Online; accessed 25-February-2016].

[65] CERN. The delphi detector at cern's lep collider. `http://delphiwww.cern.ch/offline/physics/delphi-detector.html`, 1991. [Online; accessed 14-June-2017].

[66] T. Räihä. Analysis tools for the emma experiment. *University of Oulu*, pages 34--37, 2012.

[67] J. Sarkamo. Design, construction and commissioning of the emma experiment. *University of Oulu*, pages 65--66, 2014.

[68] J. Sarkamo. Design, construction and commissioning of the emma experiment. *University of Oulu*, page 72, 2014.

[69] T. Räihä. Analysis tools for the emma experiment. *University of Oulu*, page 37, 2012.

[70] T. Antoni et al. A large area limited streamer tube detector for the air shower experiment kaskade-grande. *Nucl.Instr. and Meth. A*, 533:387--403, 2004.

[71] J. Sarkamo. Design, construction and commissioning of the emma experiment. *University of Oulu*, pages 59--61, 2014.

[72] T. Räihä. Analysis tools for the emma experiment. *University of Oulu*, pages 66,69, 2012.

[73] R. Brun et al. Root - an object oriented data analysis framework. *roceedings AIHENP'96 Workshop, Lausanne, Sep. 1996, Nucl. Inst. & Meth. in Phys. Res. A 389 (1997) 81-86*, 1996.

[74] J. Sorjonen. Special work: Reading binary files and tracking for the calibrations of muon barrel chambers for emma-experiment. *University of Jyväskylä*, 2015.

[75] J. Taylor. An introduction to error analysis. *University science books*, pages 93--95, 1997.

[76] E. Weisstein. "Lorentzian Function." From MathWorld--A Wolfram Web Resource. http://mathworld.wolfram.com/LorentzianFunction.html, 2005. [Online; accessed 3-June-2016].

Appendix A

Little endian binary format of *.emma-files. There is one Header and TDC-configuration bit-set per file.

Header

Position	Data
0x00-0x03	'E','M','M','A'
0x04-0x07	File id-number
0x08	Data format version number
0x09-0x0c	UNIX UTC time (seconds since 1.1.1980) of the file creation
0x0d-0x10	Microseconds after above time for the file creation
0x11-0x2e	reserved for future use
0x2f	number of TDC-units configured in this file

TDC-configuration

TDCs are configured at this point, position reflects the first TDC. Next TDC is in 16 bytes later.

Postion	Data
0x30	8-bit ID-number of the TDC(status/ID)
0x31	5-bit GEO Address of the TDC
0x32	Operation mode: 1 = STOP TRIGGER MATCHING, 2 = START TRIGGER MATCHING 3 =START GATING 4 =CONTINUOUS STORAGE
0x33	DATA READY mode of TDC 1 = NOT EMPTY 2 = ALMOST FULL 3 = EVENT READY
0x34-0x35	Almost full level in ALMOST FULL mode
0x36-0x37	Trigger window width
0x38-0x39	Trigger window offset
0x3a-0x3f	Reserved for future use

Data

Event consists of single Event header word (32 bits) and data words (32 bits) for all recoded hits. Bit 22 distinguishes between header and data. Bit 21 is 0 on valid data / header.

Event header

Position	Data
31-27	GEO Address of TDC
26-23	Don't care
22	1(header)
21	0(End of block)
20-0	Event serial number(clock)

Data word

Postion	Data
31	Don't care
30-24	Channel number
23	1 = start signal, 0 = ordinary signal
22	0(header)
21	0 (End of block)
20	1 = rising edge, 0 = falling edge
19-0	Measured time (LSB = 0.8ns)

File Tailer

Start of tailer

Position	data
0x00-0x03	0x00600000 - End of data
0x04-0x07	Time of closure(UNIX UTC)(seconds)
0x08-0x0b	Time of closure(microsends after above)
0x0c-0x0f	Number of events in this file

TDC count rates

Position	Data
0x00	ID-number of TDC
0x01-0x04	Count of hits on channel 0
0x05-0x08	Count of hits on channel 1
...	...
0x1fd-0x200	Count of hits on channel 127

Environment

Position	Data
0x00-0x01	Temperature 1(Tunnel air)
0x02-0x03	Temperature 2 (Control room air)
0x04-0x05	Temperature 3(VME box)
0x06-0x07	Temperature 4(Power supply)
0x08-0x09	Temperature 5
0x0a-0x0b	Temperature 6
0x0c-0x0d	Humidity 1
0x0e-0x0f	Humidity 2
0x10-0x11	Air pressure
0x12-0x13	High voltage 1
0x14-0x15	High voltage 2
0x16-0x17	Low voltage +12V
0x18-0x19	Low voltage + 5V
0x1a-0x1b	Low voltage -5V

Appendix B

TELINE T15

(23)

Trigger

Planks (calibrated): P15, P39, P18, P17
(to be calibrated): P8, P57, P14, P77, P30, P28

Plank order: P15 - P8 - P57 - P39 - P14 - P77 - P18 - P30 - P28 - P17

17.6.2011

Plank map: $\boxed{\text{map-T15-2011Jun17.plank}}$

TDC #0 (id 29): P15, P39, P18, P17, P28 (part)

TDC #1 (id 24): P8, P57, P14, P77, P30, P28 (Y1 & Y2)

HV (ref. planks): HV_G = 3975 V HV_A = 5950 V

HV (non-calib planks): HV_G = 3975 V HV_A = 5950 V

~18:00 Started calibration ./run-EMMADAQ 1000 500 3600

First file T15-L1000.emma

20.6.2011

TDC1-49 (P14-X1N) very weak
-79 puntion (P57-X3A)
P77-X2 weak

T15-L1061 P30-X4 weak
P28-X3 missing -X1-X2 weak
P39-Y1-Y2-Y3 weak
P18-Y1-Y2-Y3 weak

p = 973 mbar
T = 24°C
(after cooling)

Started again from file L1090 after SC+Planks tes

(*) in T15-L1120.emma

P28 - X3 missing, others OK

P39 - OK
P18 - OK

22.6.2011

T15

22.6.2011

TDC 0 chn 17-19, 28-31, 52-53, 96-117, 121-126 NNN

TDC 1 chn 9-11 better
chn 49 down
chn 63 pressure dependent (?)
chn 79 down - signal check
chn 96-107, 112-126

N-F P8 X2 , X4
P57 X3 A missing Y2
P14 X1 N low, Y1 . spike, getting better
P77 X2 : 20% X3:ditto
P30 X4 : ~~weak~~ really weak, other also weak
Y1 : spike
P28 X3 : missing, X1-X4 weak
Y2 : weak
P15 ok
P39 Y:t weak
P18 Y:t weak
P17 X4, Y3 OK, Y1 missing, X1, X3 spiky and weak., X2, Y2 low

23.06.2011 08:45 N-F of T15-L1123.emma

T = 24.8 °C
p = 983 mbar

P8 - OK
P57 - X3 missing, others OK
P14 - X1 bad, others OK
P77 - X2 bad, other OK
P30 - X4 bad ~~and~~ hardly missing, others OK
P28 - Y1 and Y2 OK, others bad (*)

P15 - ok
P39 - X's OK, Y's missing (*)
P18 - X's OK, Y's missing
P17 - Y1 missing, others OK

09:00 At the end of T15-L1124.emma : HV_{a} (P15, P39, P18, P17) :
3975 V → 3950 V.

P77-X2 - 83, 84, 85 tdc 1

P30-X4 - 105, 106, 107 tdc 1

T15-L1219.emma

27/6/2011

P57-X3 missing
P14-X1 very weak
"decay" P77-X2 weak
"decay" P30-X4 weak
P28-X3 missing
P17-Y1 missing

p = 991 mbar
T = 26.2 °C

Higher pressure has improved chambers a lot

P28-X3 : A, N and F missing

P14-X1 : A low, N missing, F normal

P57-X3 : A missing, N and F normal

28.06.2011 09:30 N-F of T15-L1240.emma :

p = 997 mbar
T = 24.8 °C

Similar than T15-L1219.emma

$\boxed{\text{Last file T15-L1241.emma}}$

11:00 Antto made a clipper to reduce the pulse height of the anode of P57-X3. Max is now ~200 mV.

P57-X3-A moved from chn = 79 ⇒ chn = 111.

Start from T15-L1243.emma
- in the beginning working channel was locked for P57-X3-A.

New Plank Map : $\boxed{\text{map-T15-2011Jun28.plank}}$

N-F of T15-L1243.emma : P57-X3 OK !

- others as in T15-L1240.emma

T15

26

29.06.2011
09:30

N-F of T15-LR64.emma

p = 996 mbar
T = 26 °C

P8 OK
P57 OK
P14 X1 weak, others ok
P77 X2 "decay", others OK
P30 X4 "decay", others OK
P28 X3 missing, others ok

P15, P39, P18, P17 OK (P17-Y1 not connected).

16:45 HV of non-calibrated started sparking, probably due to too high temperature.
p = 994 mbar
T = 29.8 °C

Stopped until temperature is lower.

Last file T15-LR69.emma.

03.07.2011
16:30

HV_g (P8 – P28) = 3975 V, I_g = 1.073 mA

HV_a (P8 – P28) = 5950 V, I_a = 2 μA spiking still rarely

HV_g (P15 – P17) = 3975 V, I_g = 0.691 mA

HV_a (P15 – P17) = 5950 V, I_a = 0 μA

p = 988 mBar.

T = 24.9 °C (going down)

Testing 15 min : N-F as in the top of the page.

⇒ start calibrating...

T15

27

03.07.2011
17:00 ./run-EMMADAQ 1271 500 3600

First file T15-L1271.emma
p = 988 mbar
T = 24.0 °C

Using still map-T15-2011Jun28.plank

04.07.2011
08:00 N-F of L1285.emma as previously.
T = 22.0 °C
p = 994 mbar

09:55 $HV_{GRADING}$ (P15 – P17) = 3950 V at the beginning of T15-L1288.emma

14:50 Stopped for tests of Maciek. Last file (1h) T15-L1292.emma.

17:10 Started again: First file T15-L1294.emma.
p = 995 mbar
T = 21.8 °C

05.07.2011
09:30 New Ar-dewar.

N-F of T15-L1309.emma
p = 996 mbar
T = 20.3 °C

P8, P57 OK
P14, P77, P30, P28 as before
P15, P39, P18, P17 OK

11:00 Stopped for tests of Maciek. Last file T15-L1310.emma

12:00 Started at T15-L1312.emma

T15

28

06/07/2011 T15-L1329.emma
T = 23.5 °C
p = 990 mbar

7:20
P57-X3 a bit weak
P14-X1 poor
P77-X2 very weak
P30-X4 very weak
P28-X3 missing

10:44: T15-L1333.emma – Stop for SC-tests
10:46: T15-L1335.emma – Started again
12:05: –"– 1336 –"– – Stopped
15:50: –"– 1338 –"– – Started

06.07.2011
17:00 Running in T15-L1339.emma
T = 24.0 °C
p = 989 mbar

07.07.2011
08:00 EMMAN-F of T15-L1353.emma
p = 988 mbar
T = 23.6 °C

P8, P57 OK
P14 X1 bad
P77 X2 bad "decay"
P30 X4 bad "decay"
P28 X3 missing
P15, P39, P18, P17 OK (P17-Y1 not connected)

11:50 T15-L1358 stopped for SC tests. Last file L1357.emma
17:00 T15-L1359 started
p = 987 mbar
T = 27.0 °C

17:15 Stopped due to strange behavior of non-calibrated planks. May be due to high T.

12.7.2011 T15-L1359 deleted.

T15

29

13.07.2011

15:00 Clipper in P57-X3-A was broken. Antho made a new. P14-X1-N is not counting.

Test files T15-L1370.emma ... T15-L1399.emma

P14-X1-A : chn = 63 → chn = 108

New plankmap: $\boxed{\text{map-T15-2011Jul13.plank}}$

15:30 Start ./run-EMMADAQ 1400 500 3600

First file T15-L1400.emma
p = 988 mbar
T = 20.7 °C

HV_G (P8 ... P28) = 3975 V, I_G = 1072 μA
HV_A = 5950 V, I_A = 2 μA

HV_G (P15 ... P17) = 3950 V I_G = 687 μA
HV_A = 5950 V I_A = 0 μA

14/7/11 @ 11:20, file L1418.emma
p = 993 mbar
T = 20.6 °C

I_A^{marked} = 1 μ

P8 ok, P57-X3 missing, P14-X1-N missing,
P77-X2 poor, P30-X4 poor, P28-X3 missing

Apart from P57-X3 there is not much we can do. In P57-X3-A the clipper was broken (again the resistor burned?) in L1410 ⇒ new resistors (2×7W) in. Put in in the middle of L1420.emma, without stopping DAQ.

(P57-X3 is ok in L1421.emma)

T 15 (30)

15/7/2011 ~ 8:00 T15-L1440.emma — T = 22,1 °C, p = 992 mbar

P14-X1 weak
P77-X2 weak
P30-X4 weak
P28-X3 missing
P17-Y1 missing

18.7.11 @ 9:10, T15-L1512.emma — p = 984 mbar, T = 26.0 °C

P8 & P57 ok, P14-X1-N, P77-X2, P30-X4 and P28-X3 nok. P15 - P17 ok (apart from P17-Y1).

19/7.11 @ 8:50, T15-L1536 — p = 982 mbar, T = 24.6 °C

as 18.7.11.

20/7/2011 @ 1530 T15 - L1566 — P = 986 mbar, T = 26.6 °C

P14 X1, P77 X2, P30 X4 } weak
P28 X1 & X3 missing
P17 Y1 missing

21/7/2011 @ 0900 T15-L1584 — P = 985, T = 27.3 °C

P14 X1, P77 X2, P30 X4 weak
P28 X1, X3 missing
P17 Y3 missing

in P28-X1 A broken.

(31)

[illegible] @ 13:20 [illegible] moved from [illegible] to ch #127 (in TDC #0).

* New map-file map_T15-2011Jul21.plank

Valid from T15-L1590.emma

21/7/11 @ ~ 19:00 HV shut down in non-calibrated planks. Last full file

T15-L1594.emma

22/7/11 The forecast predicts hot over the weekend. ⇒ we carry on the calibration on Monday! — p = 983 mbar, T = 27.8 °C

25/7/11 @ 9:15 According to the forecast it will be hot over the week too. Thus the Ar dewar was not ordered and we carry on our break at least for a week (until next Tuesday a week after this one). — p = 991 mbar, T = 27.7 °C

30/7/11 @ 18:10 In dewar still some liquid, p_{dewar} = 13 bar. — T = 28.4 °C

31/7/11 @ 18:30 There's still some liquid in the dewar, p_{dewar} = 12.5 bar. — T = 28.0 °C

1/8/11 @ 9:25 Still some liquid! p_{dewar} = 12 bar. — T = 25.8 °C

2/8/11 @ 9:25, @ 12:45 Still some liquid, p_{dewar} = 10 bar. — T = 22.7 °C

3/8/11 @ 9:20 Dewar is empty (3 bar)! using the Ar-bottle (empty at ~14:00) STOP. @18:20 T = 24.9 °C DOORS STILL OPEN — T = 23.5 °C

4.8.2011 @ 9:30 — T: 25,2 °C

5.8/11 @ 9:30 — T: 24,5 °C
@ 15:30 T: 19.5 °C

8/8/2011 @ 9:00 — T = 27.5 °C, p = 967 mbar

9/8/2011 @ 0900 T= — T = 24.0 °C, P = 972 mbar

10/8/11 @ 9:30 — T = 23.6 °C, p = 974 mbar

11/08/11 — T: 22.1 °C, P = 977

10:45 HV raised to ~ 4 kV

14:45 HV for reference OK
calibration NOK I(A) = 150 μA

18:00 HV for reference operational voltages

HV for calibration 2 kV

12/8/11 @ 9:30 HV for calibrated ones nominal and ok, but for non-cal even 4k seem to result in problems: — T = 29.2 °C, p = 987 mbar

$HV_G^{non\text{-}cal}$ = 3950 V, I = 1066 μA
$HV_A^{non\text{-}cal}$ = 4000 V, I = 5 μA

@ 10:00 $HV_G^{non\text{-}cal}$ = 3975 V, I = 1073 μA
H_A " " " = 4800 V, I = 7 μA (no sparking or anything).

T 15

13/8/2011 — 22.2 °C

14/8/2011 @ 13:00 — 23,3 °C

@ 20:00 — 26.0 °C

15/8/11 @ 9:20 After the week end still $HV_A^{non\text{-}cal}$ = 4k and I = 7 μA ⇒ need to find the chamber can't stand HV. Testing P8, P57 & P14 ⇒ currents 531 and 2 μA for G and A, respectively. The problem turned out to be a HV-box. and P77-X4. — 23.9 °C, p = 998 mbar

@ 17:15 Currents ok ($I_A^{non\text{-}cal}$ ~ 4 μA) after disconnecting P77-X4. Trying to run calibration over night

Same map-file, $HV_G^{non\text{-}cal}$ = 3975 V, I ~ 4 μA — p = 997 mbar, T = 22.6 °C

The last file was T15-L1594.emma. Continuing to (P77-X4 disconnected for now).

@ 15/8/ 17:19 T15-L1600.emma (500 files, 1h each).

16/8/2011 0900 — T: 23.6 °C, P = 993 mbar

T15-1615.emma

OK P8, P15
P57, P39

NOK P14 X1 missing, P14 Y1 low
P77 X1, X4 missing, X2, Y1 low
P30 X1, X2, X4, Y1 low
P28 X1, X2, Y1 low, X3 missing

} One OR cable not connected

T15

34.

16/8/2011 @ 0940 New start T15-1620.emma

@ 1300 T15-1622.emma

p = 993 mbar
T = 23.4 °C

P8 ok
P57 ok
P30 x4 poor
P15 ok
P18 ok
P14 x1 NOK
P77 x1 & x4 missing
P28 x3 missing
P39 ok
P17 Y1 missing

$HV_G^{non-cal}$ from 3975V → 3950V in the middle of T15-L1623.emma.

Current rised from 2 μA to ~~7~~ 5-6 μA.

@ 13:39 STOP, last full file T15-L1623.emma.

P77-X4 fixed (new A & G cables). New HV settings 3975V for non-cal grading (decreasing it to 3950V decreased the efficiency of several chambers!) Now current is 3μA. Carrying on to

T15-L1625.emma

START @ 14:05

17/8/11 9:15 @ L1643

p = 990 mbar
T = 23.9 °C

P8, P57 ok, P14 (X1 N function) ok, P77 (X2 poor and X1 missing), P30 (X4 poor) ok, P28 (X3 missing) ok P15 P39 P18 and P17 (Y1 missing) ok.

17/8/ ∴ P77-X1 missing. STOP @ 9:37, last full file T15-L1643.emma The problem turned out to be a disconnected HV cable.

New start @ 10:30 to

T15-L1645.emma

Now all planks are ok in N-F (apart from P14-X1, P77-X2, P30-X4, P28-X3 and P17-Y1).

19.08.2011 10:15 N-F of T15-L1691.emma

T = 23.4 °C
p = 986 mbar

Similar situation as before.

22.08.2011 10:45 N-F of T15-L1764.emma

T = 25.5 °C*
p = 992 mbar

Similar situation as before.

23.08.2011 10:30 N-F of T15-L1787.emma

T = 25.2 °C
p = 993 mbar

Similar situation as before.

24.08.2011 9:15 N-F of T15-L1810.emma

(cooled lab)
T = 22.1 °C
p = 997 mbar

Similar situation as before.

25.08.2011 8:20 N-F of T15-L1833.emma

T = 23.8 °C
p = 997 mbar

P14-X1 getting even worse
Others as before.

* The doors were opened. 1 h later T = 23.0 °C.

T15

36.

26.08.2011 09:30 N-F of T15-L1857.emma

T = 21.6 °C
p = 997 mbar

P8 and P57 ok
P14 X1
P77 X2
P30 X4
P28 X3
P15, P39 and P18 OK
P17 Y1

28.08.2011 N-F of T15-L1910.emma

T = 26.4 °C
p = 982 mbar

P8, P57 ok
P14 X1
P77 X2
P30 X4
P28 X3
P15, P18 ok
P39 Y1t low
P17 Y1

28.8.2011 @ 1430 Last full file L1911.emma

Stopping measurement for some tests.

28.8.2011 @ 1435 New start first file L1912.emma

29.08.2011 8:00 N-F of T15-L1928.emma

T = 26.6 °C
p = 979 mbar

P28, P18, P39 } several weak chambers

others similar as before

T15

37.

30/8/11 9:30 @ L1953.emma has many problems!

p = 978 mbar
T = 20.3 °C

in L1955.emma

P8 ok
P57 Y2 missing, all poor except for Y1
P14 all X nok, Y ok
P77 all ok (except for X2, as an old problem)
P30 spikes and low rates
P28 low rates

P15 ok, P39 X ok, Y low rates, P18 X ok, Y poor and P17 ok.

⇒ due to low pressure HV_G → 3975V, (3980V in non-cal). First full file: L1957.emma.

P57-Y2A not counting, card broken (signal is there). Due to a lack of time and proper cards the problem is NOT fixed (less than one week to go and Y2s are counting ~ 6 f).

31.08.2011 08:30 N-F of T15-L1976.emma

p = 980 mbar
T = 21.6 °C

P8, P57 OK
P14 X1 NOK
P77 X2 NOK
P30 X4 NOK
} same as in the beginning

P28 Y1 and Y2 OK
X1, X2 and X4 poor
X3 not counting
P15 OK
P18 + P39 X's OK, Y's poor
P17 OK (Y1 not connected)

1/9/11 @ L2001 p = 983 mbar
9:00 T = 20.8 °C

P8 ok, P57 ok (Y2 still having a card problem)
P14 ok (X1N missing still), P77 ok (X2 still poor)
P30 ok (X4 still poor) but P28 has multiple
problems (only Y1 & Y2 are ok).

P15 & P17 are ok but P39 & P18 Ys have
problems (low rates, may be due to pressure).

During L2002 HV_4^{cal} lowered to 3950 V.

12:00 STOP. Last file T15-L2004.emma

The END of T15.

Appendix C

The order of the pictures is the following: first X-chambers (FA and NA), and then Y-chambers. X1-pictures are excluded from P8, P57, P14 and P77, because of no proper data. Also, X2-chambers' picture from P77 is excluded for the same reason. The reason remaining same. Some of the bad chambers are included as an example.

1st plankmapfile

```
--Place-|-Plank-|-Signal-|-TDC#-|-FLAT-CABLE-|-TDC-CHN
------------------------------------------------------
   T15     P8      X1A      1        A1          0
   T15     P8      X1N      1        A1          1
   T15     P8      X1F      1        A1          2
   T15     P8      Y1A      1        A2         16
   T15     P8      Y1N      1        A2         17
   T15     P8      Y1F      1        A2         18
   T15     P8      X2A      1        A1          3
   T15     P8      X2N      1        A1          4
   T15     P8      X2F      1        A1          5
   T15     P8      Y2A      1        A2         19
   T15     P8      Y2N      1        A2         20
   T15     P8      Y2F      1        A2         21
   T15     P8      X3A      1        A1          6
   T15     P8      X3N      1        A1          7
   T15     P8      X3F      1        A1          8
   T15     P8      Y3A      1        A2         22
   T15     P8      Y3N      1        A2         23
   T15     P8      Y3F      1        A2         24
   T15     P8      X4A      1        A1          9
   T15     P8      X4N      1        A1         10
   T15     P8      X4F      1        A1         11
------------------------------------------------------
   T15     P57     X1A      1        B1         32
   T15     P57     X1N      1        B1         33
   T15     P57     X1F      1        B1         34
   T15     P57     Y1A      1        A2         25
   T15     P57     Y1N      1        A2         26
   T15     P57     Y1F      1        A2         27
   T15     P57     X2A      1        B1         35
   T15     P57     X2N      1        B1         36
   T15     P57     X2F      1        B1         37
   T15     P57     Y2A      1        A2         28
   T15     P57     Y2N      1        A2         29
   T15     P57     Y2F      1        A2         30
   T15     P57     X3A      1        B1         79
   T15     P57     X3N      1        B1         13
   T15     P57     X3F      1        B1         14
   T15     P57     Y3A      1        A2         44
   T15     P57     Y3N      1        B1         45
   T15     P57     Y3F      1        B1         46
   T15     P57     X4A      1        B1         41
   T15     P57     X4N      1        B1         42
   T15     P57     X4F      1        B1         43
------------------------------------------------------
```

```
T15    P14    X1A    1    B2    63
T15    P14    X1N    1    B2    49
T15    P14    X1F    1    B2    50
T15    P14    Y1A    1    C1    64
T15    P14    Y1N    1    C1    65
T15    P14    Y1F    1    C1    66
T15    P14    X2A    1    B2    51
T15    P14    X2N    1    B2    52
T15    P14    X2F    1    B2    53
T15    P14    Y2A    1    C1    67
T15    P14    Y2N    1    C1    68
T15    P14    Y2F    1    C1    69
T15    P14    X3A    1    B2    54
T15    P14    X3N    1    B2    55
T15    P14    X3F    1    B2    56
T15    P14    Y3A    1    C1    70
T15    P14    Y3N    1    C1    71
T15    P14    Y3F    1    C1    72
T15    P14    X4A    1    B2    60
T15    P14    X4N    1    B2    58
T15    P14    X4F    1    B2    59
------------------------------------------------------------
T15    P77    X1A    1    C2    80
T15    P77    X1N    1    C2    81
T15    P77    X1F    1    C2    82
T15    P77    Y1A    1    C1    73
T15    P77    Y1N    1    C1    74
T15    P77    Y1F    1    C1    75
T15    P77    X2A    1    C2    83
T15    P77    X2N    1    C2    84
T15    P77    X2F    1    C2    85
T15    P77    Y2A    1    C1    76
T15    P77    Y2N    1    C1    77
T15    P77    Y2F    1    C1    78
T15    P77    X3A    1    C2    86
T15    P77    X3N    1    C2    87
T15    P77    X3F    1    C2    88
T15    P77    Y3A    1    C1    92
T15    P77    Y3N    1    C2    93
T15    P77    Y3F    1    C2    94
T15    P77    X4A    1    C2    89
T15    P77    X4N    1    C2    90
T15    P77    X4F    1    C2    91
------------------------------------------------------------
T15    P30    X1A    1    D1    96
T15    P30    X1N    1    D1    97
T15    P30    X1F    1    D1    98
T15    P30    Y1A    1    D2    112
T15    P30    Y1N    1    D2    113
T15    P30    Y1F    1    D2    114
T15    P30    X2A    1    D1    99
T15    P30    X2N    1    D1    100
T15    P30    X2F    1    D1    101
T15    P30    Y2A    1    D2    115
T15    P30    Y2N    1    D2    116
T15    P30    Y2F    1    D2    117
T15    P30    X3A    1    D1    102
T15    P30    X3N    1    D1    103
```

```
T15    P30    X3F    1    D1    104
T15    P30    Y3A    1    D2    118
T15    P30    Y3N    1    D2    119
T15    P30    Y3F    1    D2    120
T15    P30    X4A    1    D1    105
T15    P30    X4N    1    D1    106
T15    P30    X4F    1    D1    107
-----------------------------------------------------
T15    P28    X1A    0    D2    112
T15    P28    X1N    0    D2    113
T15    P28    X1F    0    D2    114
T15    P28    Y1A    1    D2    121
T15    P28    Y1N    1    D2    122
T15    P28    Y1F    1    D2    123
T15    P28    X2A    0    D2    115
T15    P28    X2N    0    D2    116
T15    P28    X2F    0    D2    117
T15    P28    Y2A    1    D2    124
T15    P28    Y2N    1    D2    125
T15    P28    Y2F    1    D2    126
T15    P28    X3A    0    D2    118
T15    P28    X3N    0    D2    119
T15    P28    X3F    0    D2    120
T15    P28    Y3A    0    D2    124
T15    P28    Y3N    0    D2    125
T15    P28    Y3F    0    D2    126
T15    P28    X4A    0    D2    121
T15    P28    X4N    0    D2    122
T15    P28    X4F    0    D2    123
-----------------------------------------------------
T15    P15    X1A    0    A1      0
T15    P15    X1N    0    A1      1
T15    P15    X1F    0    A1      2
T15    P15    Y1A    0    B1     32
T15    P15    Y1N    0    B1     33
T15    P15    Y1F    0    B1     34
T15    P15    X2A    0    A1      3
T15    P15    X2N    0    A1      4
T15    P15    X2F    0    A1      5
T15    P15    Y2A    0    B1     35
T15    P15    Y2N    0    B1     36
T15    P15    Y2F    0    B1     37
T15    P15    X3A    0    A1      6
T15    P15    X3N    0    A1      7
T15    P15    X3F    0    A1      8
T15    P15    Y3A    0    B1     38
T15    P15    Y3N    0    B1     39
T15    P15    Y3F    0    B1     40
T15    P15    X4A    0    A1      9
T15    P15    X4N    0    A1     10
T15    P15    X4F    0    A1     11
-----------------------------------------------------
T15    P39    X1A    0    C1     64
T15    P39    X1N    0    C1     65
T15    P39    X1F    0    C1     66
T15    P39    Y1A    0    D1     96
T15    P39    Y1N    0    D1     97
T15    P39    Y1F    0    D1     98
```

```
T15    P39    X2A    0    C1     67
T15    P39    X2N    0    C1     68
T15    P39    X2F    0    C1     69
T15    P39    Y2A    0    D1     99
T15    P39    Y2N    0    D1    100
T15    P39    Y2F    0    D1    101
T15    P39    X3A    0    C1     70
T15    P39    X3N    0    C1     71
T15    P39    X3F    0    C1     72
T15    P39    Y3A    0    D1    102
T15    P39    Y3N    0    D1    103
T15    P39    Y3F    0    D1    104
T15    P39    X4A    0    C1     73
T15    P39    X4N    0    C1     74
T15    P39    X4F    0    C1     75
-----------------------------------------------------------
T15    P18    X1A    0    C2     83
T15    P18    X1N    0    C2     84
T15    P18    X1F    0    C2     85
T15    P18    Y1A    0    D1    105
T15    P18    Y1N    0    D1    106
T15    P18    Y1F    0    D1    107
T15    P18    X2A    0    C2     80
T15    P18    X2N    0    C2     81
T15    P18    X2F    0    C2     82
T15    P18    Y2A    0    D1    108
T15    P18    Y2N    0    D1    109
T15    P18    Y2F    0    D1    110
T15    P18    X3A    0    C2     86
T15    P18    X3N    0    C2     87
T15    P18    X3F    0    C2     88
T15    P18    Y3A    0    D1    111
T15    P18    Y3N    0    C2     93
T15    P18    Y3F    0    C2     94
T15    P18    X4A    0    C2     89
T15    P18    X4N    0    C2     90
T15    P18    X4F    0    C2     91
-----------------------------------------------------------
T15    P17    X1A    0    A1     16
T15    P17    X1N    0    A1     17
T15    P17    X1F    0    A1     18
T15    P17    Y1A    0    B2     -1
T15    P17    Y1N    0    B2     -1
T15    P17    Y1F    0    B2     -1
T15    P17    X2A    0    A1     19
T15    P17    X2N    0    A1     20
T15    P17    X2F    0    A1     21
T15    P17    Y2A    0    B2     31
T15    P17    Y2N    0    B2     52
T15    P17    Y2F    0    B2     53
T15    P17    X3A    0    A1     28
T15    P17    X3N    0    A1     29
T15    P17    X3F    0    A1     30
T15    P17    Y3A    0    B2     54
T15    P17    Y3N    0    B2     55
T15    P17    Y3F    0    B2     56
T15    P17    X4A    0    A1     25
T15    P17    X4N    0    A1     26
```

```
    T15      P17      X4F       0        A1          27
STOP

Before T15:

    T15      P17      Y2A       0        B2          60
```

2nd plankmapfile

```
--Place-|-Plank-|-Signal-|-TDC#-|-FLAT-CABLE-|-TDC-CHN
------------------------------------------------------
    T15      P8       X1A       1        A1           0
    T15      P8       X1N       1        A1           1
    T15      P8       X1F       1        A1           2
    T15      P8       Y1A       1        A2          16
    T15      P8       Y1N       1        A2          17
    T15      P8       Y1F       1        A2          18
    T15      P8       X2A       1        A1           3
    T15      P8       X2N       1        A1           4
    T15      P8       X2F       1        A1           5
    T15      P8       Y2A       1        A2          19
    T15      P8       Y2N       1        A2          20
    T15      P8       Y2F       1        A2          21
    T15      P8       X3A       1        A1           6
    T15      P8       X3N       1        A1           7
    T15      P8       X3F       1        A1           8
    T15      P8       Y3A       1        A2          22
    T15      P8       Y3N       1        A2          23
    T15      P8       Y3F       1        A2          24
    T15      P8       X4A       1        A1           9
    T15      P8       X4N       1        A1          10
    T15      P8       X4F       1        A1          11
------------------------------------------------------
    T15      P57      X1A       1        B1          32
    T15      P57      X1N       1        B1          33
    T15      P57      X1F       1        B1          34
    T15      P57      Y1A       1        A2          25
    T15      P57      Y1N       1        A2          26
    T15      P57      Y1F       1        A2          27
    T15      P57      X2A       1        B1          35
    T15      P57      X2N       1        B1          36
    T15      P57      X2F       1        B1          37
    T15      P57      Y2A       1        A2          28
    T15      P57      Y2N       1        A2          29
    T15      P57      Y2F       1        A2          30
    T15      P57      X3A       1        B1         111
    T15      P57      X3N       1        B1          13
    T15      P57      X3F       1        B1          14
    T15      P57      Y3A       1        A2          44
    T15      P57      Y3N       1        B1          45
    T15      P57      Y3F       1        B1          46
    T15      P57      X4A       1        B1          41
    T15      P57      X4N       1        B1          42
    T15      P57      X4F       1        B1          43
------------------------------------------------------
    T15      P14      X1A       1        B2          63
```

```
T15     P14     X1N      1       B2        49
T15     P14     X1F      1       B2        50
T15     P14     Y1A      1       C1        64
T15     P14     Y1N      1       C1        65
T15     P14     Y1F      1       C1        66
T15     P14     X2A      1       B2        51
T15     P14     X2N      1       B2        52
T15     P14     X2F      1       B2        53
T15     P14     Y2A      1       C1        67
T15     P14     Y2N      1       C1        68
T15     P14     Y2F      1       C1        69
T15     P14     X3A      1       B2        54
T15     P14     X3N      1       B2        55
T15     P14     X3F      1       B2        56
T15     P14     Y3A      1       C1        70
T15     P14     Y3N      1       C1        71
T15     P14     Y3F      1       C1        72
T15     P14     X4A      1       B2        60
T15     P14     X4N      1       B2        58
T15     P14     X4F      1       B2        59
--------------------------------------------------
T15     P77     X1A      1       C2        80
T15     P77     X1N      1       C2        81
T15     P77     X1F      1       C2        82
T15     P77     Y1A      1       C1        73
T15     P77     Y1N      1       C1        74
T15     P77     Y1F      1       C1        75
T15     P77     X2A      1       C2        83
T15     P77     X2N      1       C2        84
T15     P77     X2F      1       C2        85
T15     P77     Y2A      1       C1        76
T15     P77     Y2N      1       C1        77
T15     P77     Y2F      1       C1        78
T15     P77     X3A      1       C2        86
T15     P77     X3N      1       C2        87
T15     P77     X3F      1       C2        88
T15     P77     Y3A      1       C1        92
T15     P77     Y3N      1       C2        93
T15     P77     Y3F      1       C2        94
T15     P77     X4A      1       C2        89
T15     P77     X4N      1       C2        90
T15     P77     X4F      1       C2        91
--------------------------------------------------
T15     P30     X1A      1       D1        96
T15     P30     X1N      1       D1        97
T15     P30     X1F      1       D1        98
T15     P30     Y1A      1       D2       112
T15     P30     Y1N      1       D2       113
T15     P30     Y1F      1       D2       114
T15     P30     X2A      1       D1        99
T15     P30     X2N      1       D1       100
T15     P30     X2F      1       D1       101
T15     P30     Y2A      1       D2       115
T15     P30     Y2N      1       D2       116
T15     P30     Y2F      1       D2       117
T15     P30     X3A      1       D1       102
T15     P30     X3N      1       D1       103
T15     P30     X3F      1       D1       104
```

```
  T15    P30    Y3A    1    D2    118
  T15    P30    Y3N    1    D2    119
  T15    P30    Y3F    1    D2    120
  T15    P30    X4A    1    D1    105
  T15    P30    X4N    1    D1    106
  T15    P30    X4F    1    D1    107
---------------------------------------------------
  T15    P28    X1A    0    D2    112
  T15    P28    X1N    0    D2    113
  T15    P28    X1F    0    D2    114
  T15    P28    Y1A    1    D2    121
  T15    P28    Y1N    1    D2    122
  T15    P28    Y1F    1    D2    123
  T15    P28    X2A    0    D2    115
  T15    P28    X2N    0    D2    116
  T15    P28    X2F    0    D2    117
  T15    P28    Y2A    1    D2    124
  T15    P28    Y2N    1    D2    125
  T15    P28    Y2F    1    D2    126
  T15    P28    X3A    0    D2    118
  T15    P28    X3N    0    D2    119
  T15    P28    X3F    0    D2    120
  T15    P28    Y3A    0    D2    124
  T15    P28    Y3N    0    D2    125
  T15    P28    Y3F    0    D2    126
  T15    P28    X4A    0    D2    121
  T15    P28    X4N    0    D2    122
  T15    P28    X4F    0    D2    123
---------------------------------------------------
  T15    P15    X1A    0    A1      0
  T15    P15    X1N    0    A1      1
  T15    P15    X1F    0    A1      2
  T15    P15    Y1A    0    B1     32
  T15    P15    Y1N    0    B1     33
  T15    P15    Y1F    0    B1     34
  T15    P15    X2A    0    A1      3
  T15    P15    X2N    0    A1      4
  T15    P15    X2F    0    A1      5
  T15    P15    Y2A    0    B1     35
  T15    P15    Y2N    0    B1     36
  T15    P15    Y2F    0    B1     37
  T15    P15    X3A    0    A1      6
  T15    P15    X3N    0    A1      7
  T15    P15    X3F    0    A1      8
  T15    P15    Y3A    0    B1     38
  T15    P15    Y3N    0    B1     39
  T15    P15    Y3F    0    B1     40
  T15    P15    X4A    0    A1      9
  T15    P15    X4N    0    A1     10
  T15    P15    X4F    0    A1     11
---------------------------------------------------
  T15    P39    X1A    0    C1     64
  T15    P39    X1N    0    C1     65
  T15    P39    X1F    0    C1     66
  T15    P39    Y1A    0    D1     96
  T15    P39    Y1N    0    D1     97
  T15    P39    Y1F    0    D1     98
  T15    P39    X2A    0    C1     67
```

```
T15     P39     X2N     0     C1      68
T15     P39     X2F     0     C1      69
T15     P39     Y2A     0     D1      99
T15     P39     Y2N     0     D1     100
T15     P39     Y2F     0     D1     101
T15     P39     X3A     0     C1      70
T15     P39     X3N     0     C1      71
T15     P39     X3F     0     C1      72
T15     P39     Y3A     0     D1     102
T15     P39     Y3N     0     D1     103
T15     P39     Y3F     0     D1     104
T15     P39     X4A     0     C1      73
T15     P39     X4N     0     C1      74
T15     P39     X4F     0     C1      75
--------------------------------------------------------
T15     P18     X1A     0     C2      83
T15     P18     X1N     0     C2      84
T15     P18     X1F     0     C2      85
T15     P18     Y1A     0     D1     105
T15     P18     Y1N     0     D1     106
T15     P18     Y1F     0     D1     107
T15     P18     X2A     0     C2      80
T15     P18     X2N     0     C2      81
T15     P18     X2F     0     C2      82
T15     P18     Y2A     0     D1     108
T15     P18     Y2N     0     D1     109
T15     P18     Y2F     0     D1     110
T15     P18     X3A     0     C2      86
T15     P18     X3N     0     C2      87
T15     P18     X3F     0     C2      88
T15     P18     Y3A     0     D1     111
T15     P18     Y3N     0     C2      93
T15     P18     Y3F     0     C2      94
T15     P18     X4A     0     C2      89
T15     P18     X4N     0     C2      90
T15     P18     X4F     0     C2      91
--------------------------------------------------------
T15     P17     X1A     0     A1      16
T15     P17     X1N     0     A1      17
T15     P17     X1F     0     A1      18
T15     P17     Y1A     0     B2      -1
T15     P17     Y1N     0     B2      -1
T15     P17     Y1F     0     B2      -1
T15     P17     X2A     0     A1      19
T15     P17     X2N     0     A1      20
T15     P17     X2F     0     A1      21
T15     P17     Y2A     0     B2      31
T15     P17     Y2N     0     B2      52
T15     P17     Y2F     0     B2      53
T15     P17     X3A     0     A1      28
T15     P17     X3N     0     A1      29
T15     P17     X3F     0     A1      30
T15     P17     Y3A     0     B2      54
T15     P17     Y3N     0     B2      55
T15     P17     Y3F     0     B2      56
T15     P17     X4A     0     A1      25
T15     P17     X4N     0     A1      26
T15     P17     X4F     0     A1      27
```

```
STOP

Before T15:

    T15     P17     Y2A      0       B2          60
```

3rd plankmapfile

```
--Place-|-Plank-|-Signal-|-TDC#-|-FLAT-CABLE-|-TDC-CHN
-------------------------------------------------------
    T15     P8      X1A      1       A1           0
    T15     P8      X1N      1       A1           1
    T15     P8      X1F      1       A1           2
    T15     P8      Y1A      1       A2          16
    T15     P8      Y1N      1       A2          17
    T15     P8      Y1F      1       A2          18
    T15     P8      X2A      1       A1           3
    T15     P8      X2N      1       A1           4
    T15     P8      X2F      1       A1           5
    T15     P8      Y2A      1       A2          19
    T15     P8      Y2N      1       A2          20
    T15     P8      Y2F      1       A2          21
    T15     P8      X3A      1       A1           6
    T15     P8      X3N      1       A1           7
    T15     P8      X3F      1       A1           8
    T15     P8      Y3A      1       A2          22
    T15     P8      Y3N      1       A2          23
    T15     P8      Y3F      1       A2          24
    T15     P8      X4A      1       A1           9
    T15     P8      X4N      1       A1          10
    T15     P8      X4F      1       A1          11
-------------------------------------------------------
    T15     P57     X1A      1       B1          32
    T15     P57     X1N      1       B1          33
    T15     P57     X1F      1       B1          34
    T15     P57     Y1A      1       A2          25
    T15     P57     Y1N      1       A2          26
    T15     P57     Y1F      1       A2          27
    T15     P57     X2A      1       B1          35
    T15     P57     X2N      1       B1          36
    T15     P57     X2F      1       B1          37
    T15     P57     Y2A      1       A2          28
    T15     P57     Y2N      1       A2          29
    T15     P57     Y2F      1       A2          30
    T15     P57     X3A      1       B1         111
    T15     P57     X3N      1       B1          13
    T15     P57     X3F      1       B1          14
    T15     P57     Y3A      1       A2          44
    T15     P57     Y3N      1       B1          45
    T15     P57     Y3F      1       B1          46
    T15     P57     X4A      1       B1          41
    T15     P57     X4N      1       B1          42
    T15     P57     X4F      1       B1          43
-------------------------------------------------------
    T15     P14     X1A      1       B2         108
    T15     P14     X1N      1       B2          49
```

```
T15   P14   X1F   1   B2    50
T15   P14   Y1A   1   C1    64
T15   P14   Y1N   1   C1    65
T15   P14   Y1F   1   C1    66
T15   P14   X2A   1   B2    51
T15   P14   X2N   1   B2    52
T15   P14   X2F   1   B2    53
T15   P14   Y2A   1   C1    67
T15   P14   Y2N   1   C1    68
T15   P14   Y2F   1   C1    69
T15   P14   X3A   1   B2    54
T15   P14   X3N   1   B2    55
T15   P14   X3F   1   B2    56
T15   P14   Y3A   1   C1    70
T15   P14   Y3N   1   C1    71
T15   P14   Y3F   1   C1    72
T15   P14   X4A   1   B2    60
T15   P14   X4N   1   B2    58
T15   P14   X4F   1   B2    59
--------------------------------------------------------
T15   P77   X1A   1   C2    80
T15   P77   X1N   1   C2    81
T15   P77   X1F   1   C2    82
T15   P77   Y1A   1   C1    73
T15   P77   Y1N   1   C1    74
T15   P77   Y1F   1   C1    75
T15   P77   X2A   1   C2    83
T15   P77   X2N   1   C2    84
T15   P77   X2F   1   C2    85
T15   P77   Y2A   1   C1    76
T15   P77   Y2N   1   C1    77
T15   P77   Y2F   1   C1    78
T15   P77   X3A   1   C2    86
T15   P77   X3N   1   C2    87
T15   P77   X3F   1   C2    88
T15   P77   Y3A   1   C1    92
T15   P77   Y3N   1   C2    93
T15   P77   Y3F   1   C2    94
T15   P77   X4A   1   C2    89
T15   P77   X4N   1   C2    90
T15   P77   X4F   1   C2    91
--------------------------------------------------------
T15   P30   X1A   1   D1    96
T15   P30   X1N   1   D1    97
T15   P30   X1F   1   D1    98
T15   P30   Y1A   1   D2   112
T15   P30   Y1N   1   D2   113
T15   P30   Y1F   1   D2   114
T15   P30   X2A   1   D1    99
T15   P30   X2N   1   D1   100
T15   P30   X2F   1   D1   101
T15   P30   Y2A   1   D2   115
T15   P30   Y2N   1   D2   116
T15   P30   Y2F   1   D2   117
T15   P30   X3A   1   D1   102
T15   P30   X3N   1   D1   103
T15   P30   X3F   1   D1   104
T15   P30   Y3A   1   D2   118
```

```
     T15      P30      Y3N       1         D2          119
     T15      P30      Y3F       1         D2          120
     T15      P30      X4A       1         D1          105
     T15      P30      X4N       1         D1          106
     T15      P30      X4F       1         D1          107
--------------------------------------------------------------
     T15      P28      X1A       0         D2          112
     T15      P28      X1N       0         D2          113
     T15      P28      X1F       0         D2          114
     T15      P28      Y1A       1         D2          121
     T15      P28      Y1N       1         D2          122
     T15      P28      Y1F       1         D2          123
     T15      P28      X2A       0         D2          115
     T15      P28      X2N       0         D2          116
     T15      P28      X2F       0         D2          117
     T15      P28      Y2A       1         D2          124
     T15      P28      Y2N       1         D2          125
     T15      P28      Y2F       1         D2          126
     T15      P28      X3A       0         D2          118
     T15      P28      X3N       0         D2          119
     T15      P28      X3F       0         D2          120
     T15      P28      Y3A       0         D2          124
     T15      P28      Y3N       0         D2          125
     T15      P28      Y3F       0         D2          126
     T15      P28      X4A       0         D2          121
     T15      P28      X4N       0         D2          122
     T15      P28      X4F       0         D2          123
--------------------------------------------------------------
     T15      P15      X1A       0         A1            0
     T15      P15      X1N       0         A1            1
     T15      P15      X1F       0         A1            2
     T15      P15      Y1A       0         B1           32
     T15      P15      Y1N       0         B1           33
     T15      P15      Y1F       0         B1           34
     T15      P15      X2A       0         A1            3
     T15      P15      X2N       0         A1            4
     T15      P15      X2F       0         A1            5
     T15      P15      Y2A       0         B1           35
     T15      P15      Y2N       0         B1           36
     T15      P15      Y2F       0         B1           37
     T15      P15      X3A       0         A1            6
     T15      P15      X3N       0         A1            7
     T15      P15      X3F       0         A1            8
     T15      P15      Y3A       0         B1           38
     T15      P15      Y3N       0         B1           39
     T15      P15      Y3F       0         B1           40
     T15      P15      X4A       0         A1            9
     T15      P15      X4N       0         A1           10
     T15      P15      X4F       0         A1           11
--------------------------------------------------------------
     T15      P39      X1A       0         C1           64
     T15      P39      X1N       0         C1           65
     T15      P39      X1F       0         C1           66
     T15      P39      Y1A       0         D1           96
     T15      P39      Y1N       0         D1           97
     T15      P39      Y1F       0         D1           98
     T15      P39      X2A       0         C1           67
     T15      P39      X2N       0         C1           68
```

```
    T15    P39    X2F    0    C1     69
    T15    P39    Y2A    0    D1     99
    T15    P39    Y2N    0    D1    100
    T15    P39    Y2F    0    D1    101
    T15    P39    X3A    0    C1     70
    T15    P39    X3N    0    C1     71
    T15    P39    X3F    0    C1     72
    T15    P39    Y3A    0    D1    102
    T15    P39    Y3N    0    D1    103
    T15    P39    Y3F    0    D1    104
    T15    P39    X4A    0    C1     73
    T15    P39    X4N    0    C1     74
    T15    P39    X4F    0    C1     75
-------------------------------------------------------
    T15    P18    X1A    0    C2     83
    T15    P18    X1N    0    C2     84
    T15    P18    X1F    0    C2     85
    T15    P18    Y1A    0    D1    105
    T15    P18    Y1N    0    D1    106
    T15    P18    Y1F    0    D1    107
    T15    P18    X2A    0    C2     80
    T15    P18    X2N    0    C2     81
    T15    P18    X2F    0    C2     82
    T15    P18    Y2A    0    D1    108
    T15    P18    Y2N    0    D1    109
    T15    P18    Y2F    0    D1    110
    T15    P18    X3A    0    C2     86
    T15    P18    X3N    0    C2     87
    T15    P18    X3F    0    C2     88
    T15    P18    Y3A    0    D1    111
    T15    P18    Y3N    0    C2     93
    T15    P18    Y3F    0    C2     94
    T15    P18    X4A    0    C2     89
    T15    P18    X4N    0    C2     90
    T15    P18    X4F    0    C2     91
-------------------------------------------------------
    T15    P17    X1A    0    A1     16
    T15    P17    X1N    0    A1     17
    T15    P17    X1F    0    A1     18
    T15    P17    Y1A    0    B2     -1
    T15    P17    Y1N    0    B2     -1
    T15    P17    Y1F    0    B2     -1
    T15    P17    X2A    0    A1     19
    T15    P17    X2N    0    A1     20
    T15    P17    X2F    0    A1     21
    T15    P17    Y2A    0    B2     31
    T15    P17    Y2N    0    B2     52
    T15    P17    Y2F    0    B2     53
    T15    P17    X3A    0    A1     28
    T15    P17    X3N    0    A1     29
    T15    P17    X3F    0    A1     30
    T15    P17    Y3A    0    B2     54
    T15    P17    Y3N    0    B2     55
    T15    P17    Y3F    0    B2     56
    T15    P17    X4A    0    A1     25
    T15    P17    X4N    0    A1     26
    T15    P17    X4F    0    A1     27
STOP
```

```
Before T15:

    T15       P17       Y2A         0         B2            60
```

4th plankmapfile

```
--Place-|-Plank-|-Signal-|-TDC#-|-FLAT-CABLE-|-TDC-CHN
------------------------------------------------------
    T15       P8        X1A         1         A1             0
    T15       P8        X1N         1         A1             1
    T15       P8        X1F         1         A1             2
    T15       P8        Y1A         1         A2            16
    T15       P8        Y1N         1         A2            17
    T15       P8        Y1F         1         A2            18
    T15       P8        X2A         1         A1             3
    T15       P8        X2N         1         A1             4
    T15       P8        X2F         1         A1             5
    T15       P8        Y2A         1         A2            19
    T15       P8        Y2N         1         A2            20
    T15       P8        Y2F         1         A2            21
    T15       P8        X3A         1         A1             6
    T15       P8        X3N         1         A1             7
    T15       P8        X3F         1         A1             8
    T15       P8        Y3A         1         A2            22
    T15       P8        Y3N         1         A2            23
    T15       P8        Y3F         1         A2            24
    T15       P8        X4A         1         A1             9
    T15       P8        X4N         1         A1            10
    T15       P8        X4F         1         A1            11
------------------------------------------------------
    T15       P57       X1A         1         B1            32
    T15       P57       X1N         1         B1            33
    T15       P57       X1F         1         B1            34
    T15       P57       Y1A         1         A2            25
    T15       P57       Y1N         1         A2            26
    T15       P57       Y1F         1         A2            27
    T15       P57       X2A         1         B1            35
    T15       P57       X2N         1         B1            36
    T15       P57       X2F         1         B1            37
    T15       P57       Y2A         1         A2            28
    T15       P57       Y2N         1         A2            29
    T15       P57       Y2F         1         A2            30
    T15       P57       X3A         1         B1           111
    T15       P57       X3N         1         B1            13
    T15       P57       X3F         1         B1            14
    T15       P57       Y3A         1         A2            44
    T15       P57       Y3N         1         B1            45
    T15       P57       Y3F         1         B1            46
    T15       P57       X4A         1         B1            41
    T15       P57       X4N         1         B1            42
    T15       P57       X4F         1         B1            43
------------------------------------------------------
    T15       P14       X1A         1         B2           108
    T15       P14       X1N         1         B2            49
    T15       P14       X1F         1         B2            50
```

```
T15     P14     Y1A     1     C1      64
T15     P14     Y1N     1     C1      65
T15     P14     Y1F     1     C1      66
T15     P14     X2A     1     B2      51
T15     P14     X2N     1     B2      52
T15     P14     X2F     1     B2      53
T15     P14     Y2A     1     C1      67
T15     P14     Y2N     1     C1      68
T15     P14     Y2F     1     C1      69
T15     P14     X3A     1     B2      54
T15     P14     X3N     1     B2      55
T15     P14     X3F     1     B2      56
T15     P14     Y3A     1     C1      70
T15     P14     Y3N     1     C1      71
T15     P14     Y3F     1     C1      72
T15     P14     X4A     1     B2      60
T15     P14     X4N     1     B2      58
T15     P14     X4F     1     B2      59
------------------------------------------------------------
T15     P77     X1A     1     C2      80
T15     P77     X1N     1     C2      81
T15     P77     X1F     1     C2      82
T15     P77     Y1A     1     C1      73
T15     P77     Y1N     1     C1      74
T15     P77     Y1F     1     C1      75
T15     P77     X2A     1     C2      83
T15     P77     X2N     1     C2      84
T15     P77     X2F     1     C2      85
T15     P77     Y2A     1     C1      76
T15     P77     Y2N     1     C1      77
T15     P77     Y2F     1     C1      78
T15     P77     X3A     1     C2      86
T15     P77     X3N     1     C2      87
T15     P77     X3F     1     C2      88
T15     P77     Y3A     1     C1      92
T15     P77     Y3N     1     C2      93
T15     P77     Y3F     1     C2      94
T15     P77     X4A     1     C2      89
T15     P77     X4N     1     C2      90
T15     P77     X4F     1     C2      91
------------------------------------------------------------
T15     P30     X1A     1     D1      96
T15     P30     X1N     1     D1      97
T15     P30     X1F     1     D1      98
T15     P30     Y1A     1     D2     112
T15     P30     Y1N     1     D2     113
T15     P30     Y1F     1     D2     114
T15     P30     X2A     1     D1      99
T15     P30     X2N     1     D1     100
T15     P30     X2F     1     D1     101
T15     P30     Y2A     1     D2     115
T15     P30     Y2N     1     D2     116
T15     P30     Y2F     1     D2     117
T15     P30     X3A     1     D1     102
T15     P30     X3N     1     D1     103
T15     P30     X3F     1     D1     104
T15     P30     Y3A     1     D2     118
T15     P30     Y3N     1     D2     119
```

```
   T15     P30     Y3F       1         D2           120
   T15     P30     X4A       1         D1           105
   T15     P30     X4N       1         D1           106
   T15     P30     X4F       1         D1           107
--------------------------------------------------------
   T15     P28     X1A       0         D2           127
   T15     P28     X1N       0         D2           113
   T15     P28     X1F       0         D2           114
   T15     P28     Y1A       1         D2           121
   T15     P28     Y1N       1         D2           122
   T15     P28     Y1F       1         D2           123
   T15     P28     X2A       0         D2           115
   T15     P28     X2N       0         D2           116
   T15     P28     X2F       0         D2           117
   T15     P28     Y2A       1         D2           124
   T15     P28     Y2N       1         D2           125
   T15     P28     Y2F       1         D2           126
   T15     P28     X3A       0         D2           118
   T15     P28     X3N       0         D2           119
   T15     P28     X3F       0         D2           120
   T15     P28     Y3A       0         D2           124
   T15     P28     Y3N       0         D2           125
   T15     P28     Y3F       0         D2           126
   T15     P28     X4A       0         D2           121
   T15     P28     X4N       0         D2           122
   T15     P28     X4F       0         D2           123
--------------------------------------------------------
   T15     P15     X1A       0         A1             0
   T15     P15     X1N       0         A1             1
   T15     P15     X1F       0         A1             2
   T15     P15     Y1A       0         B1            32
   T15     P15     Y1N       0         B1            33
   T15     P15     Y1F       0         B1            34
   T15     P15     X2A       0         A1             3
   T15     P15     X2N       0         A1             4
   T15     P15     X2F       0         A1             5
   T15     P15     Y2A       0         B1            35
   T15     P15     Y2N       0         B1            36
   T15     P15     Y2F       0         B1            37
   T15     P15     X3A       0         A1             6
   T15     P15     X3N       0         A1             7
   T15     P15     X3F       0         A1             8
   T15     P15     Y3A       0         B1            38
   T15     P15     Y3N       0         B1            39
   T15     P15     Y3F       0         B1            40
   T15     P15     X4A       0         A1             9
   T15     P15     X4N       0         A1            10
   T15     P15     X4F       0         A1            11
--------------------------------------------------------
   T15     P39     X1A       0         C1            64
   T15     P39     X1N       0         C1            65
   T15     P39     X1F       0         C1            66
   T15     P39     Y1A       0         D1            96
   T15     P39     Y1N       0         D1            97
   T15     P39     Y1F       0         D1            98
   T15     P39     X2A       0         C1            67
   T15     P39     X2N       0         C1            68
   T15     P39     X2F       0         C1            69
```

```
    T15     P39     Y2A     0     D1      99
    T15     P39     Y2N     0     D1     100
    T15     P39     Y2F     0     D1     101
    T15     P39     X3A     0     C1      70
    T15     P39     X3N     0     C1      71
    T15     P39     X3F     0     C1      72
    T15     P39     Y3A     0     D1     102
    T15     P39     Y3N     0     D1     103
    T15     P39     Y3F     0     D1     104
    T15     P39     X4A     0     C1      73
    T15     P39     X4N     0     C1      74
    T15     P39     X4F     0     C1      75
-------------------------------------------------------
    T15     P18     X1A     0     C2      83
    T15     P18     X1N     0     C2      84
    T15     P18     X1F     0     C2      85
    T15     P18     Y1A     0     D1     105
    T15     P18     Y1N     0     D1     106
    T15     P18     Y1F     0     D1     107
    T15     P18     X2A     0     C2      80
    T15     P18     X2N     0     C2      81
    T15     P18     X2F     0     C2      82
    T15     P18     Y2A     0     D1     108
    T15     P18     Y2N     0     D1     109
    T15     P18     Y2F     0     D1     110
    T15     P18     X3A     0     C2      86
    T15     P18     X3N     0     C2      87
    T15     P18     X3F     0     C2      88
    T15     P18     Y3A     0     D1     111
    T15     P18     Y3N     0     C2      93
    T15     P18     Y3F     0     C2      94
    T15     P18     X4A     0     C2      89
    T15     P18     X4N     0     C2      90
    T15     P18     X4F     0     C2      91
-------------------------------------------------------
    T15     P17     X1A     0     A1      16
    T15     P17     X1N     0     A1      17
    T15     P17     X1F     0     A1      18
    T15     P17     Y1A     0     B2      -1
    T15     P17     Y1N     0     B2      -1
    T15     P17     Y1F     0     B2      -1
    T15     P17     X2A     0     A1      19
    T15     P17     X2N     0     A1      20
    T15     P17     X2F     0     A1      21
    T15     P17     Y2A     0     B2      31
    T15     P17     Y2N     0     B2      52
    T15     P17     Y2F     0     B2      53
    T15     P17     X3A     0     A1      28
    T15     P17     X3N     0     A1      29
    T15     P17     X3F     0     A1      30
    T15     P17     Y3A     0     B2      54
    T15     P17     Y3N     0     B2      55
    T15     P17     Y3F     0     B2      56
    T15     P17     X4A     0     A1      25
    T15     P17     X4N     0     A1      26
    T15     P17     X4F     0     A1      27
STOP
```

```
Before T15:

    T15      P17      Y2A        0          B2            60
```

Appendix D

P8

X2: NA and FA

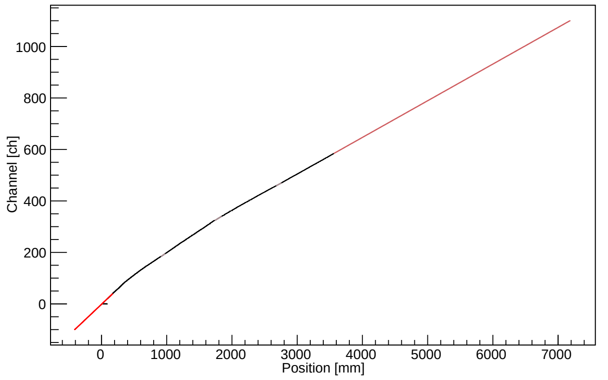

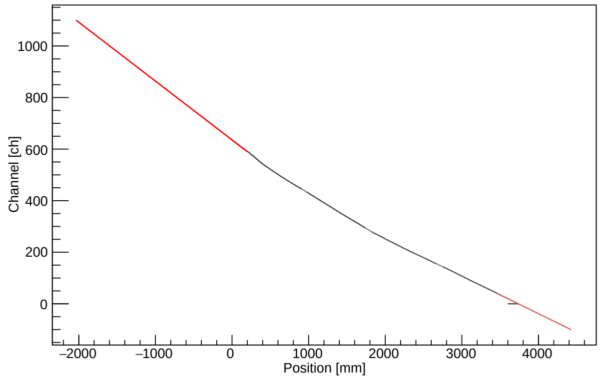

X3: NA and FA

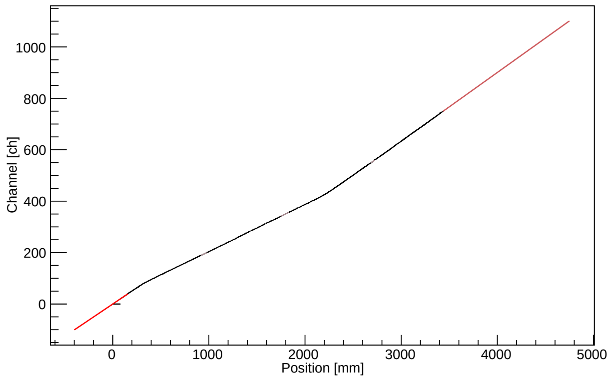

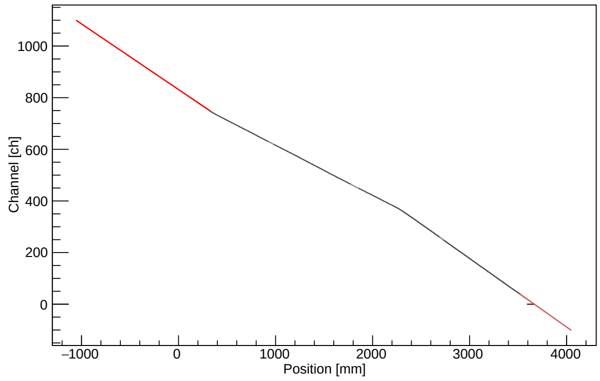

X4: NA and FA

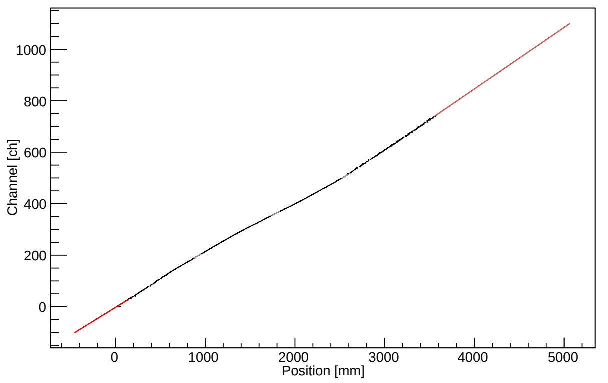

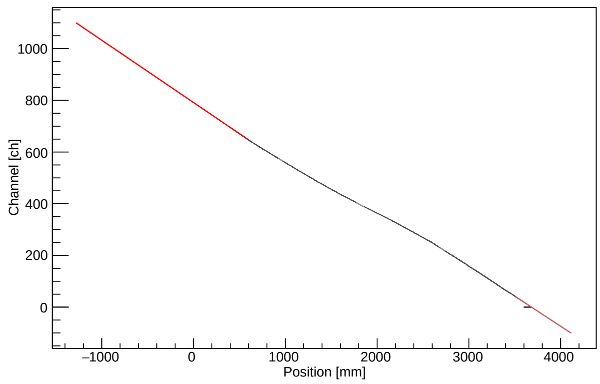

Y1: NA and FA

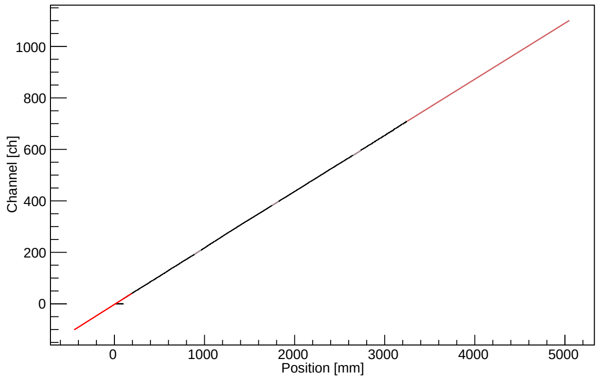

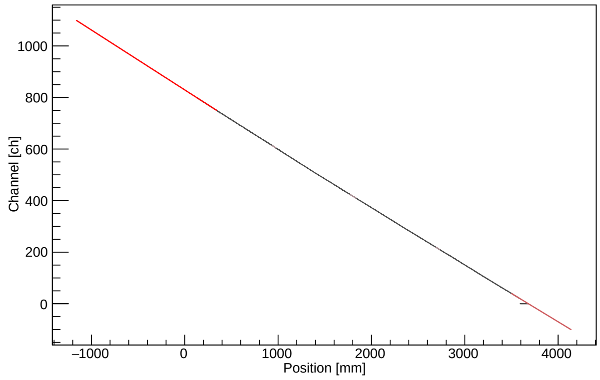

Y2: NA and FA

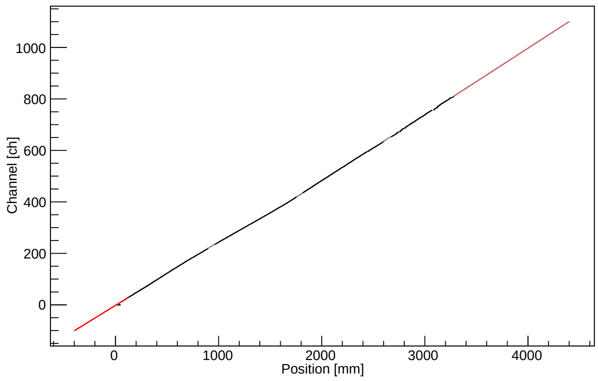

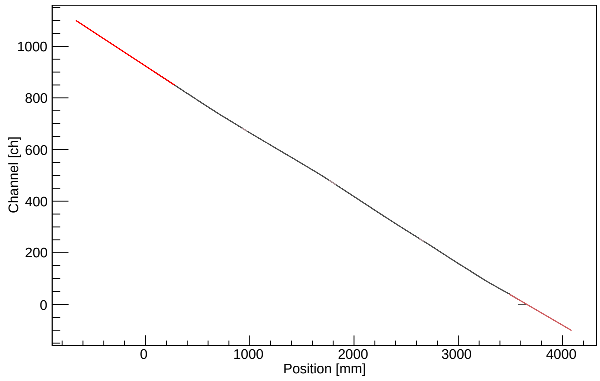

Y3: NA and FA

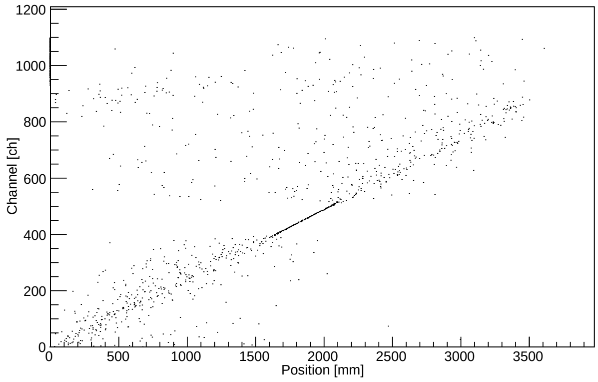

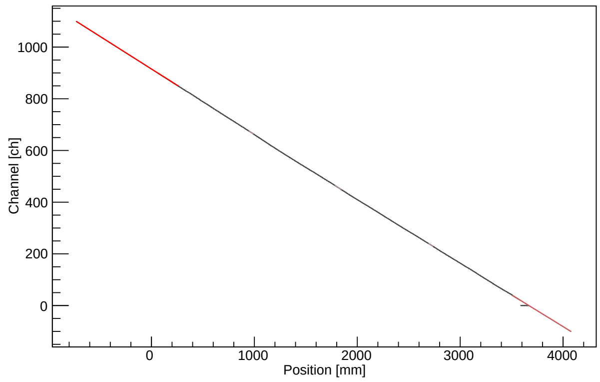

P57

X2: NA and FA

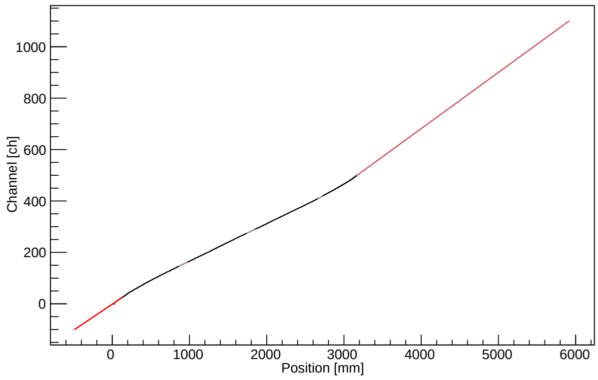

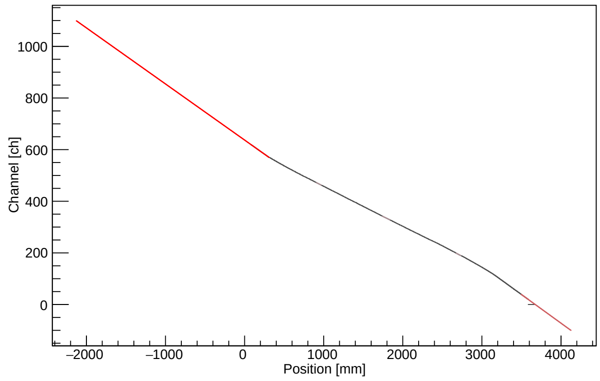

X3: NA and FA

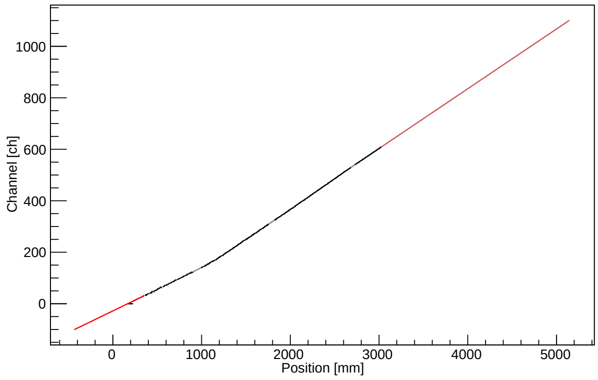

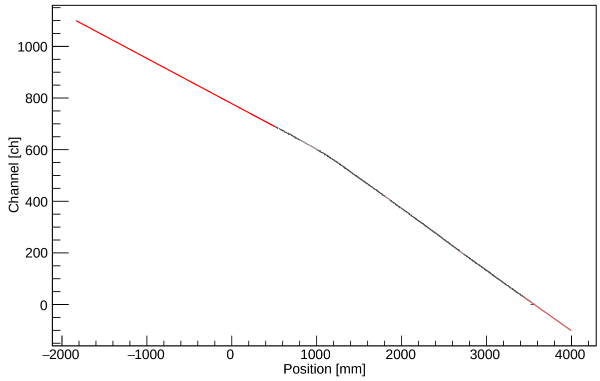

X4: NA and FA

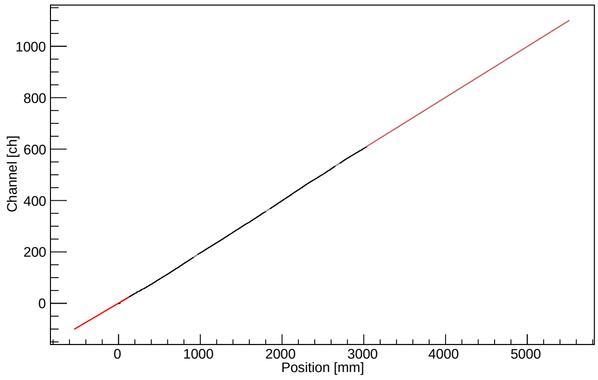

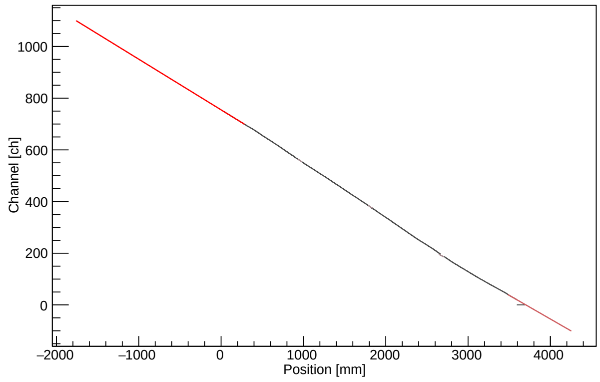

Y1: NA and FA

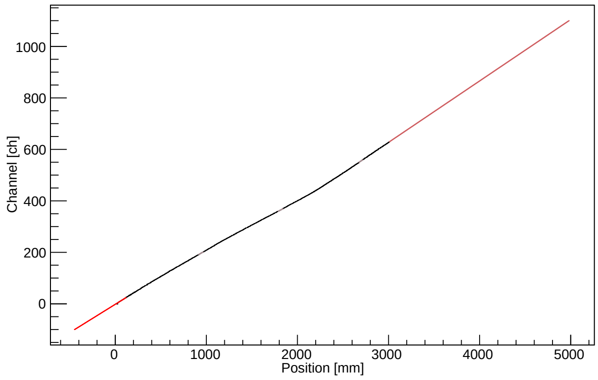

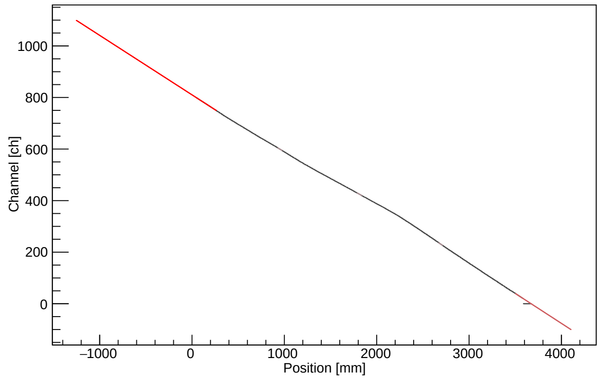

Y2: NA and FA

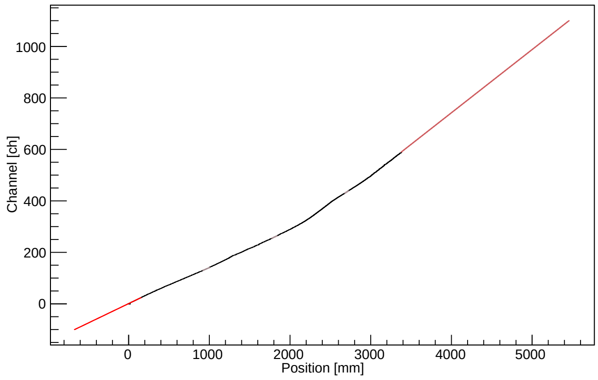

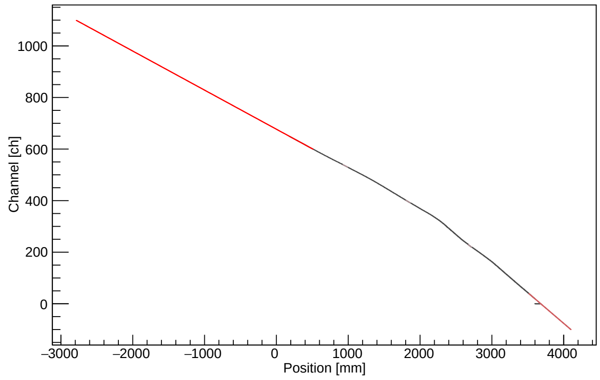

Y3: NA and FA

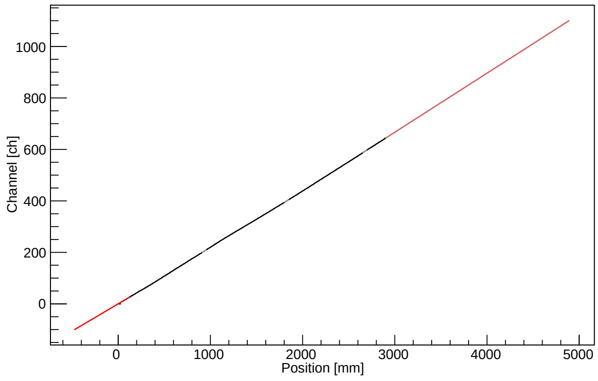

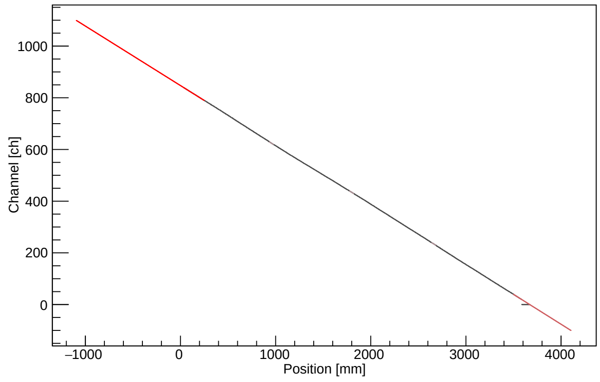

P14

X2: NA and FA

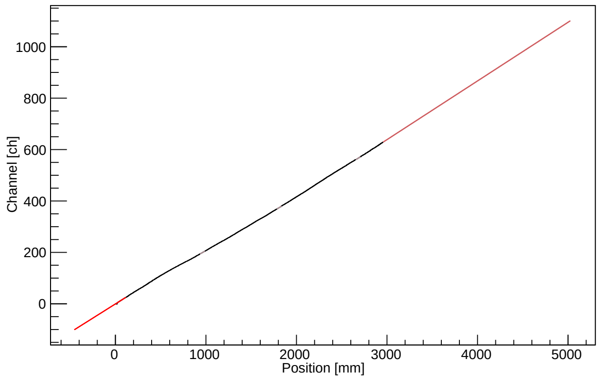

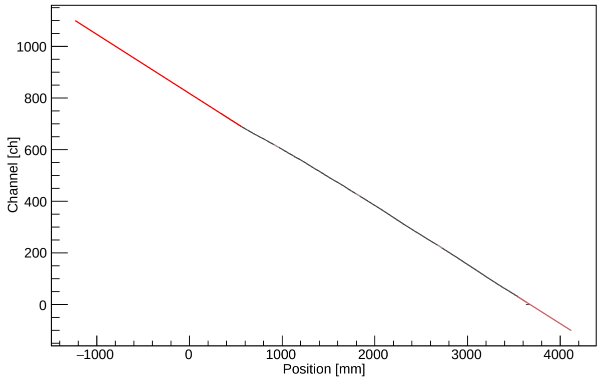

X3: NA and FA

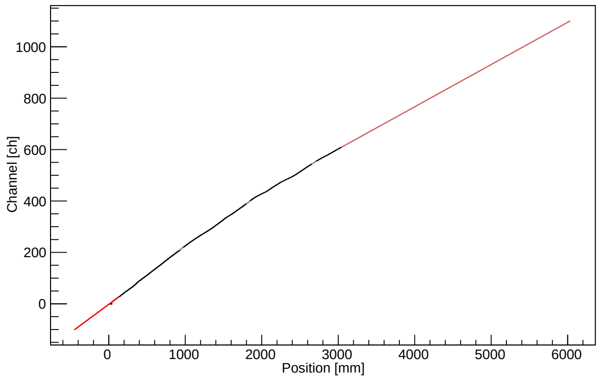

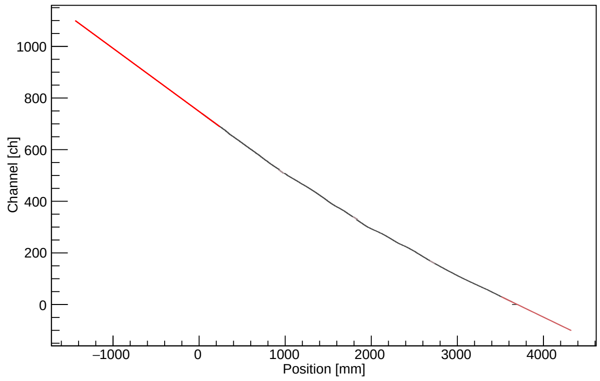

X4: NA and FA

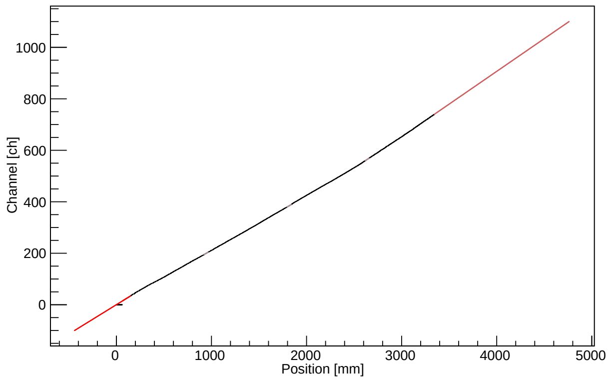

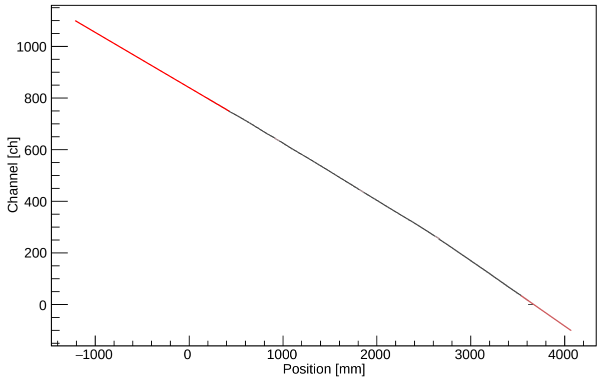

Y1: NA and FA

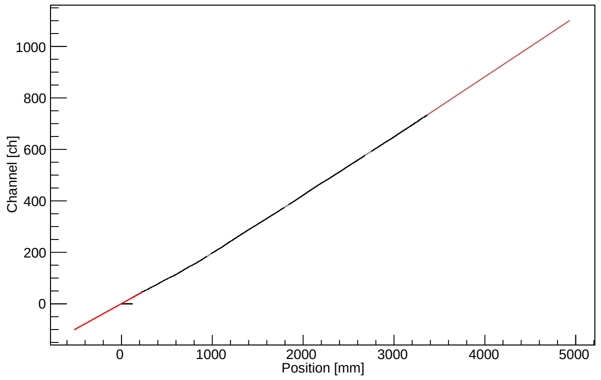

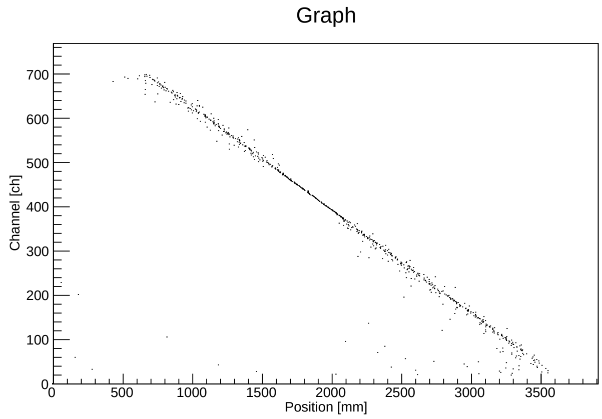

Y2: NA and FA

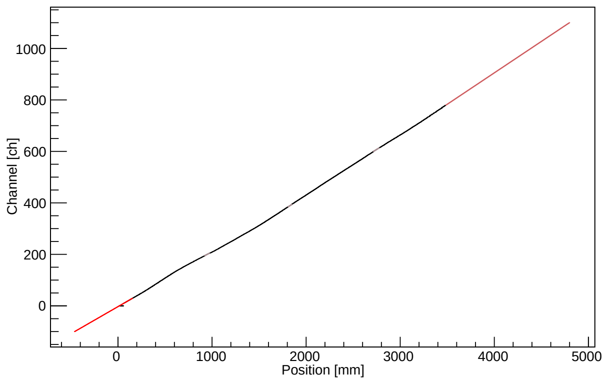

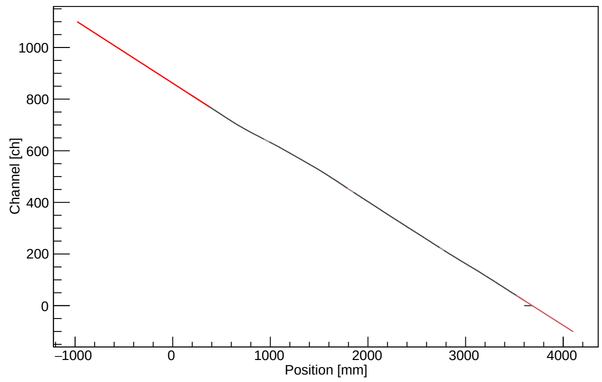

Y3: NA and FA

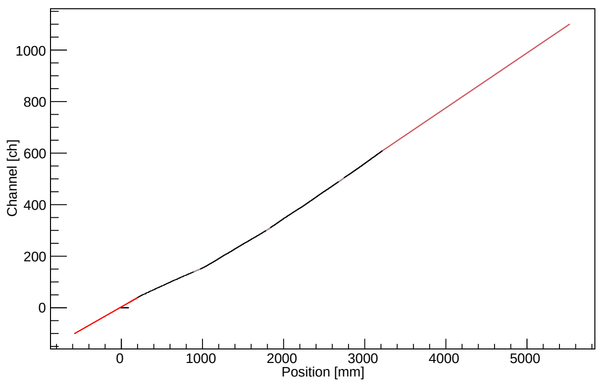

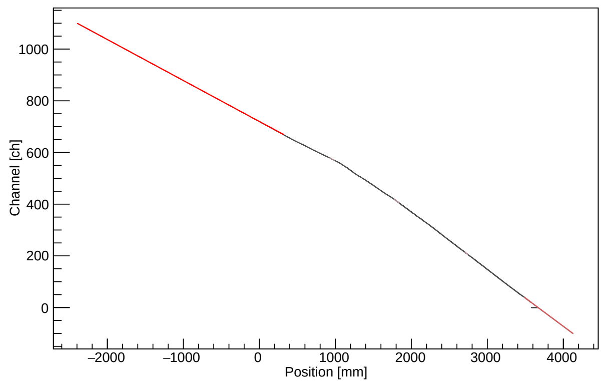

P77

X3: NA and FA

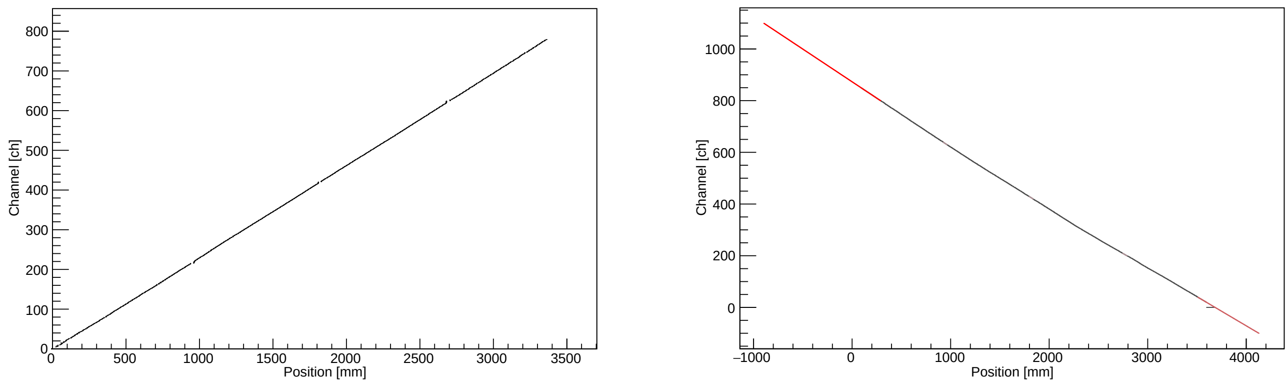

X4: NA and FA

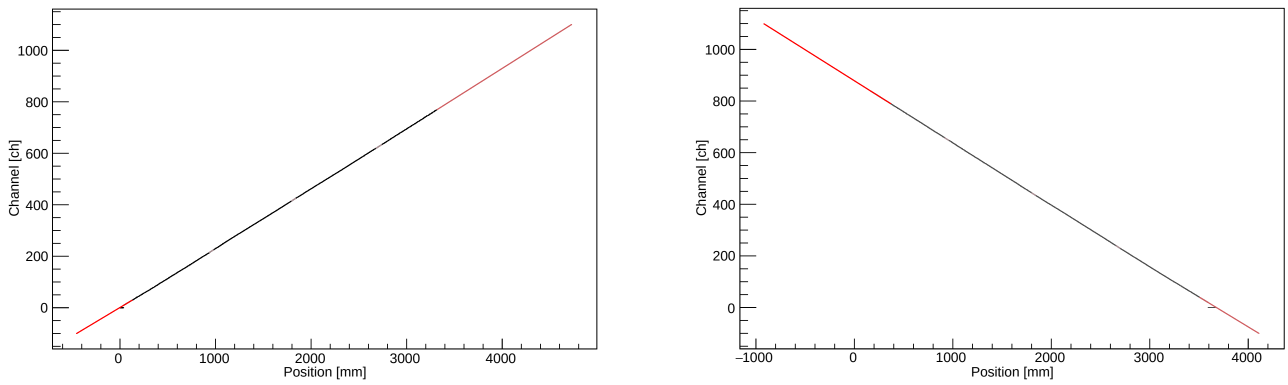

Y1: NA and FA

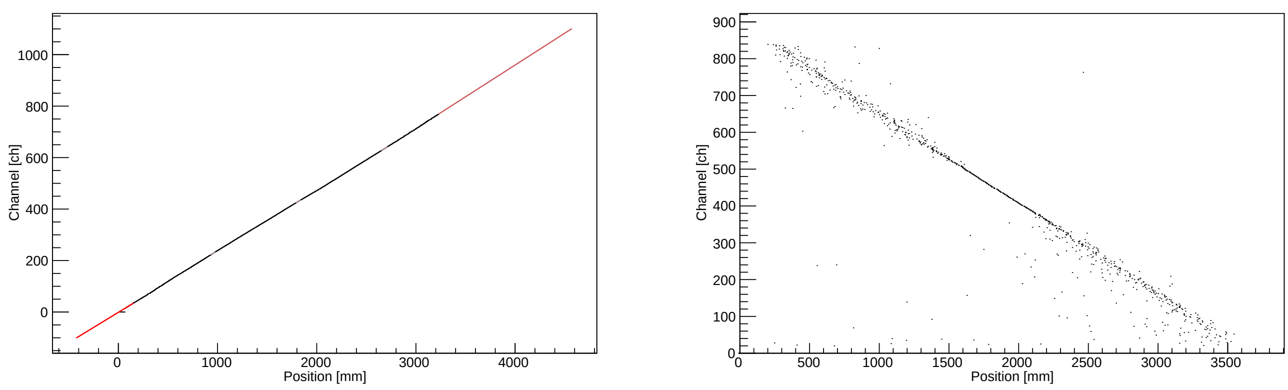

Y2: NA and FA

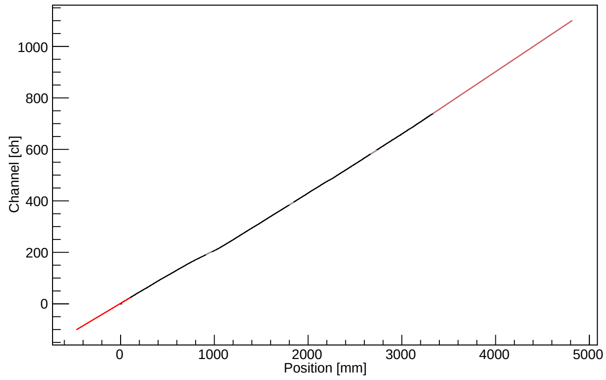

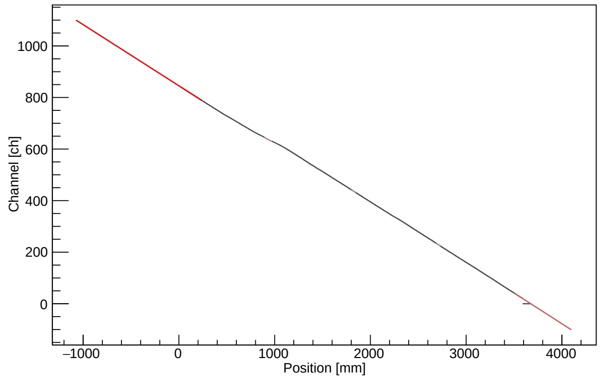

Y3: NA and FA

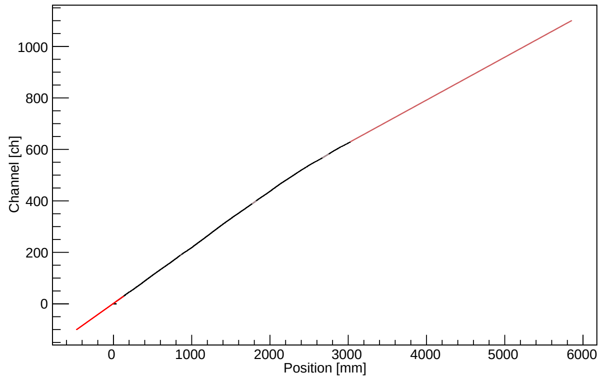

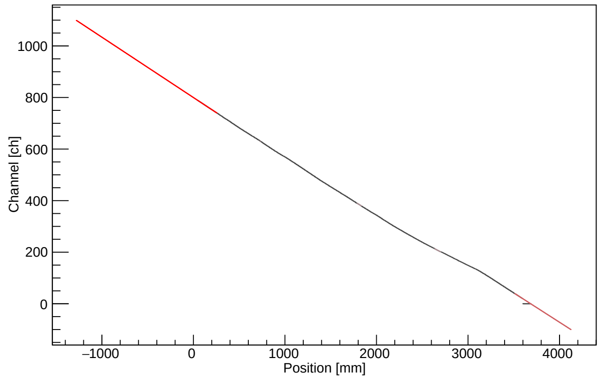

P30

X1: NA and FA

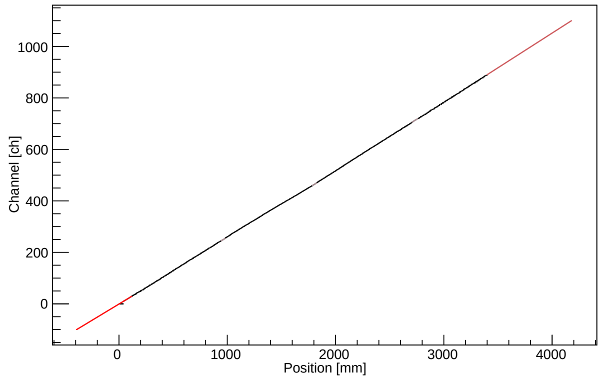

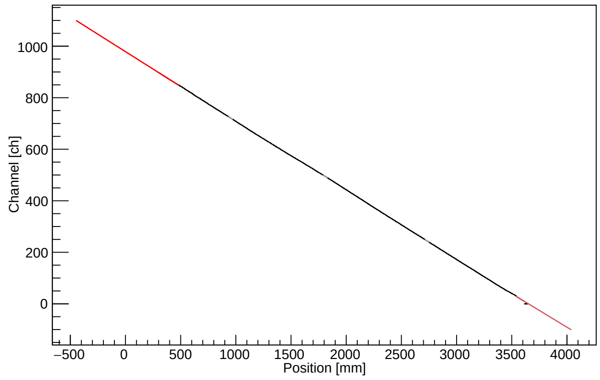

X2: NA and FA

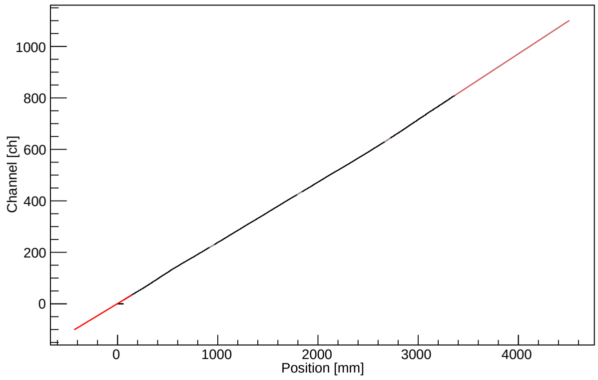

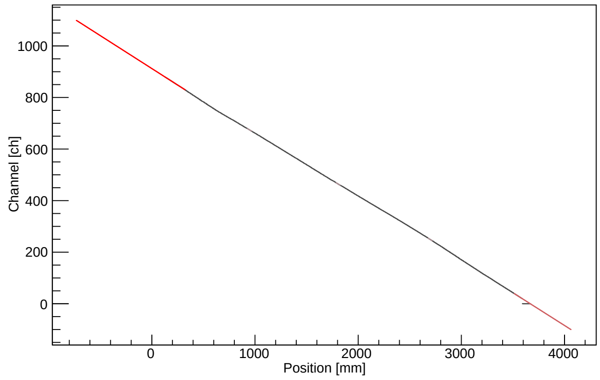

X3: NA and FA

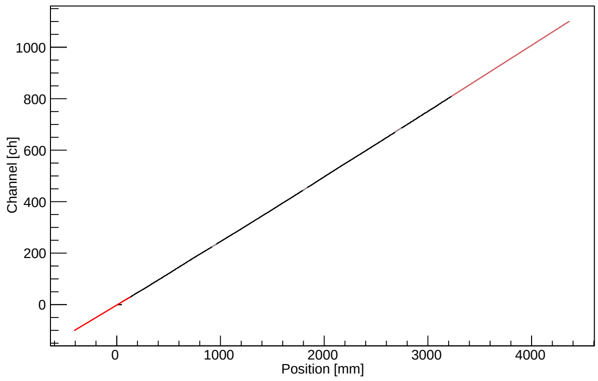

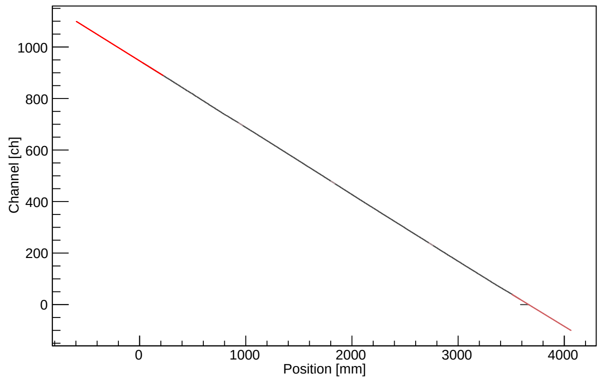

X4: NA and FA

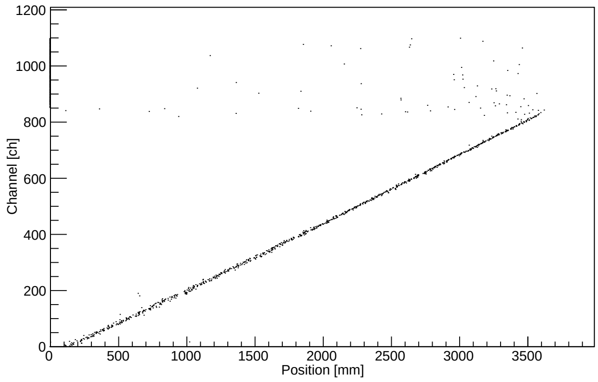

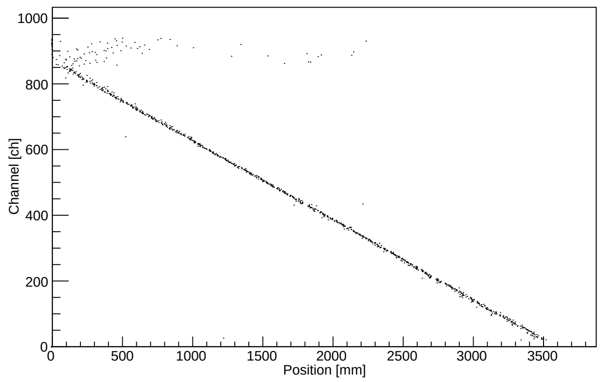

Y1: NA and FA

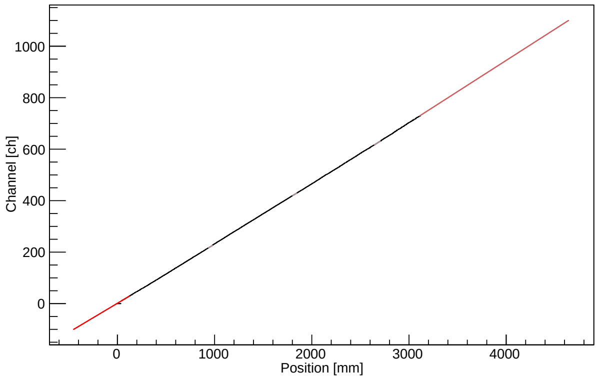

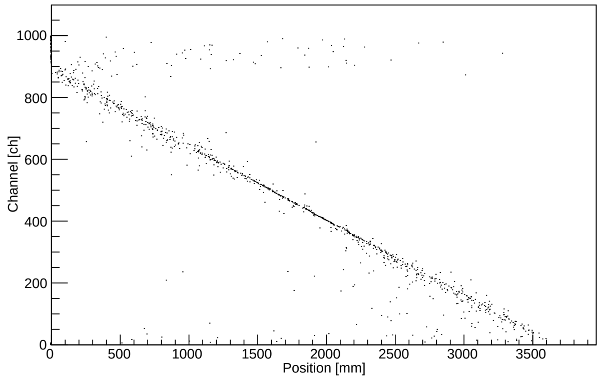

Y2: NA and FA

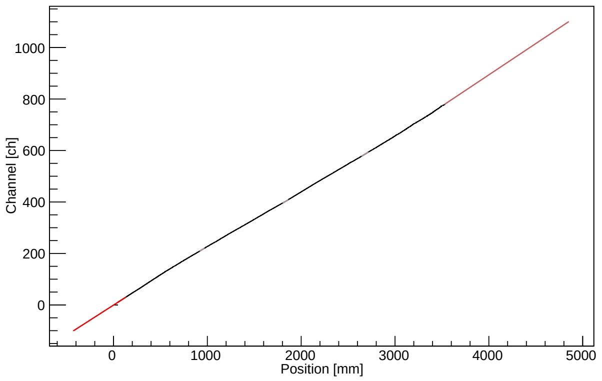

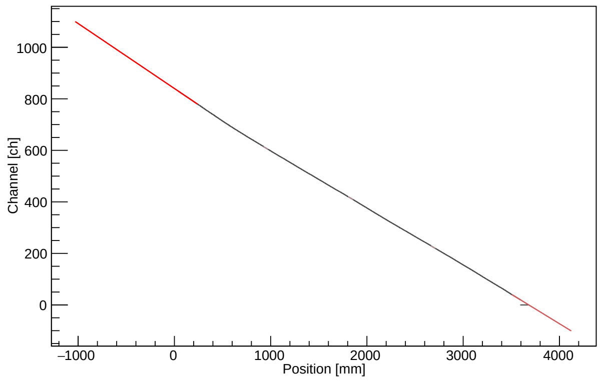

Y3: NA and FA

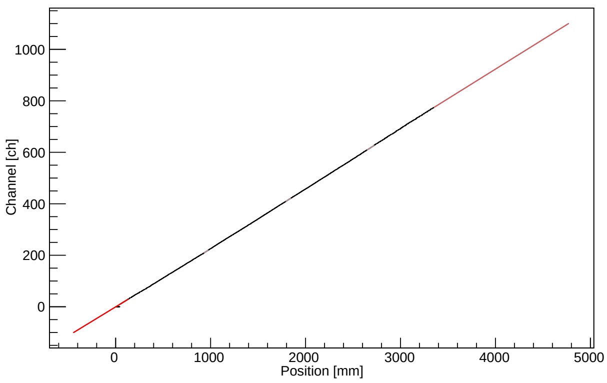

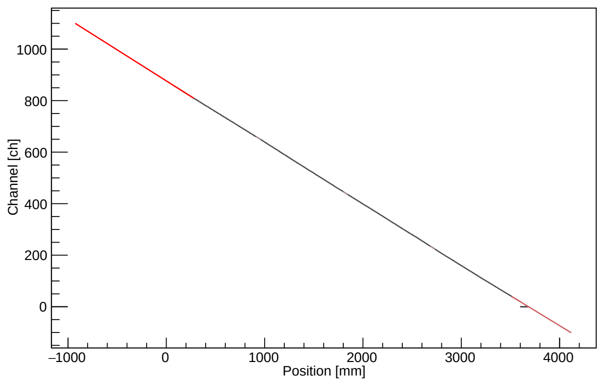

P28

X1: NA and FA

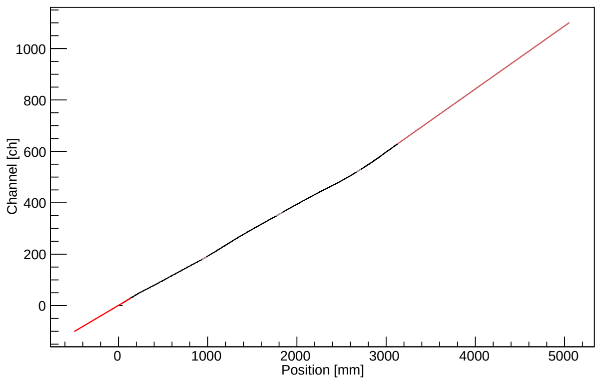

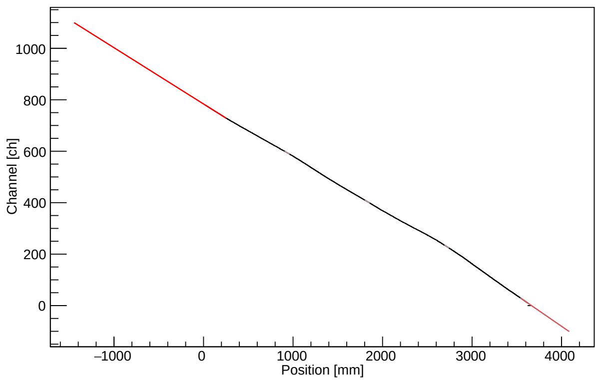

X2: NA and FA

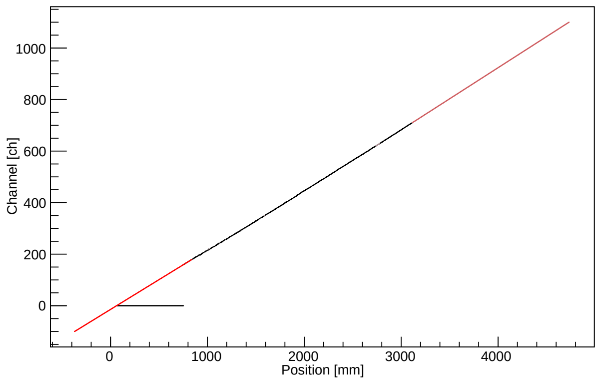

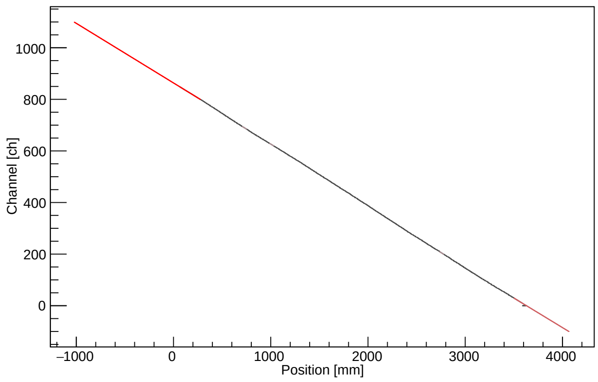

X3: NA and FA

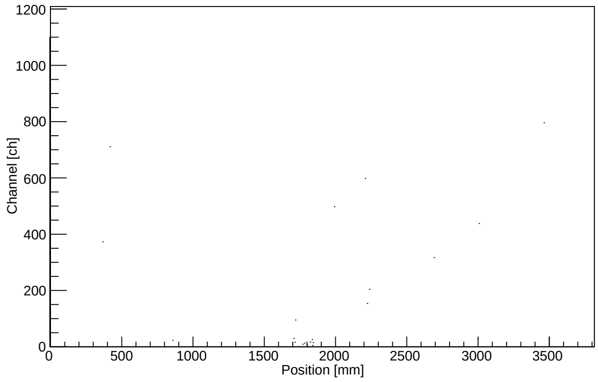

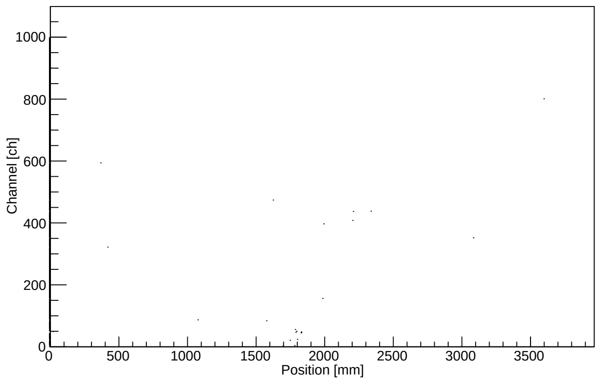

X4: NA and FA

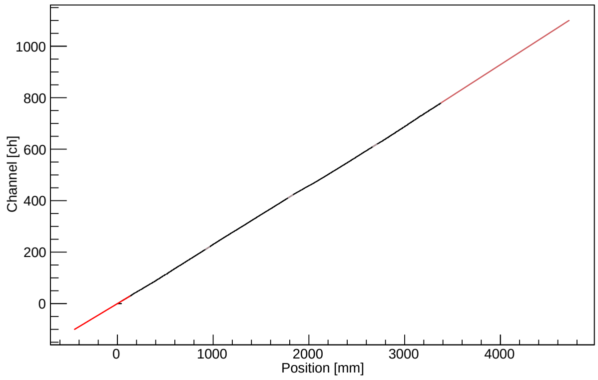

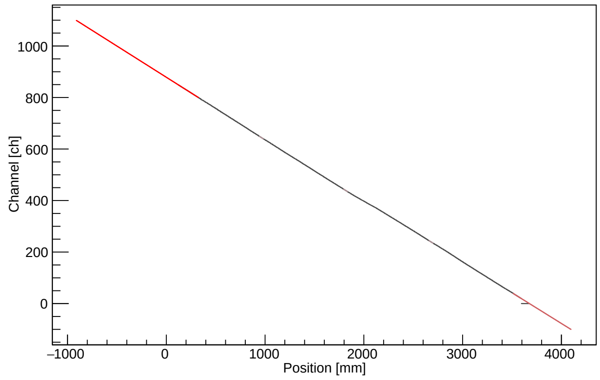

Y1: NA and FA

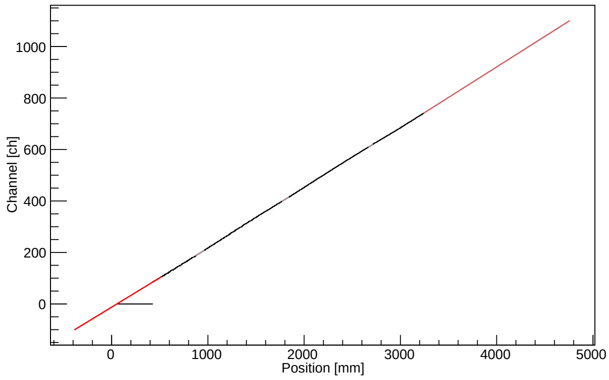

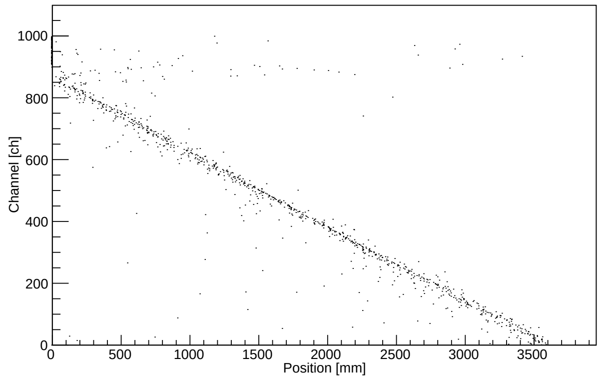

Y2: NA and FA

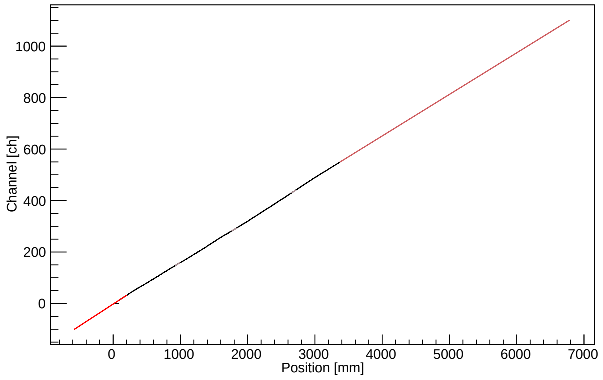

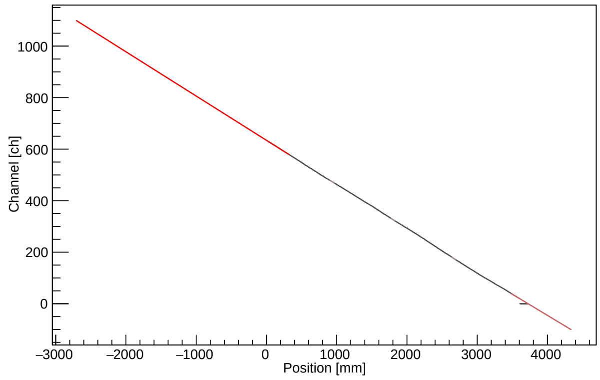

Y3: NA and FA

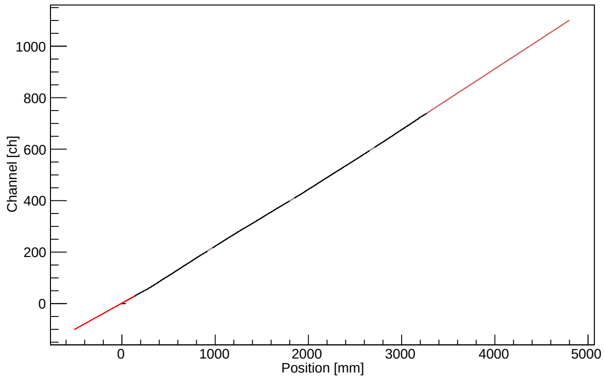

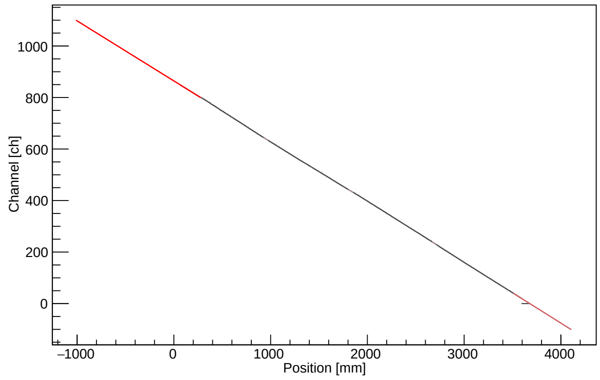

Appendix E

Residuals of uncalibrated planks with double Gaussian fit, and integral method.

P8

X2

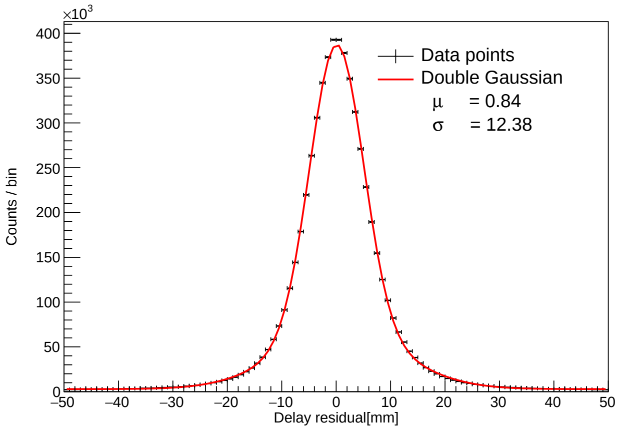

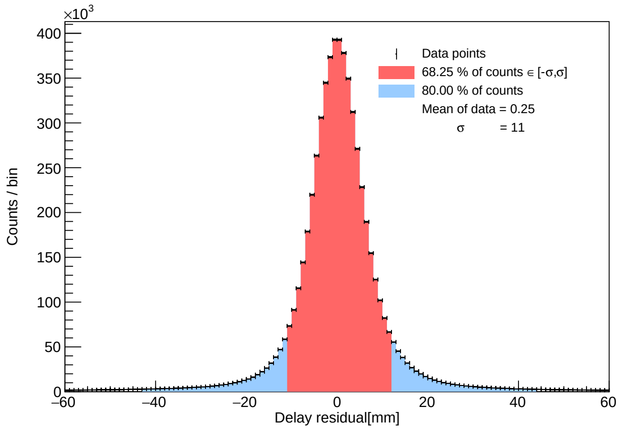

X3

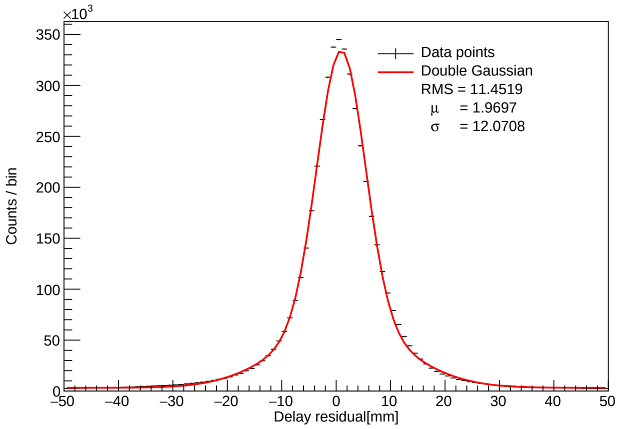

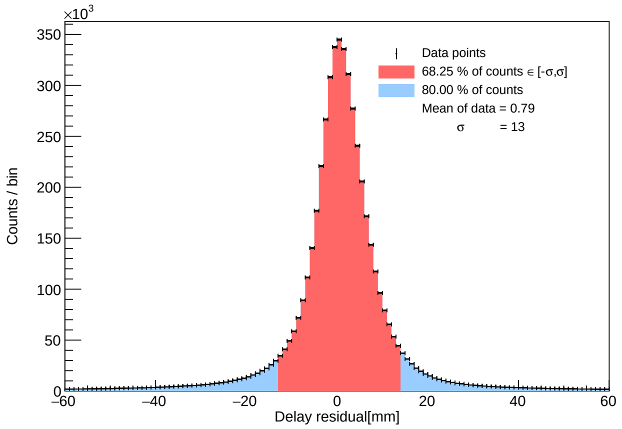

X4

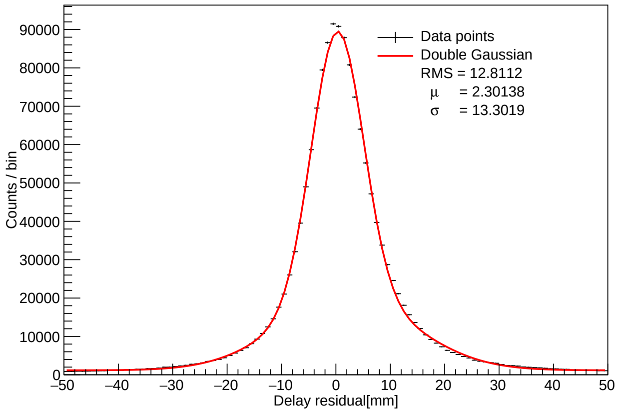
Data points
Double Gaussian
RMS = 12.8112
μ = 2.30138
σ = 13.3019
Counts / bin
Delay residual[mm]

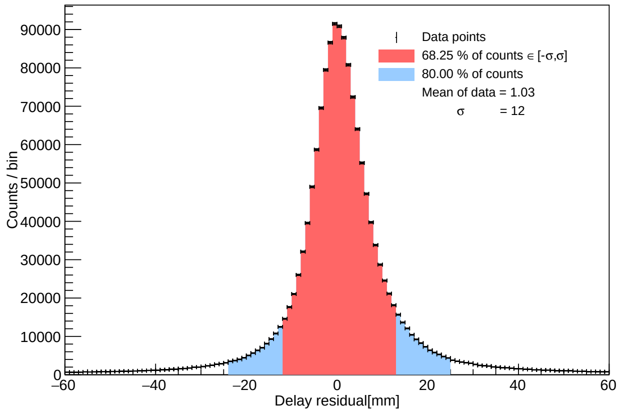
Data points
68.25 % of counts ∈ [-σ,σ]
80.00 % of counts
Mean of data = 1.03
σ = 12
Counts / bin
Delay residual[mm]

Y1

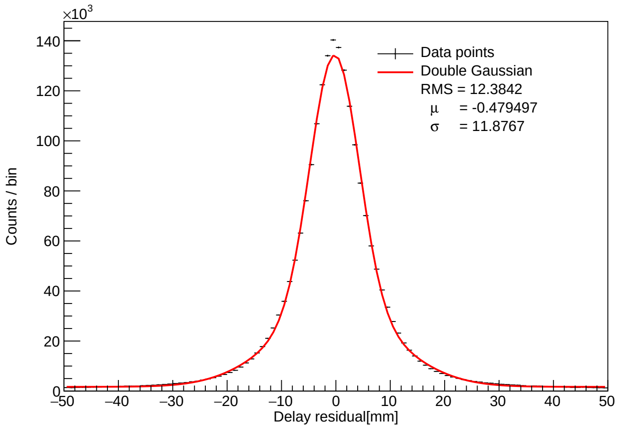
Data points
Double Gaussian
RMS = 12.3842
μ = -0.479497
σ = 11.8767
Counts / bin
Delay residual[mm]

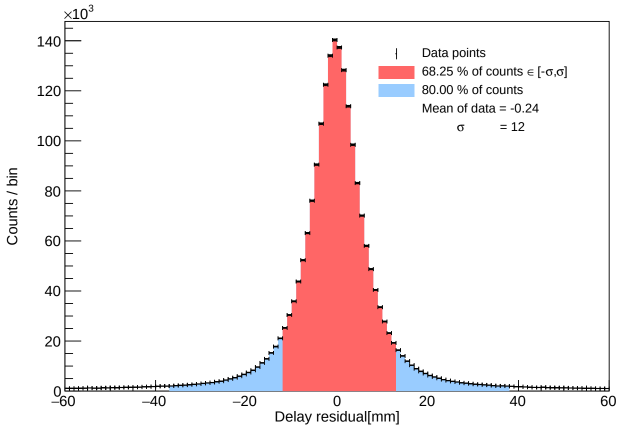
Data points
68.25 % of counts ∈ [-σ,σ]
80.00 % of counts
Mean of data = -0.24
σ = 12
Counts / bin
Delay residual[mm]

Y2

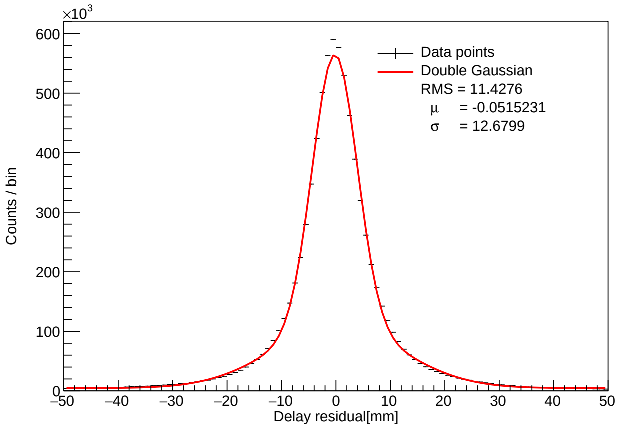
Data points
Double Gaussian
RMS = 11.4276
μ = -0.0515231
σ = 12.6799
Counts / bin
Delay residual[mm]

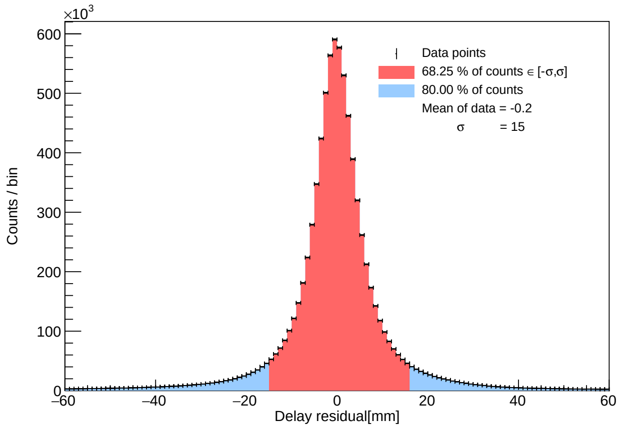
Data points
68.25 % of counts ∈ [-σ,σ]
80.00 % of counts
Mean of data = -0.2
σ = 15
Counts / bin
Delay residual[mm]

Y3

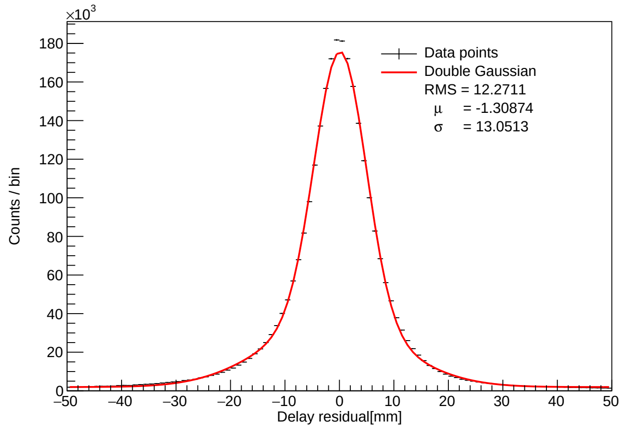
×10^3
Data points
Double Gaussian
RMS = 12.2711
μ = -1.30874
σ = 13.0513
Counts / bin
Delay residual[mm]

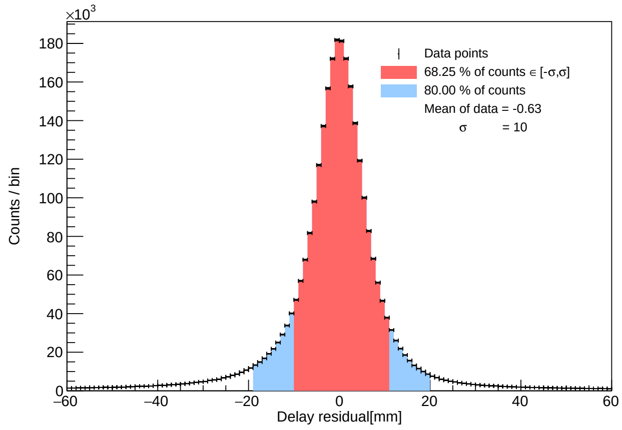
×10^3
Data points
68.25 % of counts ∈ [-σ,σ]
80.00 % of counts
Mean of data = -0.63
σ = 10
Counts / bin
Delay residual[mm]

P57

X2

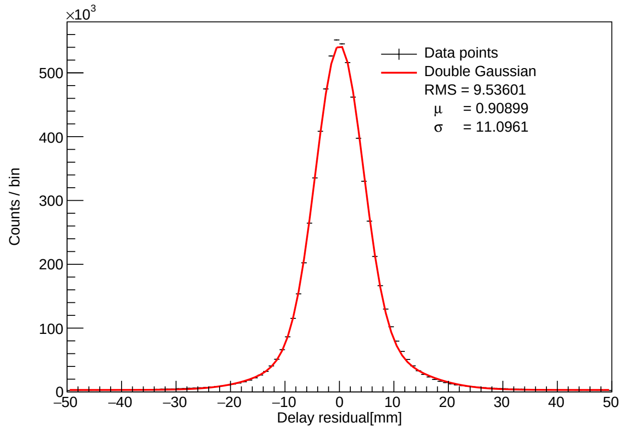
×10^3
Data points
Double Gaussian
RMS = 9.53601
μ = 0.90899
σ = 11.0961
Counts / bin
Delay residual[mm]

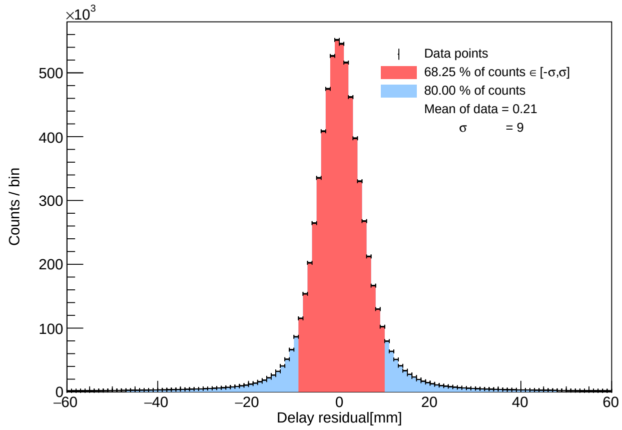
×10^3
Data points
68.25 % of counts ∈ [-σ,σ]
80.00 % of counts
Mean of data = 0.21
σ = 9
Counts / bin
Delay residual[mm]

X3

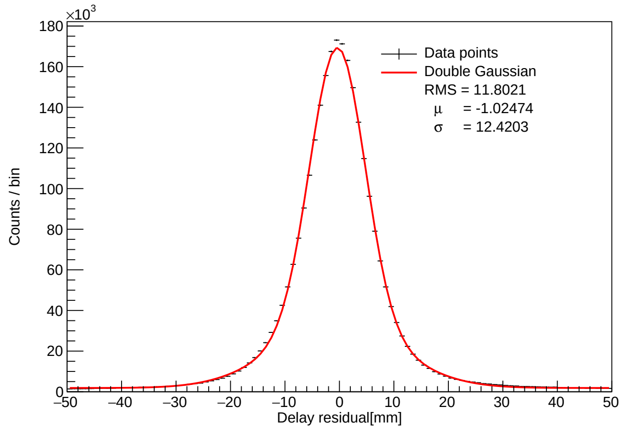
×10^3
Data points
Double Gaussian
RMS = 11.8021
μ = -1.02474
σ = 12.4203
Counts / bin
Delay residual[mm]

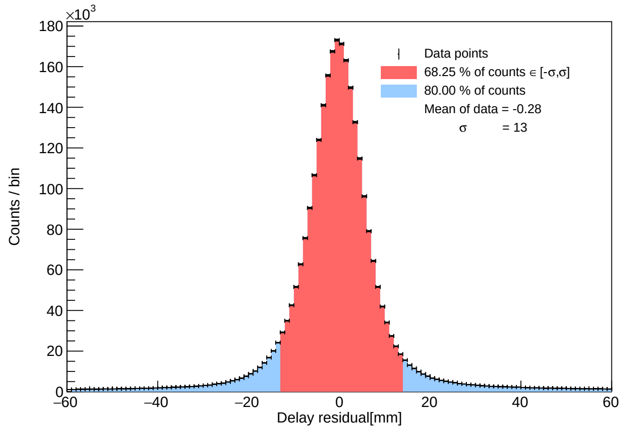
×10^3
Data points
68.25 % of counts ∈ [-σ,σ]
80.00 % of counts
Mean of data = -0.28
σ = 13
Counts / bin
Delay residual[mm]

X4

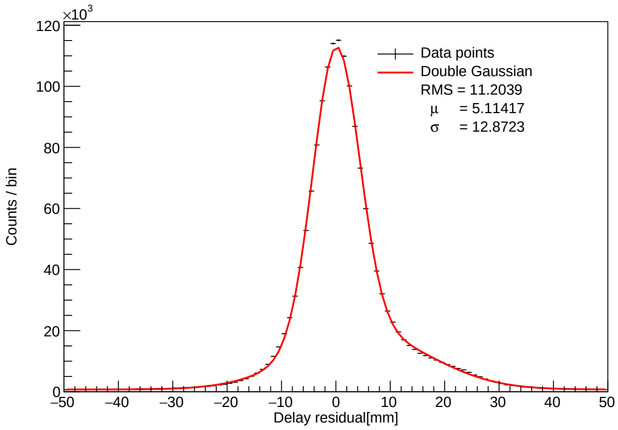
×10^3
Data points
Double Gaussian
RMS = 11.2039
μ = 5.11417
σ = 12.8723
Counts / bin
Delay residual[mm]

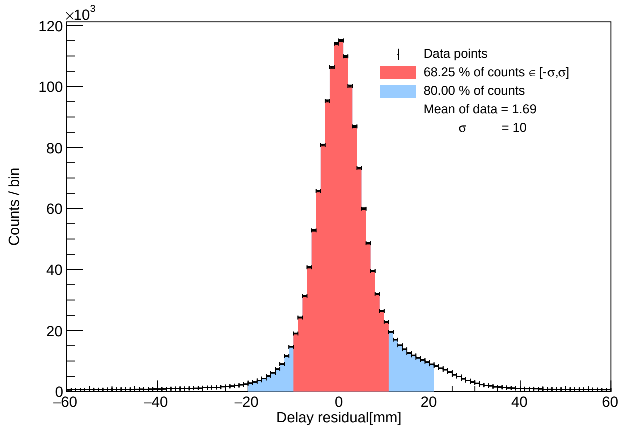
×10^3
Data points
68.25 % of counts ∈ [-σ,σ]
80.00 % of counts
Mean of data = 1.69
σ = 10
Counts / bin
Delay residual[mm]

Y1

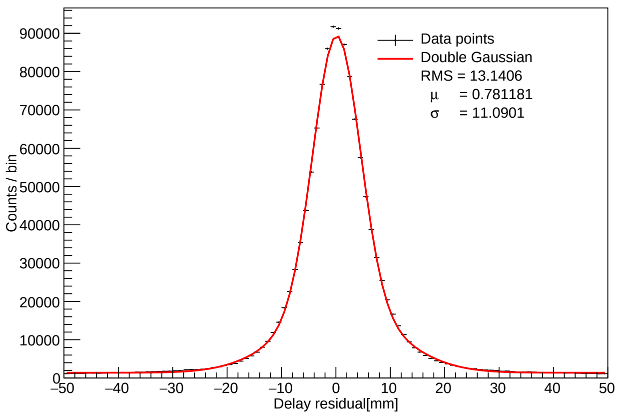
Data points
Double Gaussian
RMS = 13.1406
μ = 0.781181
σ = 11.0901
Counts / bin
Delay residual[mm]

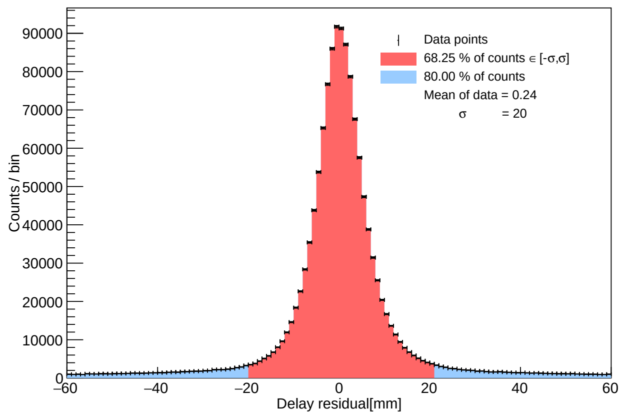
Data points
68.25 % of counts ∈ [-σ,σ]
80.00 % of counts
Mean of data = 0.24
σ = 20
Counts / bin
Delay residual[mm]

Y2

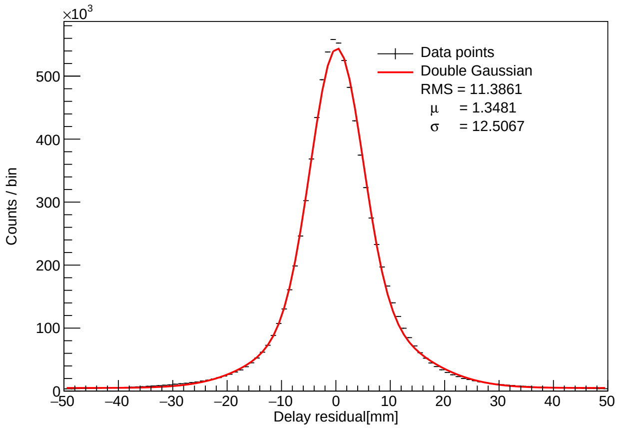
×10^3
Data points
Double Gaussian
RMS = 11.3861
μ = 1.3481
σ = 12.5067
Counts / bin
Delay residual[mm]

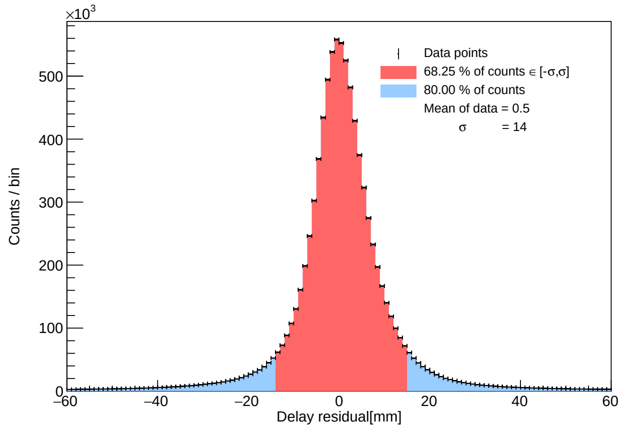
×10^3
Data points
68.25 % of counts ∈ [-σ,σ]
80.00 % of counts
Mean of data = 0.5
σ = 14
Counts / bin
Delay residual[mm]

Y3

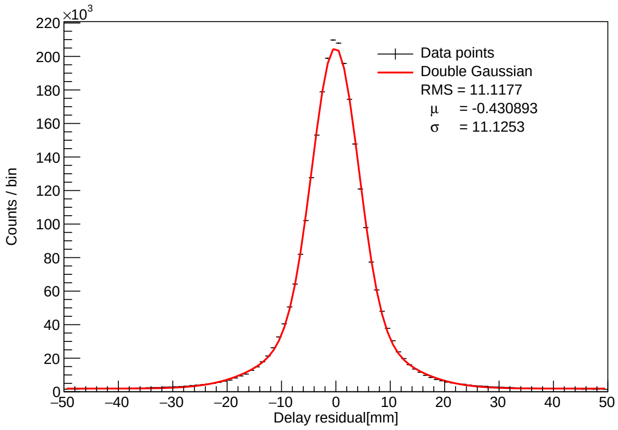
Data points
Double Gaussian
RMS = 11.1177
μ = -0.430893
σ = 11.1253
Counts / bin
Delay residual[mm]

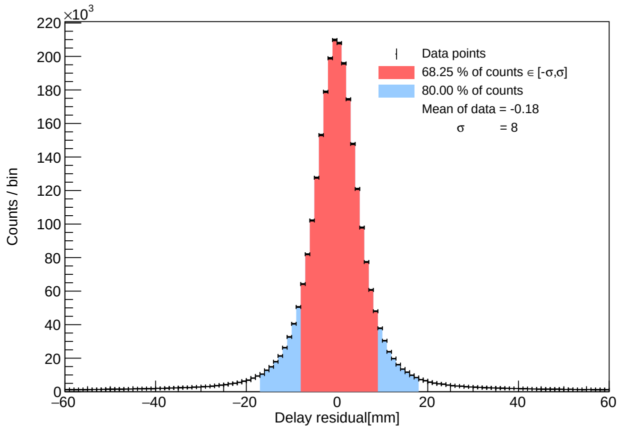
Data points
68.25 % of counts ∈ [-σ,σ]
80.00 % of counts
Mean of data = -0.18
σ = 8
Counts / bin
Delay residual[mm]

P14

X2

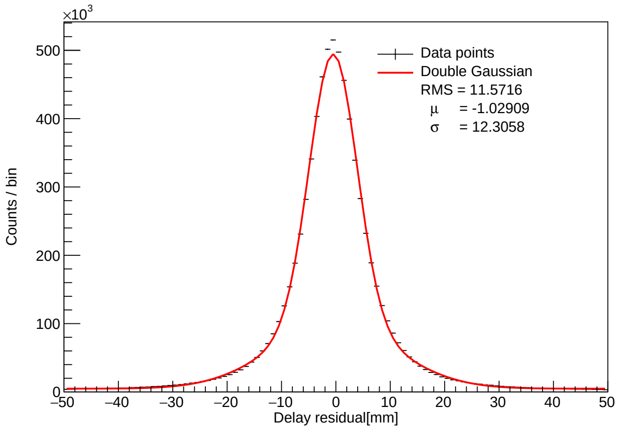
Data points
Double Gaussian
RMS = 11.5716
μ = -1.02909
σ = 12.3058
Counts / bin
Delay residual[mm]

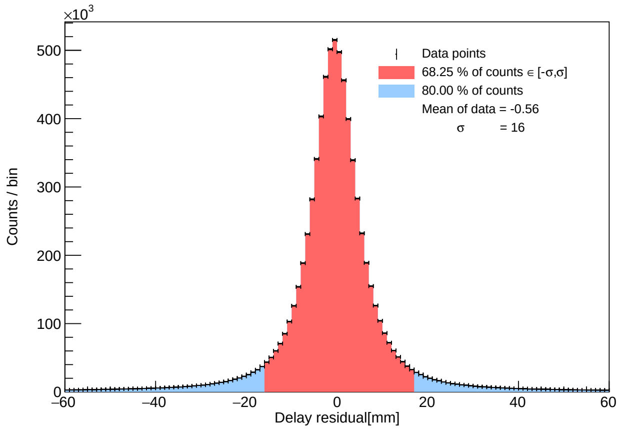
Data points
68.25 % of counts ∈ [-σ,σ]
80.00 % of counts
Mean of data = -0.56
σ = 16
Counts / bin
Delay residual[mm]

X3

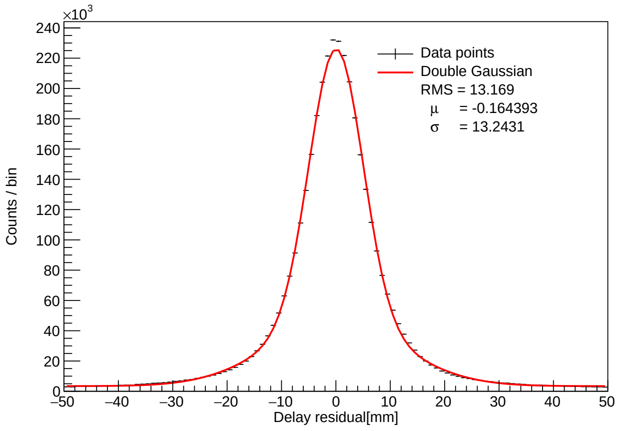
Data points
Double Gaussian
RMS = 13.169
μ = -0.164393
σ = 13.2431
Counts / bin
Delay residual[mm]

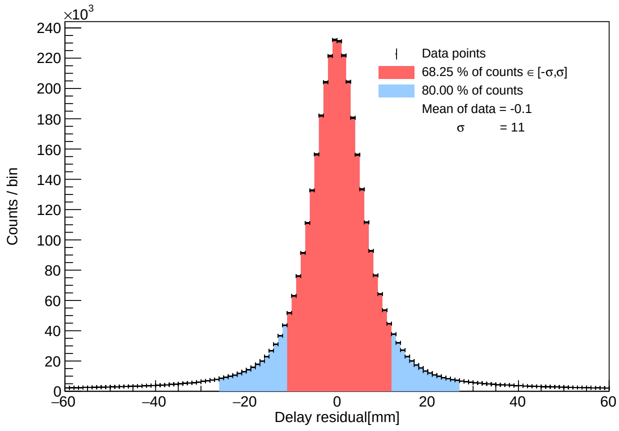
Data points
68.25 % of counts ∈ [-σ,σ]
80.00 % of counts
Mean of data = -0.1
σ = 11
Counts / bin
Delay residual[mm]

X4

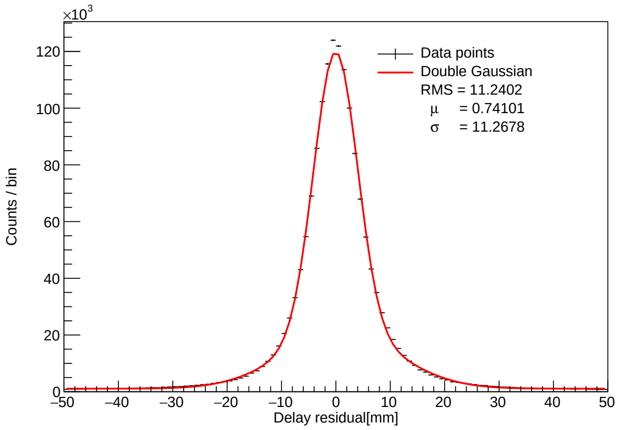
Data points
Double Gaussian
RMS = 11.2402
μ = 0.74101
σ = 11.2678
Counts / bin
Delay residual[mm]

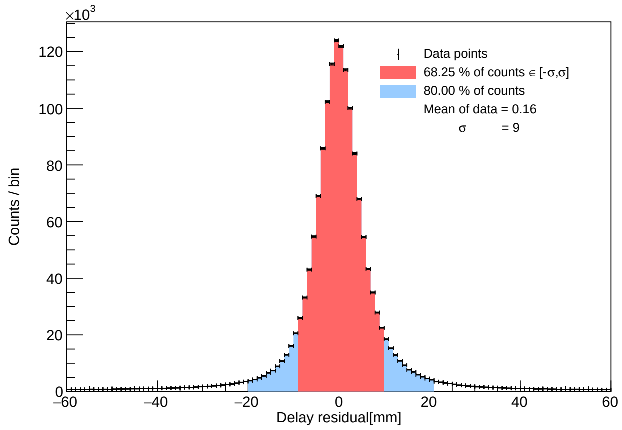
Data points
68.25 % of counts ∈ [-σ,σ]
80.00 % of counts
Mean of data = 0.16
σ = 9
Counts / bin
Delay residual[mm]

Y2

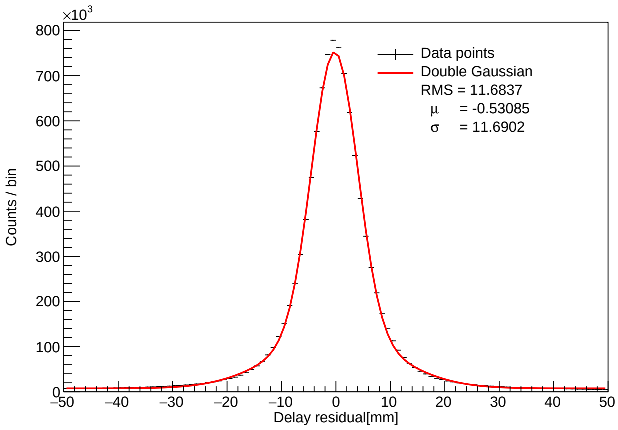
Data points
Double Gaussian
RMS = 11.6837
μ = -0.53085
σ = 11.6902
Counts / bin
Delay residual[mm]

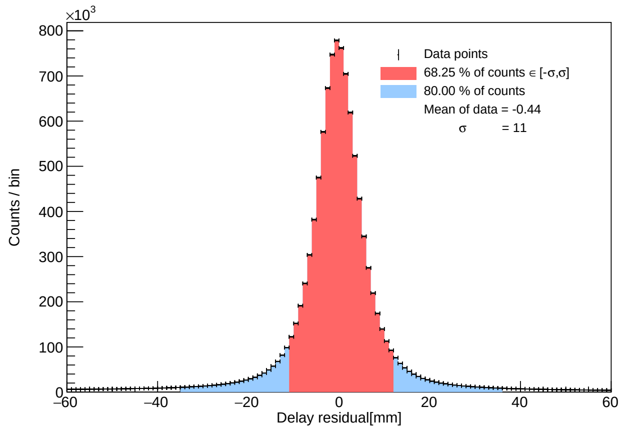
Data points
68.25 % of counts ∈ [-σ,σ]
80.00 % of counts
Mean of data = -0.44
σ = 11
Counts / bin
Delay residual[mm]

Y3

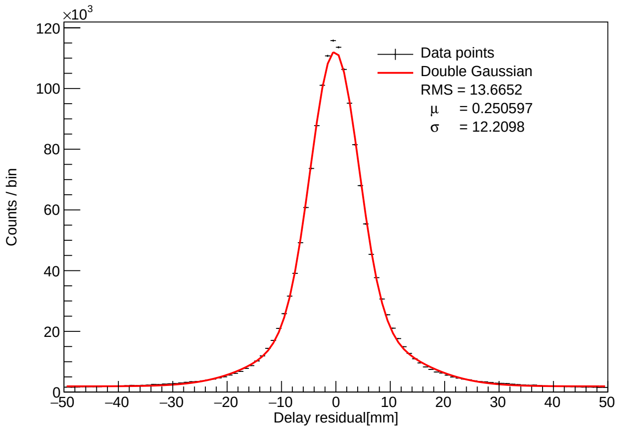
Data points
Double Gaussian
RMS = 13.6652
μ = 0.250597
σ = 12.2098
Counts / bin
Delay residual[mm]

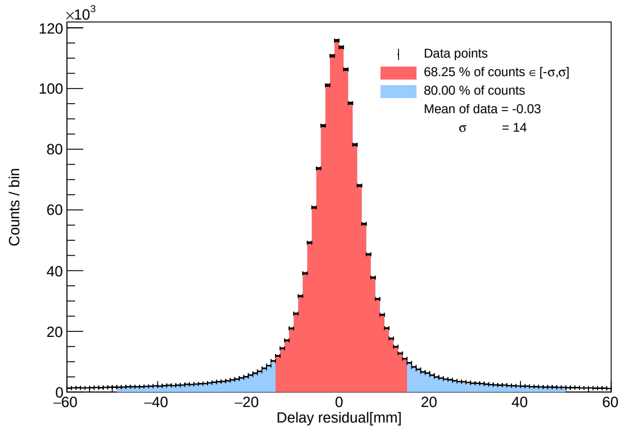
Data points
68.25 % of counts ∈ [-σ,σ]
80.00 % of counts
Mean of data = -0.03
σ = 14
Counts / bin
Delay residual[mm]

P77

X3

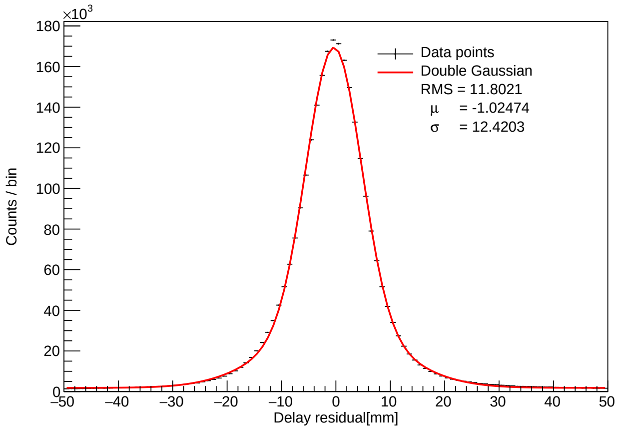
×10^3
Data points
Double Gaussian
RMS = 11.8021
μ = -1.02474
σ = 12.4203
Counts / bin
Delay residual[mm]

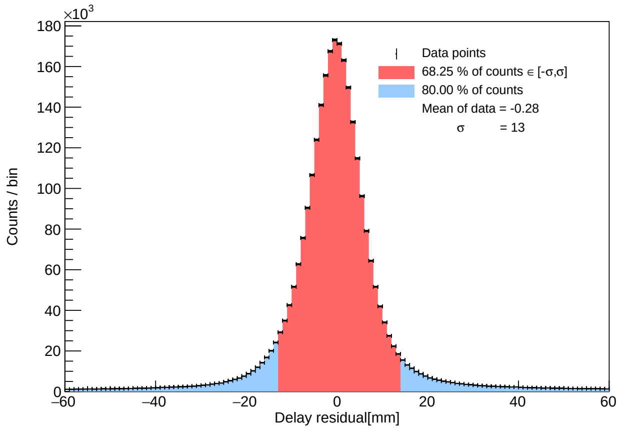
×10^3
Data points
68.25 % of counts ∈ [-σ,σ]
80.00 % of counts
Mean of data = -0.28
σ = 13
Counts / bin
Delay residual[mm]

X4

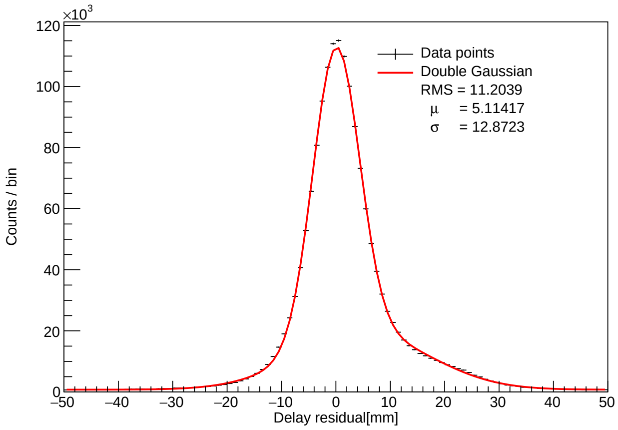
×10^3
Data points
Double Gaussian
RMS = 11.2039
μ = 5.11417
σ = 12.8723
Counts / bin
Delay residual[mm]

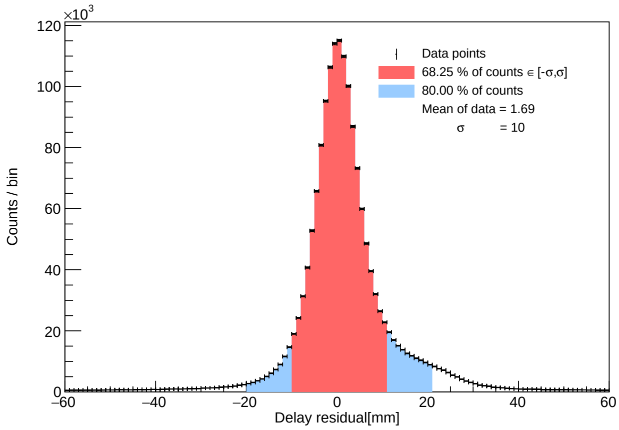
×10^3
Data points
68.25 % of counts ∈ [-σ,σ]
80.00 % of counts
Mean of data = 1.69
σ = 10
Counts / bin
Delay residual[mm]

Y2

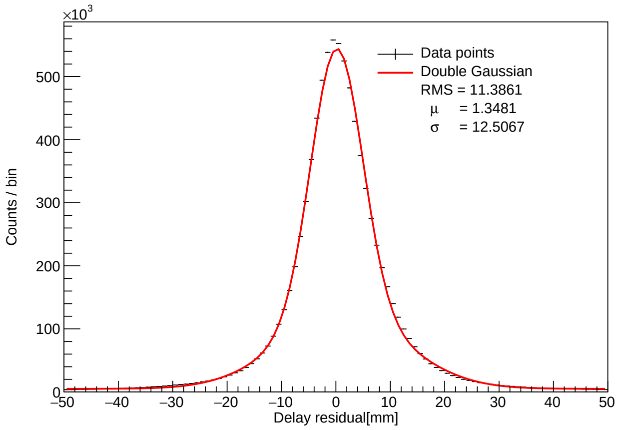
×10^3
Data points
Double Gaussian
RMS = 11.3861
μ = 1.3481
σ = 12.5067
Counts / bin
Delay residual[mm]

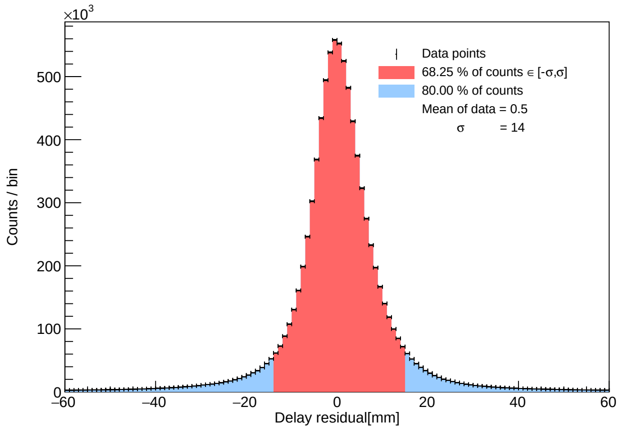
×10^3
Data points
68.25 % of counts ∈ [-σ,σ]
80.00 % of counts
Mean of data = 0.5
σ = 14
Counts / bin
Delay residual[mm]

Y3

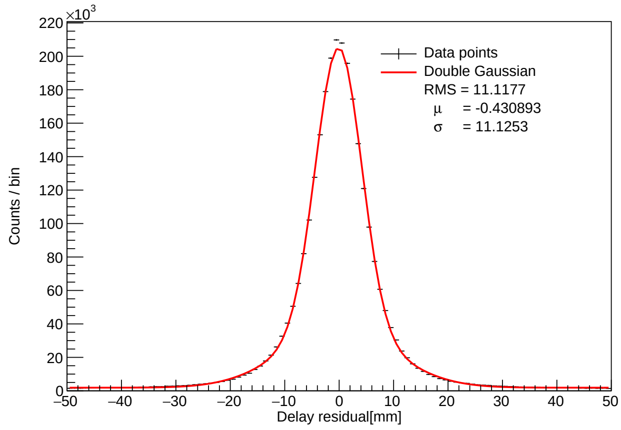
Data points
Double Gaussian
RMS = 11.1177
μ = -0.430893
σ = 11.1253
Counts / bin
Delay residual[mm]

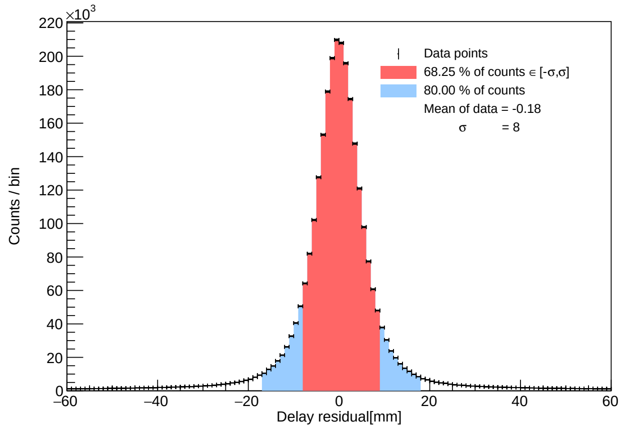
Data points
68.25 % of counts ∈ [-σ,σ]
80.00 % of counts
Mean of data = -0.18
σ = 8
Counts / bin
Delay residual[mm]

P30

X1

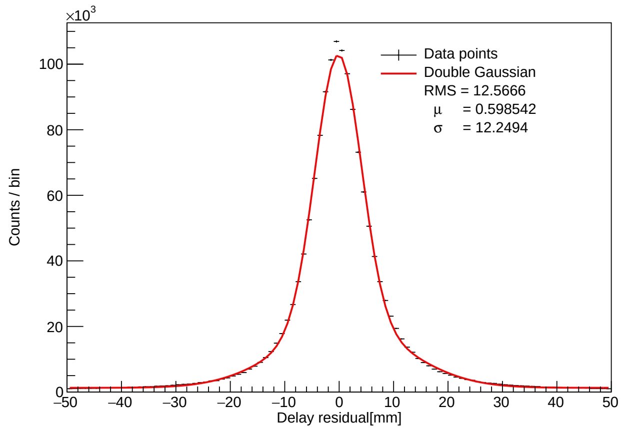
Data points
Double Gaussian
RMS = 12.5666
μ = 0.598542
σ = 12.2494
Counts / bin
Delay residual[mm]

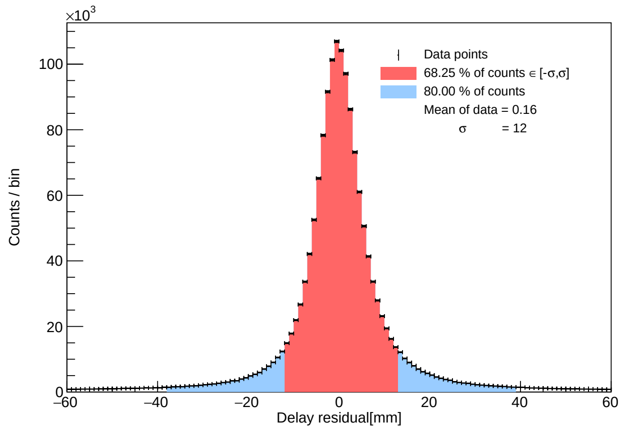
Data points
68.25 % of counts ∈ [-σ,σ]
80.00 % of counts
Mean of data = 0.16
σ = 12
Counts / bin
Delay residual[mm]

X2

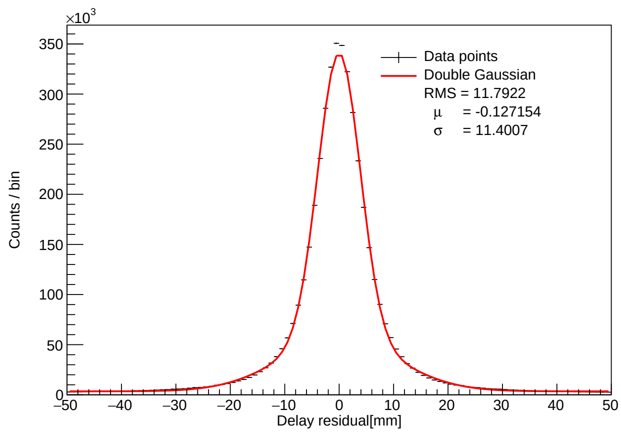
Data points
Double Gaussian
RMS = 11.7922
μ = -0.127154
σ = 11.4007
Counts / bin
Delay residual[mm]

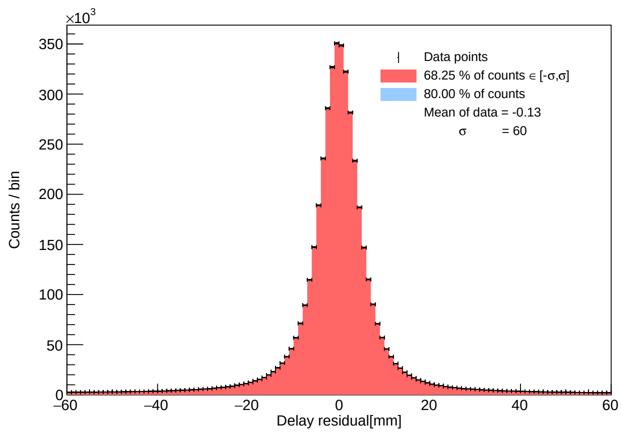
Data points
68.25 % of counts ∈ [-σ,σ]
80.00 % of counts
Mean of data = -0.13
σ = 60
Counts / bin
Delay residual[mm]

X3

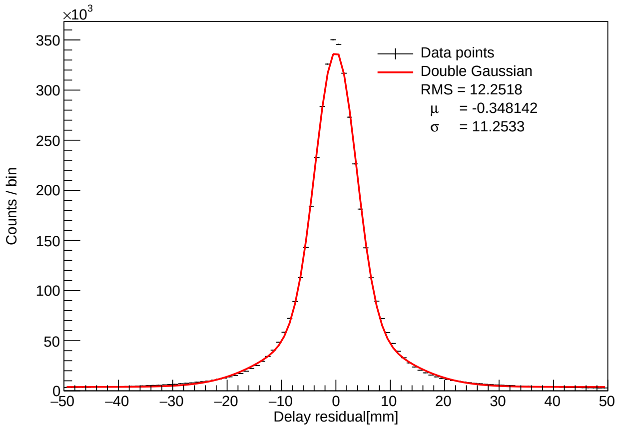
×10^3
Data points
Double Gaussian
RMS = 12.2518
μ = -0.348142
σ = 11.2533
Counts / bin
Delay residual[mm]

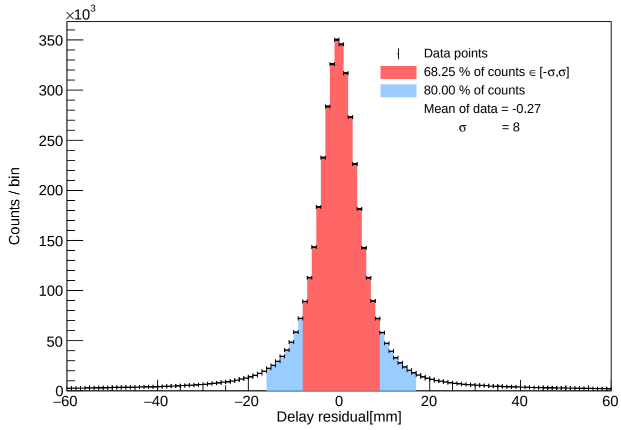
×10^3
Data points
68.25 % of counts ∈ [-σ,σ]
80.00 % of counts
Mean of data = -0.27
σ = 8
Counts / bin
Delay residual[mm]

Y2

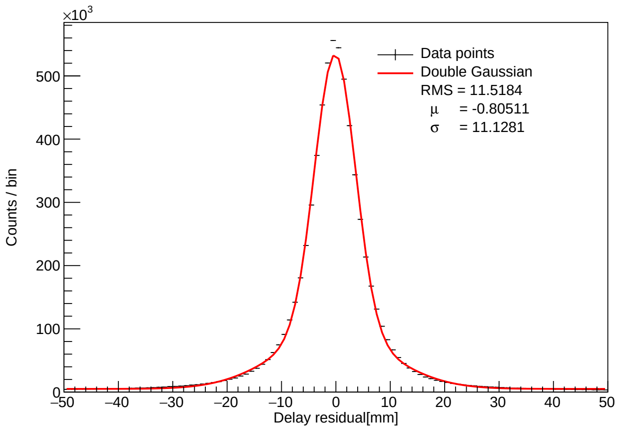
×10^3
Data points
Double Gaussian
RMS = 11.5184
μ = -0.80511
σ = 11.1281
Counts / bin
Delay residual[mm]

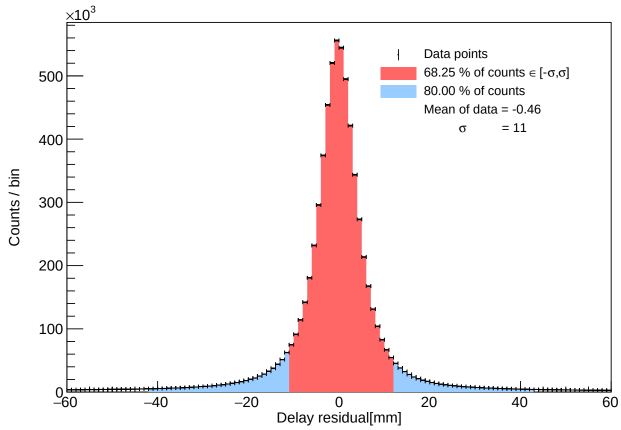
×10^3
Data points
68.25 % of counts ∈ [-σ,σ]
80.00 % of counts
Mean of data = -0.46
σ = 11
Counts / bin
Delay residual[mm]

Y3

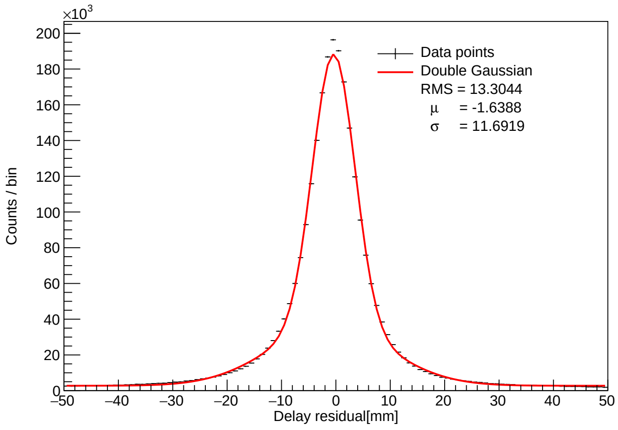
×10^3
Data points
Double Gaussian
RMS = 13.3044
μ = -1.6388
σ = 11.6919
Counts / bin
Delay residual[mm]

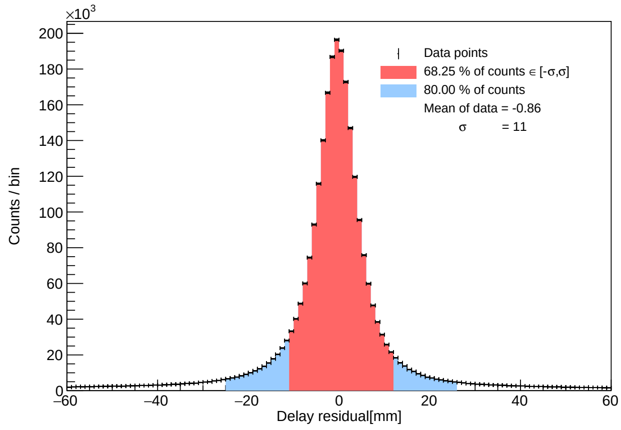
×10^3
Data points
68.25 % of counts ∈ [-σ,σ]
80.00 % of counts
Mean of data = -0.86
σ = 11
Counts / bin
Delay residual[mm]

P28

X1

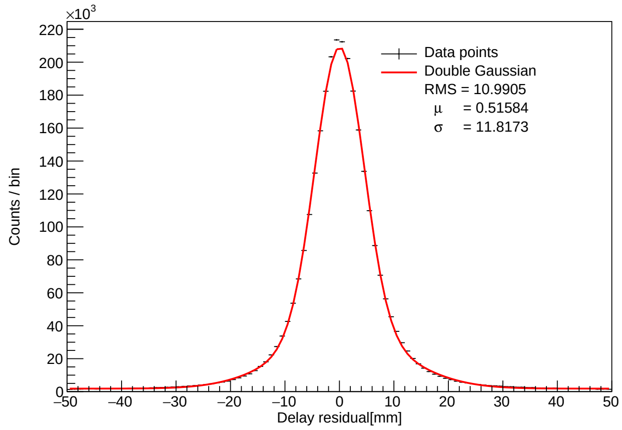
Data points
Double Gaussian
RMS = 10.9905
μ = 0.51584
σ = 11.8173
Counts / bin
Delay residual[mm]

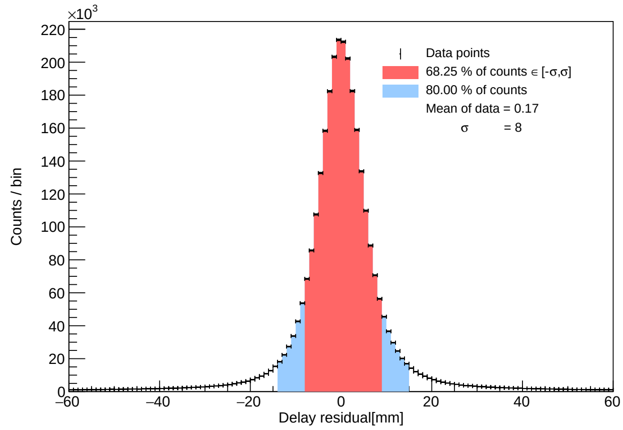
Data points
68.25 % of counts ∈ [-σ,σ]
80.00 % of counts
Mean of data = 0.17
σ = 8
Counts / bin
Delay residual[mm]

X2

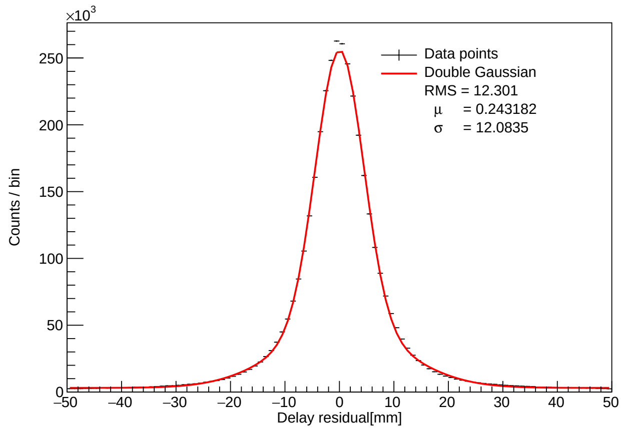
Data points
Double Gaussian
RMS = 12.301
μ = 0.243182
σ = 12.0835
Counts / bin
Delay residual[mm]

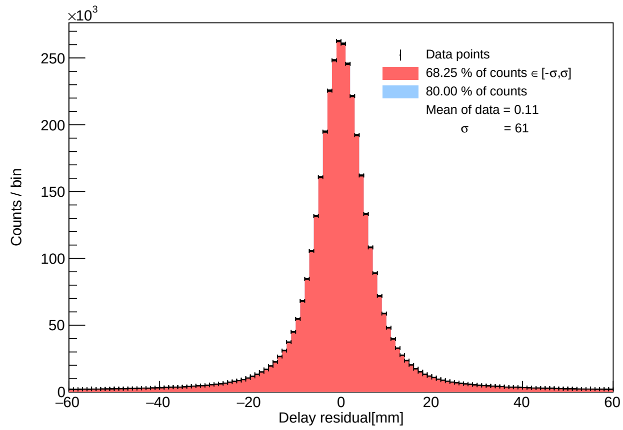
Data points
68.25 % of counts ∈ [-σ,σ]
80.00 % of counts
Mean of data = 0.11
σ = 61
Counts / bin
Delay residual[mm]

X4

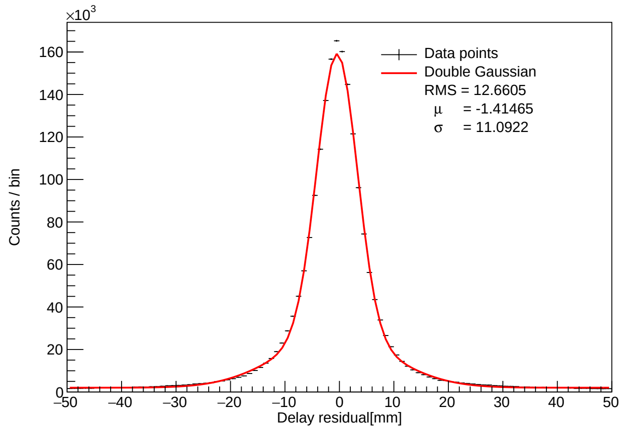
Data points
Double Gaussian
RMS = 12.6605
μ = -1.41465
σ = 11.0922
Counts / bin
Delay residual[mm]

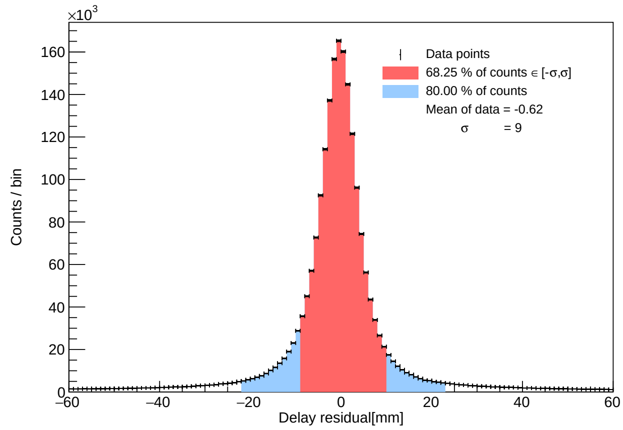
Data points
68.25 % of counts ∈ [-σ,σ]
80.00 % of counts
Mean of data = -0.62
σ = 9
Counts / bin
Delay residual[mm]

Y2

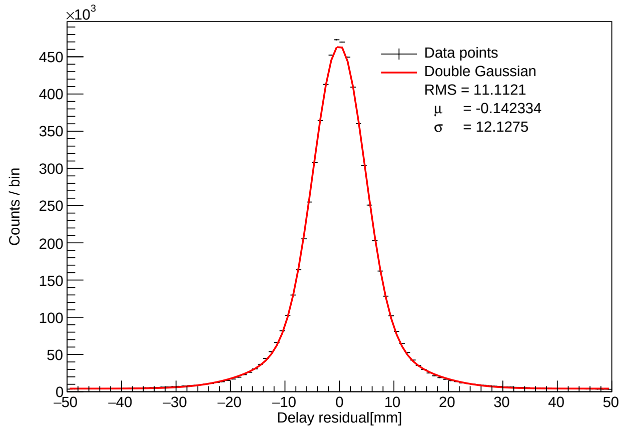

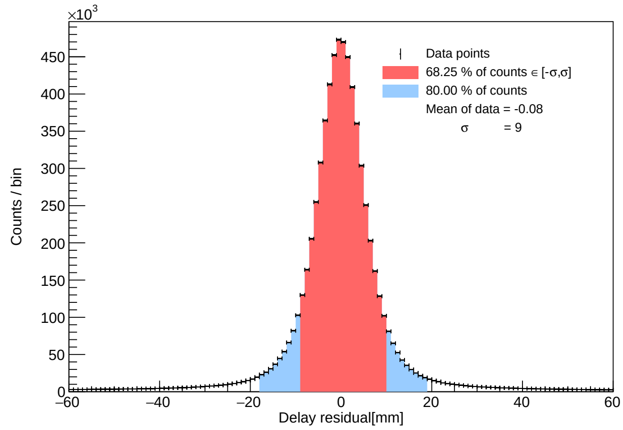

Y3

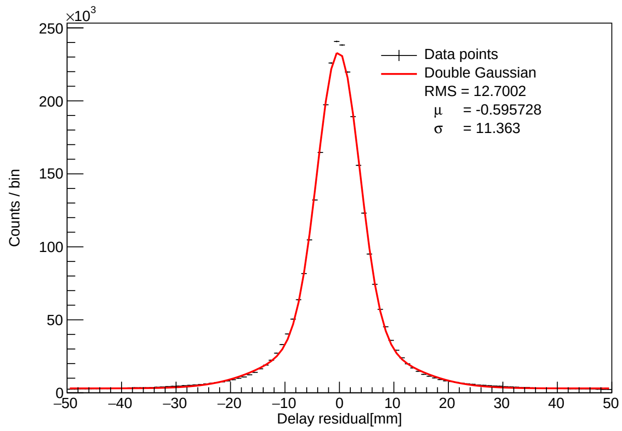

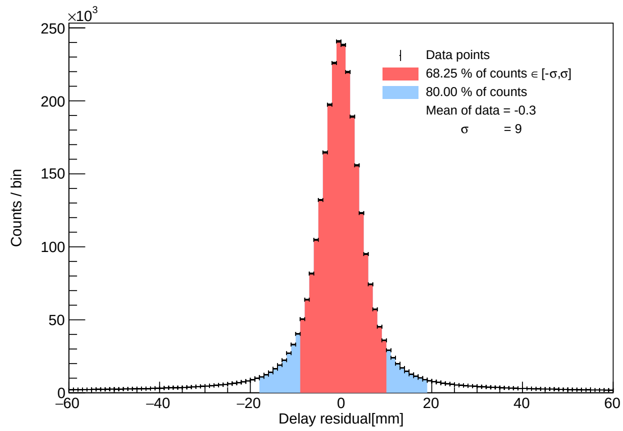

Appendix F

Anode residuals for uncalibrated planks with Lorentzian fit.

P8 and P57

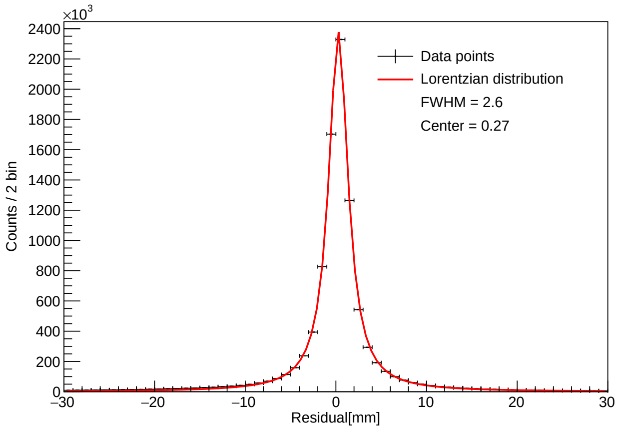

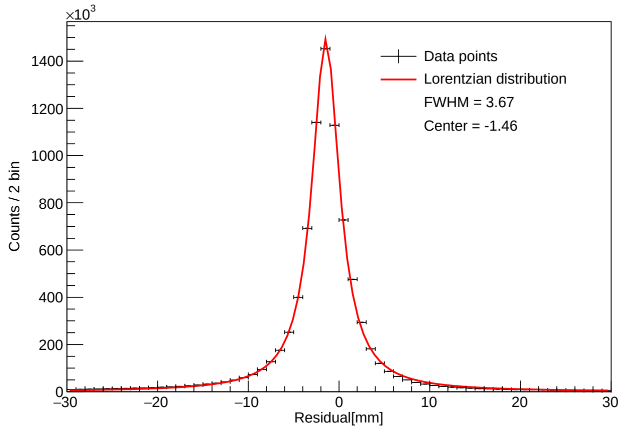

P14 and P77

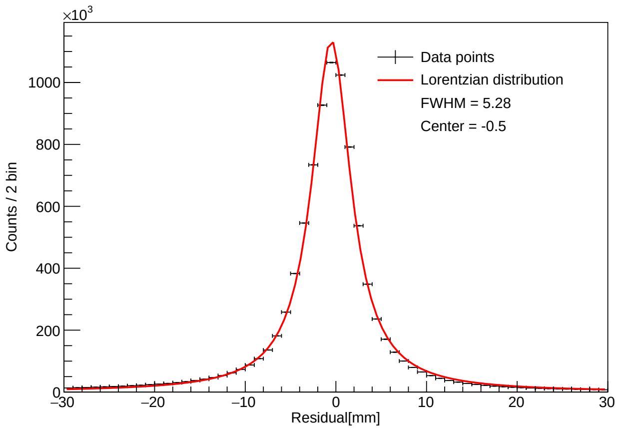

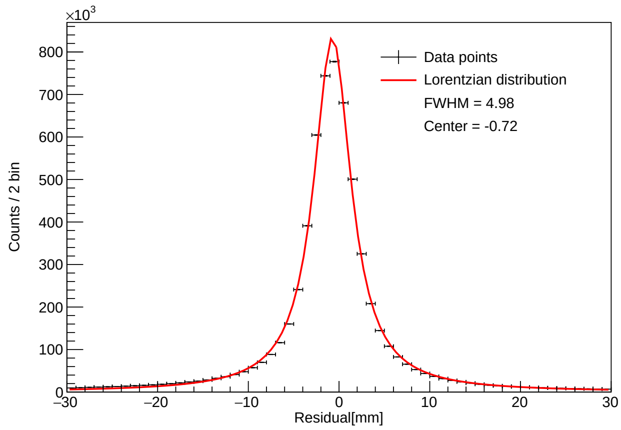

P30 and P28